50, 280 ACTA UNIVERSITATIS SZEGEDIENSIS

Acta Physica et Chemica

NOVA SERIES

TOMUS XXXVI FASCICULI 1–4

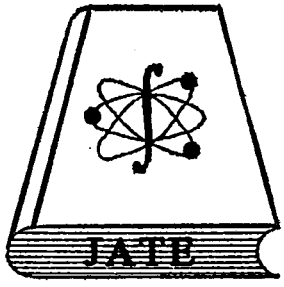

Szeged, Hungaria
1990

ACTA UNIVERSITATIS SZEGEDIENSIS

Acta Physica et Chemica

NOVA SERIES

TOMUS XXXVI FASCICULI 1-4

AUSHAF 36(1-4)1990

HU ISSN 0324-6523 Acta Univ. Szeged

HU ISSN 0001-6721 Acta Phys. et Chem.

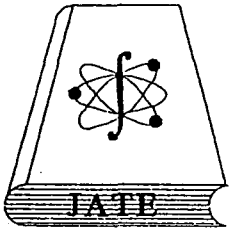

Szeged, Hungaria

1990

Kiadja:
a József Attila Tudományegyetem Természettudományi Kara
(Szeged, Aradi vértanuk tere 1.)

Szerkesztőbizottsági titkárok:
ANDOR J., BÁRDI I., MOLNÁR Á. és SÜLI Á.

Kiadványunk rövidítése:
Acta Phys. et Chem. Szeged

ANNOUNCEMENT TO EVERYONE CONCERNED !

Dear Reader,

The editorial staff regrets to announce the last issue of this Acta. Therefore, from now on, Acta copies for other journals can not be exchanged. The editorial staff and the Editor–in–Chief acknowledge and highly appreciate the cooperation of exchange partners for so many years.

After 36 years of serving the scientific publication needs of physicists and chemists at the University of Szeged (JATE), this is –to our knowledge– the only Acta, among the many university Actae, which is ceasing to exist. However, the wider editorial board, leading physicists and chemists of JATE, decided that their continuously decreasing financial funds would be spent in the future for more useful and prosperous purposes and so they sealed the fate of this Acta.

In spite of the fact that the effort to publish this Acta, home made in camera ready form, and still in higher standards and quality for always reducing costs was an unrewarding role to play and have not ever been appreciated, the select editorial staff is yet sorry for closing down the Acta Physica et Chemica Szeged.

STABILITY OF DISTRIBUTED FEEDBACK DYE LASER EXCITED BY AN EXCIMER LASER

J. SERES[1]*, J. HEBLING[2] and ZS. BOR[2]

[1]Department of Physics, Gyula Juhász Teachers' Training College,
H–6720 Szeged, Boldogasszony sgt. 6., Hungary

[2]Department of Optics and Quantum Electronics, Attila József University,
Dóm tér 9., H–6720 Szeged, Hungary

(*Received October 1, 1990*)

FOR EXCIMER LASER PUMPING, THREE POSSIBLE REASONS FOR THE FLUCTUATION IN THE DFDL OUTPUT PULSE ENERGY WERE STUDIED: THE FLUCTUATION IN THE VISIBILITY OF THE AMPLITUDE—PHASE GRATING IN THE DYE SOLUTION, THE CHANGE IN THE PUMP PULSE SHAPE ON THE 100 ps — 4 ns TIME SCALE, AND THE CHANGE IN THE PUMP BEAM INTENSITY DISTRIBUTION ALONG THE EXCITED VOLUME.

Introduction

Distributed feedback dye lasers (DFDLs) are simple sources of transform–limited picosecond pulses [1]. Both the pulse duration and the stability of the output pulse energy are relevant properties of DFDLs. The stability of a DFDL pumped by a low–pressure N_2 or an excimer laser has been measured and calculated [2,3]. The fluctuation in the exciting beam intensity was presumed to cause the fluctuation in the DFDL pulse energy. This energy fluctuation was determined from the fluctuation in the pumping laser energy and the slope of the calculated output–input energy characteristic of the DFDL. For low–pressure N_2 laser pumping, the calculations gave good agreement with the measurements [2]. However, for both TEA N_2 and excimer laser pumping, the measured fluctuation in the output energy was significantly larger than

the calculated one. TEA N_2 and excimer lasers differ from low–pressure N_2 lasers in many properties:

a) The bandwidths of TEA N_2 lasers and excimer lasers are much larger than those of low–pressure N_2 lasers. The spatial coherences of TEA N_2 and excimer lasers are small. These two differences can cause a significant fluctuation in the visibility of the amplitude–phase grating in the DFDL.

b) There are a few streaks on the cross–section of the TEA N_2 laser beam, so the intensity of the pumping varies along the excited volume of the DFDL, and therefore the amplification is modulated in space. The positions of the streaks change from shot to shot. Such a streaky structure can not be seen in the beam of a low–pressure N_2 laser.

c) Exciting pulses from excimer lasers usually have a modulation in time [3], some peaks can be observed in the pulse shape. The phase of this modulation can change from shot to shot without changing the pulse energy.

The effects of these properties on the stability of the DFDL are studied in this paper by using a time–space–dependent differential equation system to describe the lasing of the DFDL.

Theoretical model

The behaviour of the DFDL can be described by the following system of equations [4]:

$$-\frac{\partial R(x,t)}{\partial x}+\frac{\eta}{c}\frac{\partial R(x,t)}{\partial t}=\frac{1}{2}\sigma_e n(x,t)\left[R_o+R(x,t)+\frac{V}{2}S(x,t)\right]-\frac{1}{2}\rho R(x,t), \tag{1}$$

$$\frac{\partial S(x,t)}{\partial x}+\frac{\eta}{c}\frac{\partial S(x,t)}{\partial t}=\frac{1}{2}\sigma_e n(x,t)\left[S_o+S(x,t)+\frac{V}{2}R(x,t)\right]-\frac{1}{2}\rho S(x,t), \tag{2}$$

$$\frac{\partial n(x,t)}{\partial t} = I_p(x,t)\,\sigma_p\Big[N-n(x,t)\Big] - \frac{n(x,t)}{\tau} - \frac{\sigma_e\,\epsilon\lambda}{h\eta}\Big[|R|^2+|S|^2\Big]n(x,t). \qquad (3)$$

The meanings of the symbols are as follows:

x: the distance along the excited volume [cm]

N: the total concentration of dye molecules [$9\cdot10^{18}$ cm^{-3}]

n(x,t): the concentration of molecules in the S_1 excited state [cm^{-3}]

τ: the fluorescence lifetime of the S_1 state [4 ns]

η: the refractive index of the dye solution [1.32]

c: the speed of light in vacuum [$3\cdot10^8$ $m.s^{-1}$]

V: the visibility of the amplitude–phase grating in the excited volume [0.4]

σ_p: the absorption cross–section of the dye molecules at the 308 nm pump wavelength [$1.15\cdot10^{-17}$ cm^2]

σ_e: the emission cross–section of the dye molecules at the DFDL wavelength [$1.1\cdot10^{-16}$ cm^2]

R(x,t): the electric field of the DFDL light propagating in the –x direction [$V.m^{-1}$]

S(x,t): the electric field of the DFDL light propagating in the +x direction [$V.m^{-1}$]

ϵ: the permittivity of the dye solution [η^2 $8.854\cdot10^{-12}$ $AsV^{-1}m^{-1}$]

λ: the wavelength of the DFDL [555 nm]

b: the height of the excited volume [0.25 mm]

h: Planck's constant [$6.616\cdot10^{-34}$ Js]

L: the length of the pumped volume [3 mm]

ρ: the non–saturable loss of DFDL energy in the excited volume [$\approx$1 cm^{-1}]

$a = \left[N\ \sigma_p\right]^{-1}$, is the penetration depth of the pump light into the dye solution [$\approx$ 0.1 mm]

$R_0 = S_0 = \sqrt{\frac{\hbar c}{ab\epsilon\lambda L}}$, describes the spontaneous emission.

The system of equations (1)–(3) was solved on an IBM AT computer, using a numerical method. Typical excimer laser parameters were used for the calculations. The output energy of the DFDL was calculated from the formula:

$$E = \int \frac{\epsilon c b a}{\eta} |R(L,t)|^2\, dt \qquad (4)$$

Results of calculations

a) The exciting beam is split into two beams by a holographic grating in the DFDL arrangement. These two beams are reflected on the surfaces of a quartz parallelepiped. After reflection, these two beams interact in the dye solution, creating an amplitude–phase grating. In this pattern, the surfaces of the constant phase and amplitude are planes. These are perpendicular to the surface of the dye cell. For the ideal case, the visibility of the interference pattern is 1 everywhere in the excited volume. In reality, the visibility is smaller than 1. The reason for this, the bandwidth and the divergence of the excimer laser beam are not infinitely small. Therefore, the time and spatial coherence length of the exciting laser are small:
where $\Delta\lambda \approx 0.3$ nm and $\Theta \approx 0.01$ for the excimer laser. The depth of the excited

$$L_{time} = \frac{\lambda^2}{\Delta\lambda} \approx 300\ \mu m \quad (5)$$

$$L_{spatial} = \frac{\lambda}{\Theta} \approx 30\ \mu m \quad (6)$$

volume is $\approx$ 100 μm, which is significantly larger than the spatial coherence length. Therefore, the visibility is smaller than 1 and it can differ from point to point in the excited volume. A visibility value of $\approx$ 0.4 was estimated from the measurement of the amplified spontaneous emission background of the excimer laser pumped DFDL [5]. The visibility of the amplitude–phase grating can also change from shot to shot.

As an about ±10% fluctuation of the visibility seems realistic, the calculations were carried out with visibility values between 0.36 and 0.44. The results of calculations are shown in Figures 1 and 2. The output energy of the DFDL is represented as a function of pump intensity in Fig. 1. This Figure indicates that the threshold pump intensity for V = 0.4 is $I_p = 3.29 \cdot 10^{23}$ $cm^{-2}s^{-1}$. For an 8% higher intensity of this threshold, the output energy is represented as a function of the visibility (see Fig. 2). (According to Fig. 3 in [5], the DFDL creates a single pulse only if the pump intensity does not exceed the threshold intensity by more than 8%.) As it can be seen in Fig.2 a±10% fluctuation of the visibility results a±14.3% fluctuation in the DFDL pulse energy. Therefore, the fluctuation in the visibility can be the reason for the fluctuation in the DFDL output energy.

b) The cross–section of the TEA N_2 laser beam has a streaked structure; the intensity of the beam is modulated in space. This beam is focused by a cylindrical lens into a line. Because of the streaked structure of the beam, the intensity changes along the line and therefore the amplification is modulated in space. To investigate the effect of this, we described the pump intensity as a function of and time variables with the following formula:

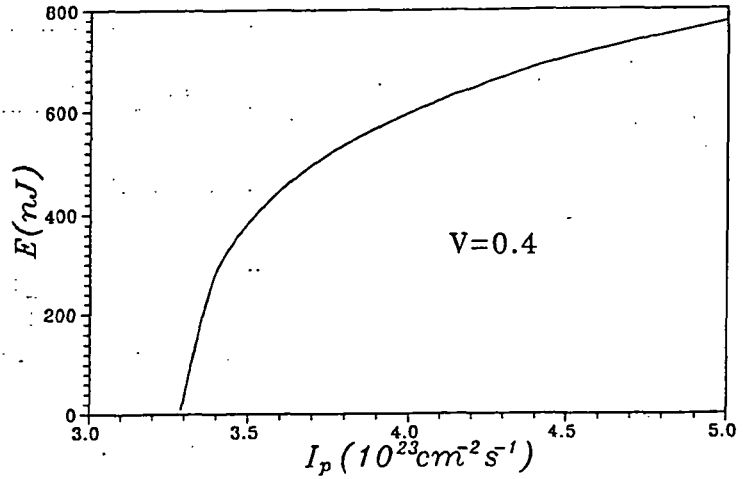

Figure 1: Single–pulse energy of the DFDL as a function of the pump intensity

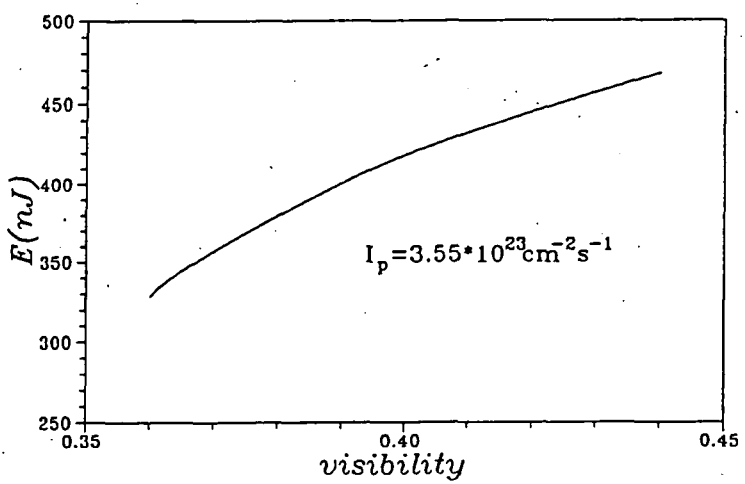

Figure 2: Single–pulse energy of the DFDL as a function of the visibility

$$I_p(x,t) = I_0 \left[1+u \sin\left[\frac{2\pi n}{L} x+\varphi\right]\right]\exp\left[-4 \ln(2)\left[\frac{t-t_p}{T}\right]^2\right] \quad (7)$$

where

t_p: the position in time of the maximum of the exciting pulse

T: the duration of the exciting pulse [9 ns]

u: the depth of the spatial modulation [0.5]

$$u = \frac{I_{max}-I_{min}}{I_{max}+I_{min}} \quad (8)$$

n: the number of streaks in the excited volume.

Usually, a small part of the focused beam is used to illuminate the dye cell, and therefore there are only a few streaks in the excited volume. The cases n = 1 and n = 2 were studied in our calculations. The results of the calculations are shown in Figures 3 and 4. The output energy is seen to depend only slightly on the spatial modulation of the pump intensity. This dependence is more significant for larger losses.

c) The exciting pulse may have a modulation in time. Such an exciting pulse was described as

$$I_p(x,t) = I_0 \left[1+u \sin\left[\frac{2\pi}{T_h} t+\varphi\right]\right]\exp\left[-4 \ln(2)\left[\frac{t-t_p}{T}\right]^2\right] \quad (9)$$

where T_h is the period of the modulation.

We chose u = 0.5. The calculations (see Fig. 5) revealed that the output energy depends on the phase of the modulation. This phase was changed by φ. The exciting intensity was chosen to be 8% higher than the threshold intensity. The measured fluc–

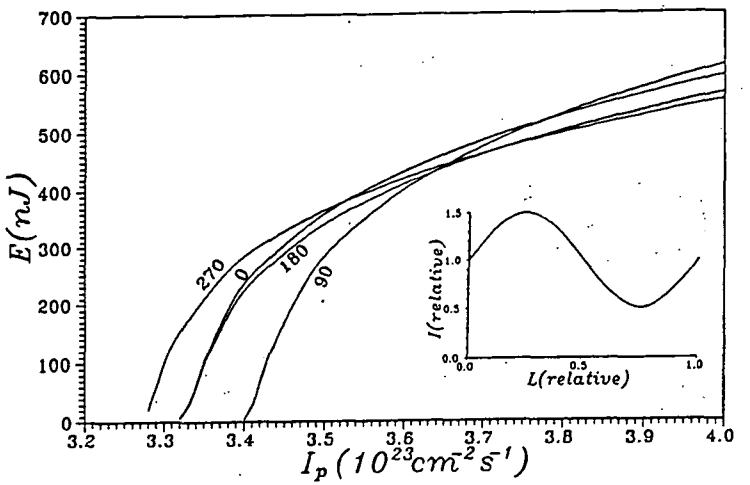

Figure 9: Single–pulse energy of the DFDL as a function of the pump intensity for different φ. The number of streaks is 1

tuation in the exciting pulse intensity was ±1%. This value was used in the calculations. For T_h = 400 ps, the results of the calculations are depicted in Fig. 5 for a few values of the phase of the modulation. It can be seen from this Figure that there is a situation (for the used parameter–set at φ=90^0) such that the energy of the DFDL fluctuates to a larger extent than ±8%, even if the phase of the modulation of the pump pulse is constant and the fluctuation in the pump intensity is only ±1%. This

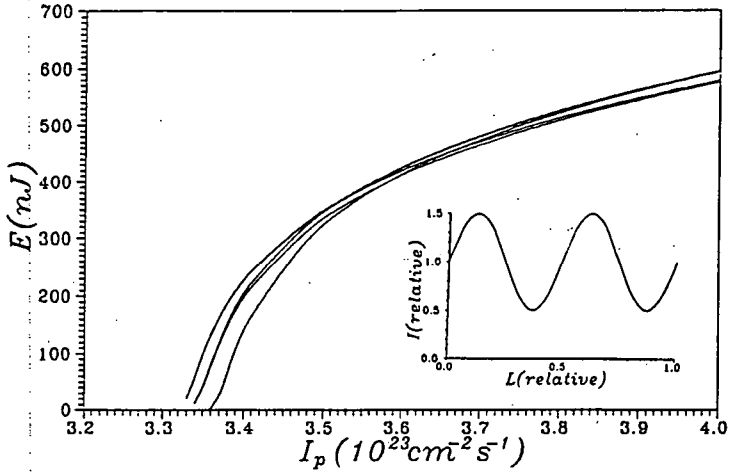

Figure 4: Single–pulse energy of the DFDL as a function of the pump intensity for different φ. The number of streaks is 2.

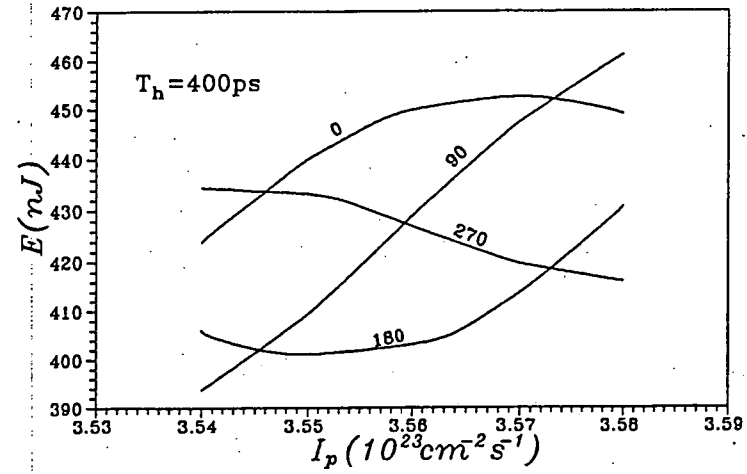

Figure 5: Fluctuation in the single–pulse energy of the DFDL at different phase φ.

sensitivity for the fluctuation in the pump intensity is about twice as large as in the case of unmodulated pumping. On the other hand, with constant pump intensity, the DFDL energy can change considerably if the phase of the modulation of the pump intensity changes from shot to shot.

Figure 6 shows the dependence of the DFDL energy fluctuation on the value ofthe modulation period. It can be seen that the fluctuation is significant if T_h is larger than 300 ps. The fluctuation is larger than 25% for T_h values between 1.4 and 2 ns. For a period time (T_h) of the modulation larger than 1 ns, the fluctuation does not decrease below 15%. Therefore, the calculations indicate that the time modulation of the pump pulse can be the reason for the fluctuation in the output energy.

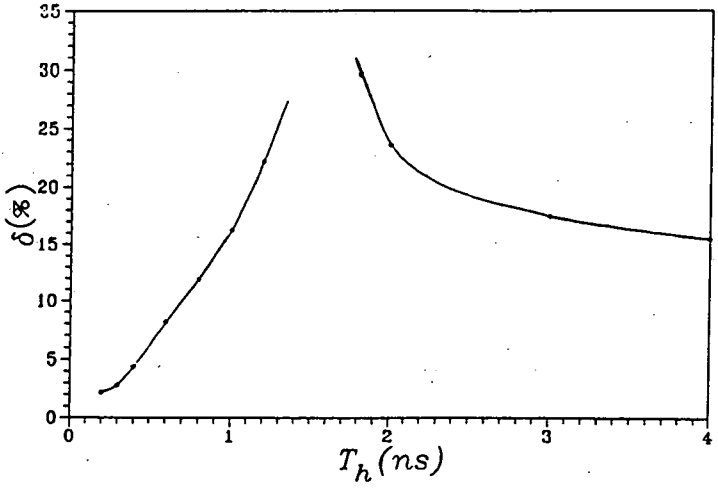

Figure 6: DFDL pulse energy fluctuation as a function of the period of the pump pulse modulation in time.

Conclusion

For TEA N_2 and excimer laser pumping, we have studied the reasons for the fluctuation in the output energy of a DFDL by using a simple model. The calculations showed that the fluctuation in the exciting pulse in time and the fluctuation in the visibility can explain the measured fluctuation. However, the fluctuation in the spatial distribution of the exciting intensity does not cause a significant fluctuation, at least for a non–saturable loss value $\rho = 1$ cm^{-1}.

References

[1] *Bor, Zs., A. Müller*: IEEE J.QE–*22*, 1524 (1986).

[2] *Bor, Zs., A. Müller, B. Rácz, F. P. Scafer*: Appl.Phys.B.*27*, 77 (1982).

[3] *Hebling, J.*: Appl.Phys.B.*47*, 267 (1988).

[4] *Duling, I.N. III, M. G. Raymer*: IEEE J.QE–*20*, 1202 (1984).

[5] *Hebling, J.*: Optics Common *64*, 539 (1987).

INVESTIGATION OF THE STABILITY OF DRUG–CONTAINING (MULPLE–PHASE) EMULSIONS

I. ERŐS[1], J. BALÁZS[2], I. CSÓKA[1] and SZ. MUSZTAFA[1]

[1]Department of Pharmaceutical Technology

A. Szent–Györgyi Medical University, Szeged, Hungary

[2]Department of Colloid Chemistry

Attila József University, Szeged, Hungary

THE AUTORS HAVE STRIVEN TO PREVENT THE DECREASE OF MULTIPLE–PHASE CHARACTER IN W/O/W EMULSIONS BY DIFFERENT TECHNOLOGICAL METHODS. PARTLY THE INTERNAL WATER PHASE OF MULTIPLE–PHASE EMULSIONS WAS GELLED BY GELATINE AND PARTLY THE VISCOSITY OF OIL PHASE WAS INCREASED BY SOLID EMULSIFIERS OF LOW HLB VALUE. THE GELATINE CONCENTRATION REQUIRED FOR STABILIZATION AND THE OPTIMAL CONCENTRATION OF SOLID EMULSIFIERS HAVE BEEN DETERMINED.

Introduction

Multiple–phase emulsions belong to the controlled drug delivery systems. The active ingredient dissolved or suspended in the internal water phase releases with an appropriate rate determined by the technologist. The following factors can be used for regulation of this rate:

– modification of drop size and surface of the internal water

– structure and compactness of emulsor film surrounding the internal wateer phase

– permeability of oil layer separating the enternal and external water phases [1].

Publications about the application of antigenic substances [2], antitumour medicines [3] and insulin [4] in w/o/w emulsions report on animal and clinical tests of promising results and good therapeutical benefit, too.

More widespreading practical use is prevented by the fact that the multiple–phase emulsions, among these w/o/w systems, are not stable. By splitting of the oil layer the external and internal water unite, hereby the multiple–phase character decreases and the multiple–phase emulsions is transformed gradually into a simple o/w emulsion. Many attempts [5–8] have been made to stabilize the multiple–phase character but this problem can't be considered as a completely solved one yet.

In our previous investigations [9] we have explained that the formation of the multiple–phase emulsion is facilitated by optimal concentration of emulsifier 1, optimal volume ratio of w/o emulsion in w/o/w emulsion, increase of viscosity of the oil and that of the external water phase and the relatively short mixing time in the second step of preparation as well.

Our further aim was to increase the stability of multiple–phase emulsions by means of:

1. Gelling the internal water phase in order to prevent the uniting of external and internal water phases.

2. Increasing the resistance and elasticity of oil layer separating the two water phases. For realizing the first step of emulsification such solid emulsifiers of relatively low HLB value were chosen which considerably increase the viscosity of oil and gel the oil as well.

Materials and methods

The oil phase of w/o/w emulsions was liquid petrolatum (Paraffinum liquidum of quality of Ph.Hg.VII).

For the preparation of w/o/w emulsions the following emulsifiers were used in the first step of emulsification: Span 20, 40, 60, 80 (Atlas GmbH, GFR), Imwitor 780 K

(Dynamit Nobel AG, GFR), Tegin (Goldschmidt AG, GFR), cetyl stearil alcohol, glycerol monostrearate, lanalcol (Ph.Hg.VII).

The concentration of emulsifiers was changed in the range of 10–12 g/100 w/o emulsion. Aqueous solution of 1% of Tween 20 was used in the second step of emulsification to form w/o/w emulsion.

The preparation of w/o emulsion, – the first step of emulsification – was performed as follows: Solid emulsifiers together with the oil phase were heated over the melting point in water bath. The water phase of the same temperature was emulsified in the melt under constant conditions. The w/o emulsion was stirred mechanically until cooling down. The second step of emulsification was performed at room temperature. Emulsions stabilized by gelatine were prepared in the above–mentioned manner.

As indicator substance ephedrine hydrochloride of 1 % wt was dissolved in the water phase of w/o emulsion for controlling the efficiency of formation and stability. The amount of chloride ion appearing in the external water phase was measured by a OP–CI–0711 P chloride selective membrane electrode, using a calibration curve. From the amount of chloride ion measured immediately after preparation the amount of formed w/o/w emulsion was determined. From the values measured after given storage time the decrease of the amount of multiple–phase emulsions and their stability we estimated.

Viscosity or emulsions were measured by Rheotest–2 rotary viscosimeter at 298 ± 1 K. Besides observation and measurement of spontaneous separation, the stability of the emulsion was determined by centrifuging for 10 minutes at a rate of 3000 rpm in centrfuge of Janetzki K–23 type.

Results and discussion

1.) The effect of geling by geletine on the properties and stability of w/o/w emulsions.

Our concept related to gelling of the internal water phase was to avoid the decrease and transformation of the multiple – phase character by preventing the uniting of the internal and external waters.

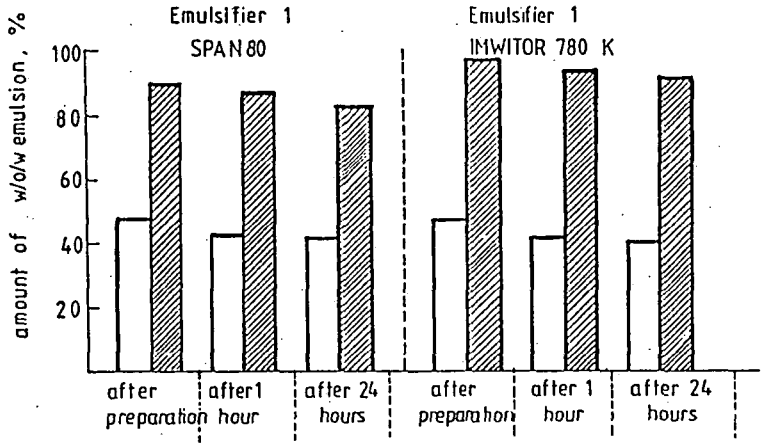

Figure 1: Stability of w/o/w emulsion without gelatine ☐ and with gelatine ▨ of 3 %.

Our hypothesis has been proved correct by Fig.1. Gelatine considerably increased the efficiency of formation of the multiple–phase emulsion and stabilized suitably the formed emulsion.

Many emulsifier of low HLB value were tested in our previous experiments to work out the first step of emulsification. The effect of the best two emulsifiers (Span 80 and Imwitor 780 K) are compared in Fig.1. Emulsifying features of Span 80 have been already known from the literature [5,6]. The excellent emulsifying capabvility of Imwitor 780 K (partial glyceride of isostearic acid, with a HLB value of 3,7) and its stabilizing effect exceeding that of Span 80 have been testified by our investigations.

Gelatine solutions of 1, 3, 4, 5 and 6 % wt were used as water phase in w/o/w emulsion to determine the optimal concentration of 1 % wt was a viscous sol, while the other systems became gelatinous ones after cooling. (it was found that gelatine concentration of 3 % wt was sufficient to stabilize effectively the multiple—phase character. In the case of systems with 4, 5 and 6 % wt gelatine concentration neither the efficiency of emulsification nor the stability of emulsions were greater (Fig.2).

Viscosity of emulsions was increased by gelatine to such an extent that the nearly ideal—viscous systems of low viscosity were transformed into structure—viscous ones (Table I).

Only data of emulsions of 24 hours are shown in Figs. 1 and 2. Investigation of multiple—phase character by means of ion—selective membrane was performed for a longer period (48 hours, 1 and 2 weeks and 1 month). Data relating to these experiments have not been published because of the instability of systems after 48 hours or 1 week. This instability became visible as separation and creaming of emulsions, respectively. This phenomenon was scarcely distinguishable but it became significant after 1 month. The multiple—phase emulsion separated into a concentrated multiple—phase emulsion (in which the multiple—phase character slightly decreased compared to the value after preparation) and water. Our investigations on the stability of distribution and the rate of separation have already been published

Table I

Rheological character and equilibrium viscosity of multiple–phase emulsion stabilized by gelatine

Emulsifying agent	Gelatine %	Rheological Character	Equilibrium viscosity (mPa.s)
Span 80	0	idealviscous	4,3
	3	structurviscous	11,5
	4	structurviscous	18,5
	5	structurviscous	34,9
	6	structurviscous	40,8
Imwitor 780 K	0	idealviscous	5,7
	3	structurviscous	19,5
	4	structurviscous	16,4
	5	structurviscous	12,5
	6	structurviscous	13,5

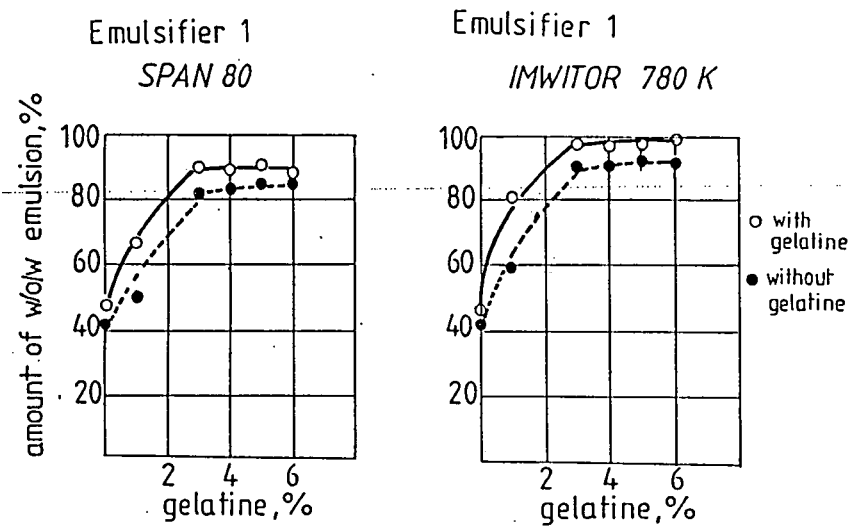

Figure 2: Effect of gelatine on the formation and stability of multiple–phase emulsion

elsewhere [10].

It can be concluded that the gelling of water phase ensures the stability of the multiple–phase character but not that of the distribution.

2.) The increase of viscosity of the oil phase by solid emulsifiers of low HLB value.

Our other effort for stabilization was the use of solid, gel forming emulsifiers in the first step of emulsification. In the basis of our previous experiments of centrifuging, cetyl stearil alcohol, glycerol monostearate, Span 40 and 60 were chosen (Table II).

Table II

Macroscopic changes after centrifuging

Solid emulsifier g/100g emulsion	10	12	14	16	18	20
Cetyl stearyl alcohol	Oo	Oo	Oo	Oo	•	•
Cetyl stearyl alcohol + Span 20	Ooo	Oo	Oo	Oo	Oo	•
Glycerol monostearate	Ooo	Oo	Oo	Oo	•	•
Glycerol monostearate + Span 20	Ooo	Oo	Oo	•	•	•
Lanalcol	Ooo	Ooo	Ooo	Oo	Oo	Oo
Lanalcol + Span 20	Oo	Oo	Oo	Oo	Oo	Oo
Span 40 + Span 20	Oo	Oo	Oo	Oo	Oo	•
Span 60	Oo	Oo	Oo	Oo	•	•
Span 60 + Span 20	Oo	Oo	Oo	Oo	•	•
TEGIN	Ooo	Ooo	Oo	Oo	Oo	•

Ooo – three layers Oo – two layers • – it remained stable

From the point of view of rheology these systems were thixotrope ones with yield point. Their equilibrium viscosity increases considerably with the amount of gel forming emulsifier (Fig. 3).

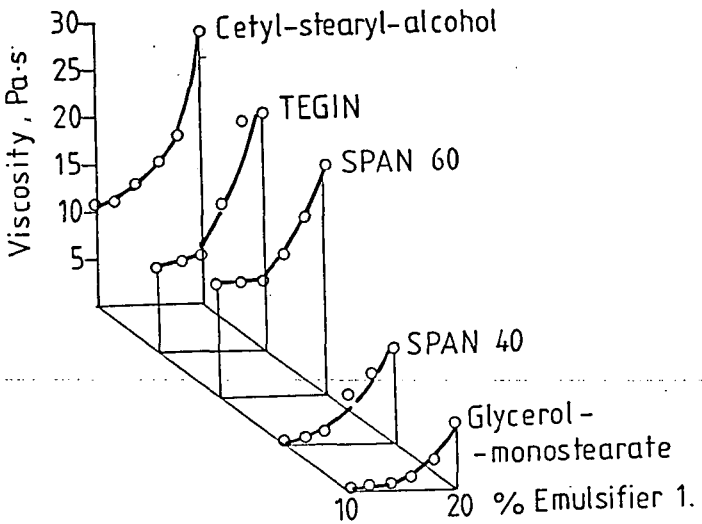

Figure 3: Connection between emulsifier concentration and equilibrium viscosity in w/o/w emulsion

Fig. 4. proves that multiple–phase emulsions can be effectively stabilized by solid emulsifiers mentioned above. Their multiple–phase character didn't change considera–bly after 72 hours. Where as in emulsions containing Span 80 this character decreased significantly during 72 hours. macroscopically these systems were stable, water or oil separation couldn't be observed even after several months following the preparation.

Since solid emulsifier of 20 % gave the character of fairly viscous or even high consistency to the system in several cases, it was abvisable to use these emulsifiers together with Span 20 liquid emulsifier in a concentration of 10–10 %.

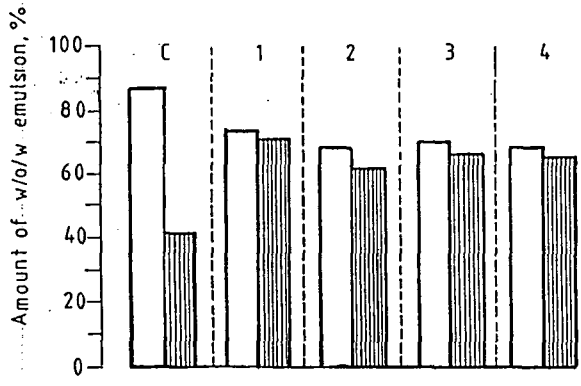

Figure 4: Effect of gel forming emulsifier 1 on the stability of multiple phase emulsions (▭ immediately after preparation, ▨ after 72 hours) C control (Span 80), 1 cetyl stearyl alcohol, 2 glycerol monostearate, 3 Span 40, 4 Span 60

Investigation of the formation of multiple–phase emulsions showed (Fig. 5) that almost each combination approached the efficiency of Span 20 – Span 80 combination. After 72 hours the multiple–phase character was unchanged in the case of cetyl stearyl alcohol – Span 20, Span 40 – Span 20 and glycerin monstearate – Span 20 systems, therefore these emulsifier mixtures have good proper stabiliziing effect. On the other hand, considerable decrease of multiple–phase character was observed in the case of Span 60 – Span 20 and Span 80 – Span 20 combinations. Explanation for this and for stabiliziing effect of different extent requires further investigations and

ditailed study of interfacial tenside film.

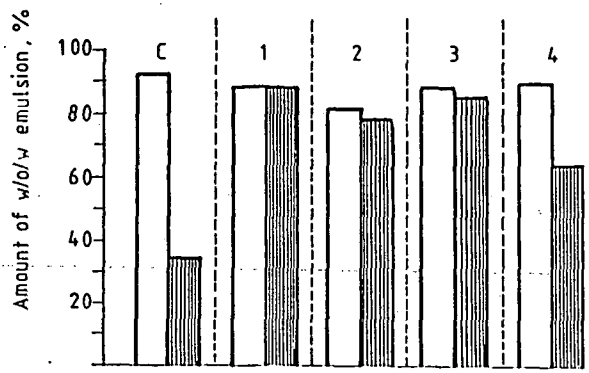

Figure 5: Conjugate effect of gel forming emulsifier and Span 20 on the stability of w/o/w emulsions (▭ immediately after preparation, ▨ after 72 hours) C control (Span 80), 1 cetyl stearyl alcohol, 2 glycerol monostearate, 3 Span 40, 4 Span 60

References

[1] *Florence, A. T., J. A. Omotosho and T. L. Whateley:* Polymers and Aggregate Systems (ed. M. Rusoff) VCH Publisher, Inc. Weinheim. 1989. p. 163.

[2] *Hill, A. V., K. G. Hibbitt, A. Shears:* A. W. Britt J. Exp. Phatol. *55*, 194 (1973).

[3] *Takahashi, T., S. Ueda, K. Kono, S. Majima:* T. Cancer *38*, 1507

(1976).

[4] *Sichiri, M., R. Kawomori, M. Yoshida, M. Etani, M. Hoshi, K. Izumi, Y. Shigeta, H. Abe:* M Diabetes *24*, 971 (1975).

[5] *Florence, A. T., D. Whitehill:* J. pharm. pharamacol. *34*, 687 (1982).

[6] *Abd–Elbary, A., S. A. Noyr, F. F. Mansour. Pharm. Ind. 46*, 964 (1984).

[7] *Madgassi S., M. Frenkel, N Garti:* Drug. Dev. Ind. Pharm. *11*, 791 (1985).

[8] *Oza, K. P., S. G. Frank:* J. Disp. Sci. Techn. *10*, 187 (1989).

[9] *Balázs J., I. Erős, M. Tasi, M. Péter:* Acta Phys. Chem. *34*, 121 (1988).

[10] *Erős, I., Csóka, I., Balázs:* 2nd International Congress on Cosmetics and Household Chemicals, Budapest 1990., Abstracts p. 64.

A PC COMPUTER PROGRAM MINIMIX FOR THE CALCULATION OF THE STABILITY CONSTANTS OF $M_qL_pL'_{p'}$, TYPE MIXED OR THE MIXTURE OF M_qL_p and $M_{q'}L'_{p'}$, COMPLEXES FROM SPECTROPHOTOMETRIC MEASUREMENTS

F. GAIZER*

Institute of Inorganic and Analytical Chemistry, Attila József University,

Dóm tér 7, H–6720 Szeged, Hungary

and

H. B. SILBER

San José State University, School of Chemistry,

San José, California, 95192, USA

(*Received May 21, 1990*)

THE PC COMPUTER PROGRAM MINIMIX HAS BEEN CONSTRUCTED IN BASIC AND FORTRAN PROGRAMING LANGUAGE FOR THE CALCULATION OF STABILITY CONSTANTS AND MOLAR ABSORPTIVITIES OF THE $M_qL_pL'_{p'}$, TYPE MIXED OR THE MIXTURE OF M_qL_p AND $M_{q'}L'_{p'}$, COMPLEXES FROM SPECTROPHOTOMETRIC MEASUREMENTS. BY THE FORTRAN VERSION OF THIS PROGRAM THE EQUILIBRIA OF THE $M_qL_pL_p, H_r$ PROTONATED/DEPROTONATED COMPLEXES CAN ALSO BE TREATED.

Introduction

In our previous papers we published desk computer programs for 16 Kbyte computers to evaluate stability constants from potentiometric [1] and spectrophotometric [2] measurements. In the present paper we introduce a more complex program which is capable of calculating the optimum value of stability constants and molar absorp–

* Present permanent address: Department of Chemistry, Janus Pannonius University, H–7624 Pécs, Ifjúság u. 6., Hungary

tivities of mixed ligand complexes of type $M_qL_pL'_{p'}$ from spectrophotometric measurements. The program also applies to mixtures of complexes such as M_qL_p and $M_{q'}L'_{p'}$, but it cannot be used for metals bound to only a single ligand (M_qL_p alone). The present program MINIMIX written in BASIC programming language differs from the previous ones not only in the problem to be solved, but in its capability of evaluating measurements at any number of wavelengths. By the FORTRAN version of this program, which is available upon request, the equilibria of mixed ligand complexes of type $M_qL_pL'_{p'}H_r$, *i.e.*, protonated (+r) or hydroxo (−r) complexes, can be treated too.

Fundamentals

For the formation of mixed ligand complexes the following equilibria can be written (the charges on the components are omitted for simplicity):

$$q\,M + p\,L + p'\,L' \rightleftharpoons M_qL_pL'_{p'} \quad \text{or}$$
$$q\,M + p\,L + p'\,L' + r\,H^+ \rightleftharpoons M_qL_pL'_{p'}H_r\,.$$

For these equilibria the following cumulative formation constant can be written and are used in this program:

$$\beta = [M_qL_pL'_{p'}H_r] \cdot [M]^{-q} \cdot [L]^{-p} \cdot [L']^{-p'} \cdot [H^+]^{-(r)}$$

In the present BASIC program the last term is not included.

Assuming the validity of BEER's law, the absorbance (A) of a solution in 1 cm path length can be written as the sum of the absorbances of each component:

$$A = \epsilon_M \cdot [M] + \epsilon_L \cdot [L] + \epsilon_{L'} \cdot [L'] + \sum_j \epsilon_j \cdot c_j,$$

where $c_j = \beta_j \cdot [M]^{q_j} \cdot [L]^{p_j} \cdot [L']^{p'_j} \cdot [H^+]^{(r_j)}$. If we assume the composition of complexes (q, p, p', and r values) formed in the system studied and their stability constants (β values), we can calculate the concentration of free species ([M], [L] and [L'] by solving the mass balance equations written for the total concentrations of components (T_M, T_L and $T_{L'}$) [3], and having these values we can calculate the concentration of the individual c_j complexes. If we assume molar absorptivities for each of the absorbing species too, we can calculate the absorbance (A_c) and compare it with the measured one (A_m) for each solution. If the agreement is not satisfactory, the program adjusts the assumed parameters (β and ϵ values) until satisfactory agreement is reached, or a completely new calculation with another model (with new q, p, p' and r values) is required. Consequently the steps of the evaluation with a model are as follows: First, we assume the stoichiometric coefficients of the complexes formed; second, β and ϵ values are estimated. Third, the program calculates the concentration of the free species and complexes, and from these then calculates the absorbancies.

To calculate the optimum values of the parameters resulting in the minimum sum of the unweighted squares of residuals in absorbances, the same method is used in this program as in MINISPEF [2].

The program

With the exception of renumbering and a few changes detailed later, the portions of the program (lines 260–295) were kept identical with that of MINISPEF [2]. The names of variables and arrays have been kept, only a few new ones had to be introduced. To make the usage of the program easier, we reduced the number of input variables to the minimum, based on our experiences. In order to help user in extending or modifying the program, the arrays and their dimensions have been summarized

in Table I.

In the main program, the following substantial changes have been made:

- It is capable of treating data from measurements made at a maximum of four wavelengths.
- The error in the individual parameters are saved and may be printed out.
- The values of the elements of correction vector appear on the screen. This facilitates following the refinement cycles and the "behavior" of each parameter during refinements.
- On the basis of our systematic examination, we have found it necessary to modify automatically the value of individual increments after each refinement cycle. As an optimum value for the increment, half of the error in each parameter was found. In spite of this modification, it is advisable to try different starting values for increments, if the interaction between the reactants is weak or there are parameters which have only a slight effect on the sum of the square of residuals. Leaving out the T(J) = U7/2 statement in the line 680, no modification of increments is made.

The function of subroutines EQUSOL and PRINT has not been changed, but the former one has been extended to solve equation systems with three unknowns. It seemed to be expedient to locate them in a separate subroutine (CPXES) for the calculation of the concentration of complexes.

Instructions for the use of the program

The percentage distribution of complexes is calculated by the formula

$$\% = \frac{q_j * C_{ij} * 100}{T}, \quad \text{where:}$$

Table I

Name of Array	Chemical notation or Reference	Identifier in the Program	Dimension of the Array
Total concentrations	T_M, T_L, $T_{L'}$	M, L, CZ	MP
Concentration of free species	[M], [L], [L']	A, B, Z	MP
Measured and calculated absorbances	A_m, A_c	E, El	MP x NW
Stoichiometric coefficients of complexes	q, p, p'	Q1, P1, R1	NC
Parameters	log β, ϵ	P	NP
Increments of parameters		T	NP
Errors in parameters	$\sigma(\log\beta)$, $\sigma(\epsilon)$	ER	NP
Complexes	$M_qL_pL'_p$,	C1	MP x NC
Serial No. parameters to be refined		S1	PF
Serial No. of wavelength involved into refinement		SW	NW
Transposed of gradient matrix	G^{T*}	G	PFx(NW x MP)
Product of the gradient matrix and its transposition	$C = G^T \times G^*$	C	PF x PF
Inverse of C	C^{-1*}	C5	PF x PF
Error vector	$y_i - y_i^{o*}$	D	NW x MP
Absorbances calculated by the starting values of parameters	y_i^{o*}	F	NW x MP
Product of transposed gradient matrix and error vector	$G^T \times d^*$	G1	PF
Correction vector	h^*	G2	PF
Cumulative stability constans	β	E2	NC
Molar absorptivites	ϵ	E3	NWx(NC + 3)

Abbreviations: NC: No. of complexes; NP: No. of parameters (= NC + NW * (NC + 3))
NW: No. of wavelengths; MP: No. of measured points; PF: No. of parameters to be refined.
*) Ref. 3.

if N%=1 then T = TOT M, if N%=2 then T = TOT L, if N%=3 then T = TOT L'.

Divisors (X1, X2, X3). To make easier the typing of TOT concentrations of reactants, their multiplied values can be input; *e.g.*, if the concentrations are in mM, then the divisor X1 = 1000, etc. (see line 85).

Factors generating initial values of free species are necessary for solving mass balance equations by iterative methods. These initial values are calculated in the following way:

- $[M] = T_M * FM$, $[L] = T_L * FL$ and $[L'] = T_{L'} * FZ$. (line 840 and 1015).

The input of parameters into the array P must be made in the following order: first by β's, then the respective molar absorptivity of complexes, then ϵ_M, ϵ_L and $\epsilon_{L'}$, for the first, second, etc. wavelength. The serial number of parameters obtained in this way is used in the refinement or search procedure.

Experimental points involved in the calculations: there are options to use only one part of the experimental points, such as with only every second, third, etc. points.

Task: The program can execute three tasks:

1.) Optimizing simultaneously a maximum of 4 parameters given by their serial numbers.

2.) Search for the value of one of the parameters between input limits and by input step.

3.) Search for the value of one of the parameters between limits and steps generated by the actual value of parameter to be searched for. *E.g.*, if the value of the parameter searched for is P and the value of T3 is given for the lower limit of the search, the actual starting value will be T3 * P, etc., for T4 and T5 (line 335).

Note: 1.) The search is carried out only into the direction of higher values.

2.) If the value of the parameter to be searched for is negative, the step–
–factor T4 must be negative, too.

Print: For uneven numbers the output appears only on the screen.

For even numbers it is sent to the printer also.

Printout options: Depending upon the number chosen, various printing options are allowed:

if R% = 1 or 2: Refined parameters and their errors, square of residuals and standard deviation are shown.

if R% = 3 or 4: All the parameters and their errors, square of residuals and standard deviation are shown.

if R% = 5 or 6: The measured and calculated absorbances and the difference between them for the wavelengths involved into the calculations and the percentage distribution of complexes, that of free metal and free ligand are shown.

Wavelength(s) involved into refinements must be given by their input serial number.

Control number (V1): After execution of a task, it is possible to continue the calculations at different points of the programs (see lines 375 and 695). Options:

if V1 = 1: Calculation with new experimental data (from line 20)

if V1 = 2: New model (new Q, P, P', R values, from line 120)

if V1 = 3: Calculations with another points (from line 175)

if V1 = 4: New task (from line 265)

if V1 = 5: New refinement cycle (from line 385)

if V1 = 6: End of calculations.

Acknowledgement

This work was done under the Grant AX–659. The Robert A. Welch Foundation of Houston, Texas. One of the authors (F.G.) expresses his gratitude to the Foundation for the financial support.

References

[1] *Gaizer, F., A. Puskás:* Talanta, *28*, 565 (1981).

[2] *Gaizer, F., A. Puskás:* Talanta, *28*, 925 (1981).

[3] *Gaizer, F., M. Máté:* Acta Chim. Acad. Sci. Hung., *103*, 355 (1980).

```
0 REM MINIMIX-MW4
5 DIM A(50),B(50),C(4,4),C1(50,8),C5(4,4),CZ(50),D(200),E(50,8),E1(50,8)
10 DIM E2(8),E3(4,11),ER(52),F(200),G(4,200),G1(4),G2(4),L(50),M(50),P(52)
15 DIM P1(8),Q1(8),R1(8),S1(4),SW(4),T(52),Z(50):ZI=LOG(10):TI=1/ZI:E5=1000
20 PRINT "? # OF MSD POINTS":INPUT N1:PRINT "? # OF PARAMETERS":INPUT N2
25 PRINT "? # OF CPXES":INPUT N3:PRINT "? PERCENTAGE DISTRIBUTION RELATED TO
    1: TOT M,   2: TOT L,   3: TOT L'   -   SEE INSTRUCTIONS":INPUT N4%
30 PRINT "PRINTING OF MSD. DATA ?  -  NO: 0,  YES: 1":INPUT R%
35 PRINT "? DIVISOR OF TOT M TO BE INPUT":INPUT X1
40 PRINT "? DIVISOR OF TOT L TO BE INPUT":INPUT X2
45 PRINT "? DIVISOR OF TOT L' TO BE INPUT":INPUT X3
50 PRINT "? FACTOR GENERATING [M] FROM TOT M":INPUT FM
55 PRINT "? FACTOR GENERATING [L] FROM TOT L":INPUT FL
60 PRINT "? FACTOR GENERATING [L'] FROM TOT L'":INPUT FZ
65 PRINT "? # OF WAVELENGTHS":INPUT NW
70 FOR I=1 TO N1:PRINT  "? TOT M";I:READ M(I):PRINT "? TOT L";I:READ L(I)
75 PRINT "? TOT L'";I:READ CZ(I)
80 FOR J=1 TO NW:PRINT "? ABSORBANCE FOR WAVELENGTH #";J:READ E(I,J):NEXT J
85 M(I)=M(I)/X1:L(I)=L(I)/X2:CZ(I)=CZ(I)/X3:V2=E5
90 NEXT I
95 IF R%=0 THEN 105
100 LPRINT "        MEASURED DATA, CONCNS IN MMOL, AND ABSORBANCES":LPRINT
105 PRINT "        MEASURED DATA, CONCNS IN MMOL, AND ABSORBANCES":PRINT
110 FOR I=1 TO N1:PRINT USING "####.### ";I,M(I)*V2,L(I)*V2,CZ(I)*V2,E(I,1),E(I
2),E(I,3),E(I,4):NEXT I:IF R%=0 THEN 120
115 FOR I=1 TO N1:LPRINT USING "####.### ";I,M(I)*V2,L(I)*V2,CZ(I)*V2,E(I,1),E(
,2),E(I,3),E(I,4):NEXT I
120 FOR I=1 TO N3:PRINT "? Q FOR CPX #";I:INPUT Q1(I)
125 PRINT "? P FOR CPX #";I:INPUT P1(I):PRINT "? P' FOR CPX #";I:INPUT R1(I)
130 NEXT I
135 FOR I=1 TO N3:PRINT "? LOG BETA OF CPX #";I:INPUT P(I):
    PRINT "? ITS INCREMENT":INPUT T(I):NEXT I
140 I=N3+1:FOR J=1 TO NW:PRINT "WAVELENGTH #";J:FOR J1=1 TO N3
145 PRINT "? MOLAR ABSORPTIVITY OF CPX #";J1:INPUT P(I):
    PRINT "? ITS INCREMENT":INPUT T(I):I=I+1:NEXT J1
150 PRINT "? MOLAR ABSORPTIVITY OF METAL": INPUT P(I):
    PRINT "? ITS INCREMENT":INPUT T(I):I=I+1
155 PRINT "? MOLAR ABSORPTIVITY OF THE FIRST LIGAND"
160 INPUT P(I):PRINT "? ITS INCREMENT":INPUT T(I):I=I+1
165 PRINT "? MOLAR ABSORPTIVITY OF THE SECOND LIGAND":INPUT P(I)
170 PRINT "? ITS INCREMENT":INPUT T(I):I=I+1:NEXT J
175 PRINT "? SERIAL # OF THE FIRST EXPT. POINT TO BE EVALUATED":INPUT K
180 PRINT "? SERIAL # OF THE LAST EXPT. POINT TO BE EVALUATED":INPUT V
185 PRINT "? STEP BETWEEN THE EXPT. POINTS":INPUT N:T1=1:V2=1:MK=1
260 REM ************************************************************
265 PRINT "?  TASK;  OPTIONS:   0: REFINEMENT;  1: SEARCH WITH INPUT DATA;
                               2: SEARCH WITH GENERATED DATA":INPUT F
270 PRINT "? PRINT FORMAT;  OPTIONS 0-6,  SEE INSTRUCTIONS":INPUT R%
275 PRINT "? # OF WAVELENGTHS TO BE INVOLVED INTO CALCULATIONS":INPUT NWF
280 FOR LW=1 TO NWF:PRINT "? SERIAL # OF WAVELENGTH #";LW;"INVOLVED INTO CALCULA
TIONS":INPUT SW(LW):NEXT LW
285 GOSUB 830:GOSUB 1280:U1=U:IF F=0 THEN 385
```

```
290 REM *** SEARCH PROCEDURE FOR PARAMETER VALUE **********************
295 PRINT "? STARTING VALUE OR FACTOR OF PARAMETER TO BE SEARCHED FOR":INPUT T3
300 PRINT "? STEP VALUE OR FACTOR OF PARAMETER TO BE SEARCHED FOR":INPUT T4
305 PRINT "? UPPER LIMIT OR FACTOR OF PARAMETER TO BE SEARCHED FOR":INPUT T5
310 PRINT "? SERIAL # OF PARAM. TO BE SEARCHED FOR":INPUT T6
315 PRINT "? PRINT FORMAT, OPTIONS 0-6, SEE INSTRUCTIONS":INPUT R%
320 PRINT "? # OF STEPS AFTER U-MINIMUM":INPUT T7
325 PRINT "? WHERE TO GO AFTER EXECUTION THIS TASK; OPTIONS 1-6, SEE INSTRUCTION
S":INPUT V1
330 IF F=1 THEN 340
335 T3=P(T6)*T3:T4=P(T6)*T4:T5=P(T6)*T5
340 P(T6)=T3:V2=T6:GOSUB 830:GOSUB 1280:T8=H:T9=P(T6):GOTO 360
345 V2=T6:GOSUB 830:GOSUB 1280:IF H>T8 THEN 355
350 T8=H:T9=P(T6):GOTO 360
355 T7=T7-1:IF T7=0 THEN 365
360 P(T6)=P(T6)+T4:IF P(T6)<=T5 THEN 345
365 P(T6)=T9:PRINT USING "THE OPTIMUM VALUE OF PARAMETER : -########.######";T9
370 PRINT USING "THE SERIAL NUMBER OF PARAMETER :                ###";T6:V2=T6
375 ON V1 GOTO 20,120,175,265,385:END:REM ******************************
380 REM *** REFINEMENT PROCEDURE FOR PARAMETER VALUES ******************
385 PRINT "*** REFINEMENT FOLLOWS !***"
390 PRINT "? # OF PARAMETERS TO BE REFINED":INPUT F1:F2=1
395 PRINT "? WHERE TO GO AFTER EXECUTION THIS TASK; OPTIONS 1-6, SEE INSTRUCTION
S":INPUT V1
400 PRINT "PRINT FORMAT;  OPTIONS 0-6,  SEE INSTRUCTIONS":INPUT R%
405 FOR J=1 TO F1: C(F1,F1)=0:C5(F1,F1)=0:NEXT J
410 FOR J=1 TO F1:PRINT "? SERIAL # OF PARAMETER #";J;"TO BE REFINED":INPUT S1(J
):NEXT J
415 REM *** ERROR VECTOR, D ***
420 KW=0:FOR NN=1 TO NWF:LW=SW(NN):FOR I=K TO V STEP N:KW=KW+1:D(KW)=E(I,LW)-E1(
I,LW):F(KW)=E1(I,LW):NEXT I:NEXT NN
425 REM *** G MATRIX ***
430 FOR K1=1 TO F1:J=S1(K1):P(J)=P(J)+T(J):T6=J:V2=J:GOSUB 830:KW=0:FOR NN=1 TO
NWF:LW=SW(NN)
435 FOR I=K TO V STEP N:KW=KW+1:G(K1,KW)=(E1(I,LW)-F(KW))/T(J):NEXT I:NEXT NN
440 P(J)=P(J)-T(J):V2=1:NEXT K1
445 REM *** C MATRIX ***
450 FOR K1=1 TO F1:FOR K2=1 TO F1:C(K1,K2)=0:FOR I=1 TO KW
455 C(K1,K2)=C(K1,K2)+G(K1,I)*G(K2,I): NEXT I
460 C(K2,K1)=C(K1,K2):NEXT K2:NEXT K1
465 REM *** INVERSION OF MATRIX C INTO C5 ***
470 FOR I=1 TO F1:FOR K1=1 TO F1:C5(I,K1)=0:C5(K1,I)=0:NEXT K1:C5(I,I)=1
475 NEXT I:C5(F1,F1)=1:FOR K1=1 TO F1:V3=C(K1,K1):FOR I=1 TO F1
480 C(K1,I)=C(K1,I)/V3:C5(K1,I)=C5(K1,I)/V3:NEXT I:FOR L=1 TO F1
485 IF L-K1=0 THEN 500
490 V3=C(L,K1):FOR I=1 TO F1
495 C(L,I)=C(L,I)-V3*C(K1,I):C5(L,I)=C5(L,I)-V3*C5(K1,I):NEXT I
500 NEXT L:NEXT K1
505 REM *** MULTIPL. OF ERROR VECT. AND G-TRANSP. ***
510 FOR I=1 TO F1:S=0:FOR J=1 TO V STEP N:S=S+G(I,J)*D(J):NEXT J:G1(I)=S:NEXT I
```

```
515 REM *** CORRECTION VECTOR, G2 ***
520 FOR I=1 TO F1:S=0:FOR J=1 TO F1
525 S=S+C5(I,J)*G1(J):NEXT J:G2(I)=S:NEXT I:A6=1:I6=1
530 FOR K1 = 1 TO F1:J=S1(K1):IF J<=N3 THEN 550
535 F3=P(J)+G2(K1)
540 IF F3>0 THEN 550
545 G2(K1)=-P(J)
550 NEXT K1
555 IF F2=0 THEN 570
560 PRINT "U1=",U1
565 K6%=R%:R%=0:I6=0:K7=1:A6=.5:GOTO 575
570 PRINT "REFINED PARAMETERS:":PRINT
575 FOR K1=1 TO F1:J=S1(K1):P(J)=P(J)+G2(K1)*A6:NEXT K1
580 IF I6<1 THEN 610
585 FOR K1=1 TO F1:J=S1(K1)
590 IF J<=N3 THEN 605
595 IF P(J)>0 THEN 605
600 P(J)=0
605 NEXT K1
610 V2=S1(F1):GOSUB 830
615 IF I6>0 THEN 680
620 IF K7=0 THEN 635
625 U2=U:PRINT "U2=",U2
630 K7=0:GOTO 575
635 U3=U:PRINT "U3=",U3:R%=K6%:U4=U1-2*U2+U3:IF U4>0 THEN 655
640 A6=1:IF U3>U1 THEN 650
645 A6=1:GOTO 660
650 A6=0:PRINT "CONCAVE ALFA, IS MADE EQUAL WITH",A6:GOTO 665
655 U4=(U1-U3)/(4*U4):A6=.5+U4
660 PRINT "ALFA=",A6
665 A6=1-A6:I6=1:IF ABS(A6)<3 THEN 675
670 A6=2
675 A6=-A6:GOTO 570
680 U1=U:FOR I=1 TO F1:J=S1(I):U7=SQR(ABS(C5(I,I)))*H:ER(J)=U7:T(J)=U7/2
685 NEXT I:GOSUB 1280
690 PRINT "CORR. VECTOR:":FOR J=1 TO F1:PRINT USING" +##.##### ";G2(J),J:NEXT J
695 ON V1 GOTO 20,120,175,265,385:END:REM ****************************
830 REM EQUSOLV ******************************************************
835 FOR I=1 TO N3:E2(I)=EXP(ZI*P(I)):NEXT I:IK=N3:FOR JJ=1 TO NW:FOR II=1 TO N3+
3:IK=IK+1:E3(JJ,II)=P(IK):NEXT II:NEXT JJ:U=0:S2=0:TOL=.002
840 MK=MK-1:A=L(K)*FL:B=M(K)*FM:Z=CZ(K)*FZ
845 FOR I=K TO V STEP N:IF V2>N3 GOTO 985
850 KK=0:MKK=0:IX=0:ITT=0:CA=L(I):CB=M(I):CZ=CZ(I):AT=CA*TOL:BT=CB*TOL:ZT=CZ*TOL
:TYA=AT/1000:TYB=BT/1000:TYZ=ZT/1000:ITER=0
855 IF MK<0 THEN GOTO 870
860 IF (MK >=0) AND (I=K) THEN GOTO 1000
865 IF (MK>=0) AND (I>K) THEN GOTO 875
870 A=A(I):B=B(I):Z=Z(I)
875 MKK=MKK+1:IF MKK>30 THEN GOTO 1000
880 NRM=1:GOSUB 1165
885 YA=CASZ-CA:YB=CBSZ-CB:YZ=CZSZ-CZ:AYA=ABS(YA):AYB=ABS(YB):AYZ=ABS(YZ)
890 IF (AYA>AT) THEN GOTO 905
895 IF (AYB>BT) THEN GOTO 905
```

```
900 IF AYZ<=ZT THEN GOTO 980
905 IF AYA<TYA THEN YA=0
910 IF AYB<TYB THEN YB=0
915 IF AYZ<TYZ THEN YZ=0
920 AY=0-YA:BY=0-YB:ZY=0-YZ
925 DET=DA*DB*DZ+DBA*DZB*DAZ+DZA*DAB*DBZ-DZA*DB*DAZ-DZB*DBZ*DA-DZ*DBA*DAB
930 DT1=AY*DB*DZ+BY*DZB*DAZ+ZY*DAB*DBZ-ZY*DB*DAZ-DZB*DBZ*AY-DZ*BY*DAB
935 DT2=DA*BY*DZ+DBA*ZY*DAZ+DZA*AY*DBZ-DZA*BY*DAZ-ZY*DBZ*DA-DZ*DBA*AY
940 DT3=DA*DB*ZY+DBA*DZB*AY+DZA*DAB*BY-DZA*DB*AY-DZB*BY*DA-ZY*DBA*DAB
945 A=A+DT1/DET:IF A<0 THEN GOTO 1000
950 IF A>CA THEN GOTO 1000
955 B=B+DT2/DET:IF B<0 THEN GOTO 1000
960 IF B>CB THEN GOTO 1000
965 Z=Z+DT3/DET:IF Z<0 THEN GOTO 1000
970 IF Z > CZ THEN GOTO 1000
975 GOTO 875
980 A(I)=A:B(I)=B:Z(I)=Z
985 FOR NN=1 TO NWF:LW=SW(NN):E1(I,LW)=B(I)*E3(LW,N3+1)+A(I)*E3(LW,N3+2)+Z(I)*E3
(LW,N3+3)
990 FOR LC=1 TO N3:E1(I,LW)=E1(I,LW)+C1(I,LC)*E3(LW,LC):NEXT LC
995 DE=E(I,LW)-E1(I,LW):S2=S2+1:U=U+DE^2:NEXT NN:GOTO 1155
1000 AT=10*AT/(ITER+1):BT=10*BT/(ITER+1):ZT=10*ZT/(ITER+1):A=A(I):B=B(I):Z=Z(I)
1005 IF ITER=1 THEN GOTO 1020
1010 IF MK<0 THEN GOTO 1020
1015 A=CA*FL:B=CB*FM:Z=CZ*FZ
1020 ITER=ITER+1:DIA=A:DIB=B:DIZ=Z
1025 GA=2:GB=2:GZ=2:NRM=0
1030 GOSUB 1165
1035 ITT=ITT+1:IF ITT>500 THEN GOTO 1150
1040 DE=CA-CASZ:ADE=ABS(DE):IF ADE<=AT THEN GOTO 1070
1045 IF DE<=0 THEN GOTO 1055
1050 DIA=GA*DIA:A=A+DIA:GOTO 1060
1055 GA=.5:DIA=GA*DIA:A=A-DIA
1060 DLA=A/1000:IF DIA>DLA THEN GOTO 1030
1065 GA=2:DIA=A:GOTO 1025
1070 DE=CB-CBSZ:ADE=ABS(DE):IF ADE<=BT THEN GOTO 1100
1075 IF DE<=0 THEN GOTO 1085
1080 DIB=GB*DIB:B=B+DIB:GOTO 1090
1085 GB=.5:DIB=GB*DIB:B=B-DIB
1090 DLB=B/1000:IF DIB>DLB THEN GOTO 1025
1095 GB=2:DIB=B:GOTO 1025
1100 DE=CZ-CZSZ:ADE=ABS(DE):IF ADE<=ZT THEN GOTO 1140
1105 IF DE<=0 THEN GOTO 1115
1110 DIZ=GZ*DIZ:Z=Z+DIZ:GOTO 1125
1115 GZ=.5:DIZ=GZ*DIZ:Z=Z-DIZ
1120 IF DE<0 THEN GOTO 1025
1125 DLZ=Z/1000:IF DIZ>DLZ THEN GOTO 1025
1130 GZ=2:DIZ=Z:GOTO 1030
1135 GOTO 980
1140 IF ITER=2 THEN GOTO 980
1145 AT=ITER*AT/10:BT=ITER*BT/10:ZT=ITER*ZT/10:A(I)=A:B(I)=B:Z(I)=Z:ITT=0:MKK=0:
GOTO 875
1150 PRINT "UNSUCCESSFUL ITERATION!":GOTO 1140
1155 NEXT I:RETURN
1160 RETURN
```

```
1165 REM CPXES FOR MIXED LIGAND CPXES **********************************
1170 CASZ=A:CBSZ=B:CZSZ=Z:IF NRM=0 THEN GOTO 1180
1175 DA=1:DB=1:DZ=1:DAB=0:DAZ=0:DBZ=0
1180 FOR L=1 TO N3:JP=P1(L):JQ=Q1(L):JZ=R1(L)
1185 C1(I,L)=E2(L)*Z^JZ*B^JQ*A^JP:CPX=C1(I,L)
1190 CASZ=CASZ+JP*CPX:CBSZ=CBSZ+JQ*CPX:CZSZ=CZSZ+JZ*CPX:IF NRM=0 GOTO 1205
1195 DA=DA+(CPX/A)*JP*JP:DB=DB+(CPX/B)*JQ*JQ:DZ=DZ+(CPX/Z)*JZ*JZ
1200 DAB=DAB+JP*JQ*CPX:DBZ=DBZ+JQ*JS*CPX:DAZ=DAZ+JP*JS*CPX:NEXT L
1205 IF NRM=0 THEN GOTO 1215
1210 DBA=DAB/A:DAB=DAB/B:DZB=DBZ/B:DBZ=DBZ/Z:DZA=DAZ/A:DAZ=DAZ/Z
1215 RETURN
1280 REM PRINT ***********************************************************
1290 IF R%=0 THEN GOTO 1680
1300 IF F>0 THEN PRINT "VALUE OF PARAM. SEARCHED FOR:  ";P(T6)
1310 IF F>0 AND R%>=2 THEN LPRINT "VALUE OF PARAM. SEARCHED FOR:  ";P(T6)
1320 IF F>0 THEN GOTO 1430
1330 IF R%>2 THEN GOTO 1380
1340 IF F1>0 THEN PRINT "REFINED PARAMETERS AND THEIR ERRORS:"
1350 FOR I=1 TO F1:J=S1(I):PRINT J,P(J),ER(J):NEXT I:IF R%=1 THEN GOTO 1430
1360 IF F1 >0 THEN LPRINT "REFINED PARAMETERS AND THEIR ERRORS:":LPRINT
1370 FOR I=1 TO F1:J=S1(I):LPRINT J,P(J),ER(J):NEXT I:GOTO 1430
1380 PRINT "PARAMETERS AND THEIR ERRORS:"
1390 FOR I=1 TO N2:PRINT USING "  ####.####  ";I,P(I),ER(I):NEXT I
1400 IF R%=3 OR R%=5 THEN GOTO 1430
1410 LPRINT" ":LPRINT "PARAMETERS AND THEIR ERRORS:"
1420 FOR I=1 TO N2:LPRINT USING "  ####.####  ";I,P(I),ER(I):NEXT I
1430 PRINT USING"SQUARE OF RESIDUALS:  .###### ";U
1440 IF R%=2 OR R%=4 THEN LPRINT USING"SQUARE OF RESIDUALS:  .###### ";U
1450 IF R%=6 THEN LPRINT USING"SQUARE OF RESIDUALS:  .###### ";U
1460 H=SQR(U/(S2-F1-1)):PRINT USING"STANDARD DEVIATION:   .###### ";H:PRINT
1470 IF R%=2 OR R%=4 THEN LPRINT " ":LPRINT USING"STANDARD DEVIATION:   .######
";H:LPRINT
1480 IF R%=6 THEN LPRINT :LPRINT USING"STANDARD DEVIATION:   .###### ";H:LPRINT
1490 IF R%<5 THEN GOTO 1680
1500 FOR JJ=1 TO NWF:J=SW(JJ):PRINT " WAVELENGTH # ",J:PRINT:FOR I=K TO V STEP N
:PRINT USING " +##.###  ";E(I,J),E1(I,J),E(I,J)-E1(I,J),I:NEXT I:NEXT JJ
1510 IF R%=5 THEN GOTO 1540
1520 FOR JJ=1 TO NWF:J=SW(JJ):LPRINT " WAVELENGTH # ",J:LPRINT:FOR I=K TO V STEP
 N:LPRINT USING " +##.###  ";E(I,J),E1(I,J),E(I,J)-E1(I,J),I:NEXT I:NEXT JJ
1530 ON N4% GOTO 1540,1590,1640
1540 PRINT "PERCENTAGE DISTRIBUTION OF TOT M IN CPXES AND FREE M"
1550 IF R%=6 THEN LPRINT "PERCENTAGE DISTRIBUTION OF TOT M IN CPXES AND FREE M"
1560 FOR I=K TO V STEP N:PRINT USING "  ###.##  ";C1(I,1)*100/M(I),C1(I,2)*100/M
(I),C1(I,3)*100/M(I),B(I)*100/M(I),I:NEXT I
1570 IF R%=5 THEN GOTO 1680
1580 FOR I=K TO V STEP N:LPRINT USING "  ###.##  ";C1(I,1)*100/M(I),C1(I,2)*100/
M(I),C1(I,3)*100/M(I),B(I)*100/M(I),I:NEXT I:GOTO 1680
1590 PRINT "PERCENTAGE DISTRIBUTION OF TOT L IN CPXES"
1600 IF R%=6 THEN LPRINT "PERCENTAGE DISTRIBUTION OF TOT L IN CPXES"
1610 FOR I=K TO V STEP N:PRINT USING "  ###.##  ";C1(I,1)*100/L(I),C1(I,2)*100/L
(I),A(I)*100/L(I),I:NEXT I
```

```
1620 IF R%=5 THEN GOTO 1680
1630 FOR I=K TO V STEP N:LPRINT USING "  ###.##  ";C1(I,1)*100/L(I),C1(I,2)*100/
L(I),A(I)*100/L(I),I:NEXT I:GOTO 1680
1640 PRINT "PERCENTAGE DISTRIBUTION OF TOT L' IN CPXES"
1650 IF R%=6 THEN PRINT "PERCENTAGE DISTRIBUTION OF TOT L' IN CPXES"
1660 FOR I=K TO V STEP N:PRINT USING "  ###.##  ";C1(I,1)*100/CZ(I),C1(I,2)*100/
CZ(I),Z(I)*100/CZ(I),I:NEXT I:IF R%=5 THEN GOTO 1680
1670 FOR I=K TO V STEP N:LPRINT USING "  ###.##  ";C1(I,1)*100/CZ(I),C1(I,2)*100
/CZ(I),Z(I)*100/CZ(I),I:NEXT I
1680 RETURN
3000 REM DATA FOR MINIMIX-MW4
3010 REM DATA 24, 22, 2, 1, 1, 1000,1000,1000, .9,.9,.9,  4
3020 DATA 53.095,   95.115,  1404.88,  .261, .214, .160, .148
3030 DATA 53.095,  190.23,   1309.77,  .289, .237, .195, .162
3040 DATA 53.095,  285.34,   1214.66,  .292, .252, .210, .171
3050 DATA 53.095,  380.46,   1119.54,  .305, .265, .211, .179
3060 DATA 53.095,  475.56,   1024.44,  .318, .281, .234, .190
3070 DATA 53.095,  570.69,    923.31,  .329, .295, .259, .201
3080 DATA 53.095,  665.8,     834.20,  .337, .304, .253, .205
3090 DATA 53.095,  760.93,    739.07,  .335, .309, .260, .211
3100 DATA 53.095,  856.03,    643.97,  .350, .321, .269, .220
3110 DATA 53.095,  951.16,    548.84,  .355, .331, .281, .229
3120 DATA 53.095, 1046.30,    453.70,  .358, .335, .282, .230
3130 DATA 53.095, 1141.40,    358.60,  .361, .338, .285, .232
3140 DATA 109.48,   95.115,  1404.88,  .523, .370, .305, .255
3150 DATA 109.48,  190.23,   1309.77,  .557, .441, .354, .284
3160 DATA 109.38,  285.34,   1214.66,  .582, .485, .384, .307
3170 DATA 109.38,  380.46,   1119.54,  .604, .521, .420, .335
3180 DATA 109.38,  475.56,   1024.44,  .620, .547, .440, .346
3190 DATA 105.57,  643,       923.31,  .625, .561, .454, .363
3200 DATA 109.48,  665.8,     834.20,  .667, .593, .484, .384
3210 DATA 109.48,  760.93,    739.07,  .675, .617, .509, .409
3220 DATA 109.48,  856.03,    857.00,  .687, .631, .520, .415
3230 DATA 109.48,  951.16,    548.84,  .695, .641, .525, .424
3240 DATA 109.48, 1046.30,    453.70,  .711, .659, .552, .441
3250 DATA 109.48, 1141.40,    358.60,  .719, .671, .564, .454
3260 REM DATA 1,1,0, 1,0,1, .17, .12, -1.3, .2
3270 REM DATA 5, .25, 5, .25, 5, .25, 0, .1, 0, .1
3280 REM DATA 5, .25, 5, .25, 5, .25, 0, .1, 0, .1
3290 REM DATA 5, .25, 5, .25, 5, .25, 0, .1, 0, .1
3300 REM DATA 5, .25, 5, .25, 5, .25, 0, .1, 0, .1
3310 REM DATA 1, 24, 1
3320 REM DATA 1,1, 1,1, 0,2,20, 3,2,2,4
3330 REM DATA 2,1, 1,1, .9, .01, 1.2, 3,2,2,4
3340 REM DATA 0,1, 1,1, 3,5,2, 3,4,5,  3,4,2, 3,4,5
3350 REM DATA 0,1, 1,2, 3,5,2, 8,9,10, 3,4,2, 8,9,10
3360 REM DATA 0,1, 1,3, 3,5,2, 13,14,15, 3,4,2, 13,14,15
3370 DATA 0,1, 1,4, 3,5,2, 18,19,20, 3,4,2, 18,19,20
3380 DATA 1,4, 4, 1,2,3,4, -1.00, 1, -0.99, 2,1,1,4
3390 DATA 0,1, 1,1, 3,5,2, 3,4,5,  3,4,2, 3,4,5
3400 DATA 0,1, 1,2, 3,5,2, 8,9,10, 3,4,2, 8,9,10
3410 DATA 0,1, 1,3, 3,5,2, 13,14,15, 3,4,2, 13,14,15
3420 DATA 0,1, 1,4, 3,5,2, 18,19,20, 3,4,2, 18,19,20
3430 DATA 0,4, 4, 1,2,3,4, 2,6,6, 1,2
```

CHEMISTRY IN A SPIN

SIDNEY F. A. KETTLE*

Institute of Inorganic and Analytical Chemistry,

Attila József University

Dóm tér 7., H–6720 Szeged, Hungary

(*Received December 13, 1990*)

THE IMPORTANCE OF CONSIDERING RELATIVISTIC EFFECTS, BEING IN CLOSE CONNECTIONS WITH THE ELECTRON SPIN, IN UNDERSTANDING OF BONDING PROPERTIES IN MOLECULES IS EMPHASIZED, ILLUSTRATED BY CHEMICAL EXAMPLES AND SHOWN HOW THESE EFFECTS CAN BE TREATED QUALITATIVELY BY GROUP THEORETICAL TOOLS, ESPECIALLY THOSE CALLED DOUBLE GROUPS.

The theory of relativity is essential to our understanding of bonding in molecules. Electron spin is a relativistic phenomenon and is relevant to the simplest system. Elementary lectures refer to the fact, sooner or later, we must use the quantum number j ($=l+s$) rather than l and s separately. We are aware that the (relativistic) phenomenon of spin–orbit coupling exists and that the use of j is linked to the importance of spin–orbit coupling. Yet it is usual to assume that all this can be forgotten even when discussing the bonding in compounds of the heavier elements. Of course, relativity is a "difficult" topic but this does not make its neglect a valid approximation. Indeed, it does not take much of a literature survey to point out theneed to take relativistic phenomena on board. For instance, down the series Co, Rhand Ir the spin–orbit coupling constants for the 4+ ions (ions for which data are

* Permanent address: School of Chemical Sciences, University of East Anglia, Norwich NR4 7TJ, ENGLAND, U.K.

available for all three elements) are 650, 1570 and 5000 cm^{-1} respectively – an order of–magnitude change, moving from an energy typical of a vibration to one typical of a low–energy electronic excitation. Perhaps more obvious is a comparison of the relative energies of the Pb–Pb single bond (1.0eV) and the corresponding spin–orbit coupling energy –1.32eV. How can one hope to correctly describe the Pb–Pb bond unless the importance of spin–orbit coupling is considered, even if it is subsequently dismissed? Similarly, a recent approximate study of the bonding in an equilateral triangular array of Pt atoms concluded that the bonding energy is 7.12 $kJ.mol^{-1}$ on a non–relativistic basis but is 36.43 $kJ.mol^{-1}$ on a relativistic basis [1]. Therefore, we must surely conclude that we must make a serious attempt to include relativistic phenomena in our qualitative description of heavy–metal clusters. Of course, relativistic calculations are much more difficult to do than non–relativistic ones and, in particular, it becomes much more difficult to include the effects of electron–electron repulsion. So, detailed calculations are limited to simple systems but still we can learn a great deal from them. So, as one relevant example, it seems clear that although Ag–H and Au–H are very similar at the non–relativistic level, they become very different when relativistic effects are included (see the energy level diagram in Fig.1). This not only accounts for the different colours of silver and gold (a transition in metallic silver moves to much lower energy in gold) but, almost certainly, for the very different chemistries of the two elements. Further manifes– tations of relativistic phenomena are the low melting point of mercury, the inert pair effect (both manifestations is from the fact that a pair of *s* electrons have become a bit similar to those in He) and a contribution to the lanthanide contraction.

Relativistic atomic orbitals differ in one major way from their non–relativistic

counterparts. They are a superposition of four "bits". Each "bit" is quite like one of the familiar atomic orbitals but the fact the orbitals are superpositions means that the

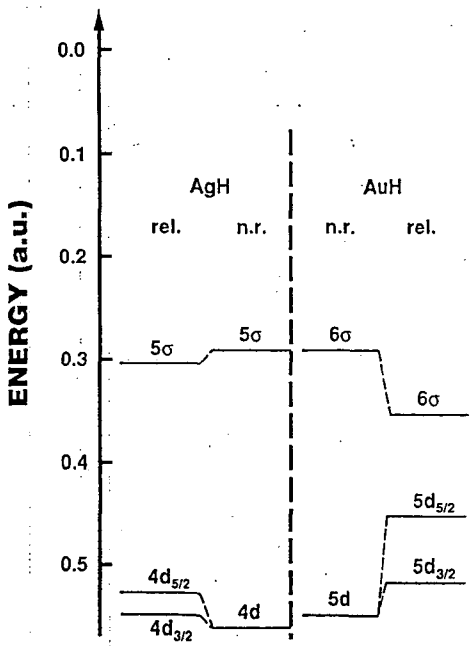

Figure 1: Energy level diagrams of AgH and AuH

nodal pattern inherent in one "bit" will not normally coincide with those of the other "bits". So, overall, there are no nodes. All of this makes it difficult to draw relativistic orbitals and they tend to be pictured as electron densities. Even this is not really satisfactory because relativistic orbitals have intrinsic angular momentum which cannot be "cancelled–out" (such cancelling–out is the way that the standing waves p_x and p_y are obtained from the angular momentum containing functions p_1 and p_{-1}). The result is that the subject is made yet more difficult by half–true statements,

intended to help saying: "both the functions $s_{1/2}$ and $p_{1/2}$ are spherically symmetrical" or "$p_{1/2}$ consists of a σ bonding component and a π antibonding component". Although a proper description of bonding in heavy–element compounds must surely use such orbitals there is a half–way house. This is to use functions appropriate to j, to use spin–orbit functions. Again, however, these functions are shrouded in mystery and no–one seems to attempt to draw them. Yet the group–theory associated with them is well–developed – it is the theory of the so–called "double groups". These are usually introduced as a mathematical trick but, in fact, a reality can be attached to them.In Fig. 2 is given the character table of the C_{2v} double group, usually denoted C^*_{2v}, together with the nodal patterns associated with each of its irreducible representations.

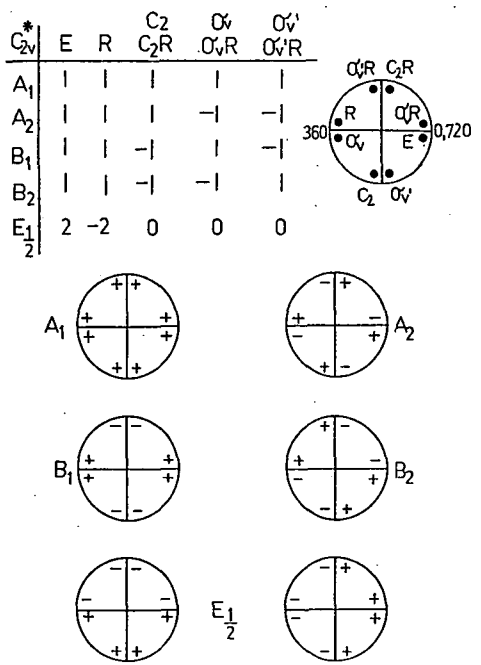

Figure 2: Character table and nodal patterns of the C^*_{2v} (double) group

It will be noticed that it is possible to give standing–wave pictures of the (two) spin = ± 1/2 functions (these are the components of the $E_{1/2}$ basis).

As an example I now give a double–group description of the metal–metal bonding in the $Pt_3(CO)_6$ cluster. It will help to take a result from the reference cited earlier, that in a Pt_3 cluster there is a "hole" of 0.768 electrons in the d–shell [1]. This hole is a result of an enhanced occupation of the 6s–shell (relativistic effects lower the energies of s–electrons, a phenomenon which is manifest in mercury being a liquid and in the inert–pair effect). For the moment, for simplicity, we take the d–electron hole as unity. Regarding the Pt as square–planar (three CO groups and the Pt_2 unit forming the square plane) then simple crystal field theory places the hole in the d_{x2-y2} orbital. The electron is therefore in an $E_{1/2}$ orbital of the C^*_{2v} group, that shown earlier. Now, because electrons in Pt–CO bonding orbitals spend part of their time on the CO ligands, where relativistic effects are small, the consequences of relativistic effects will be most important for the Pt–Pt bonding. The symmetry of the $Pt_3(CO)_6$ unit is D_{3h} and so we work in the D^*_{3h} (double) group. It is a simple matter to show that the $E_{1/2}$ functions of C^*_{2v} form a basis for the $E_{1/2} + E_{3/2} + E_{5/2}$ irreducible representations of D^*_{3h}. We do not know the relative ordering of these levels; it depends on the relative importance of spin–orbit coupling and bonding (although, in the event, our conclusions will depend only on the relative position of $E_{3/2}$ and this probably does not depend on the winner). Let us take bonding to be the winner, so that the (node–dependent) energy sequence is that given above. If the first two spin–orbitals are filled then the d–orbital hole is 0.667 electrons, not too far from the result of calculations [1] on Pt_3. A double–group picture of the $E_{3/2}$ functions is given in Fig. 3. To get the electron density associated with these functions we simply have to square them, whereupon the phase pattern which forced the use of a rotation of

720° as the identity changes to one compatible with the real–world identification of 360° as identity. Occupancy of $E_{3/2}$ as the HOMO corresponds to bumps of high electron density by every 60°, so that we would expect that if two $Pt_3(CO)_6$ units stack together, free from crystal environment constraints, that they would be rotated 30° relative to each other.

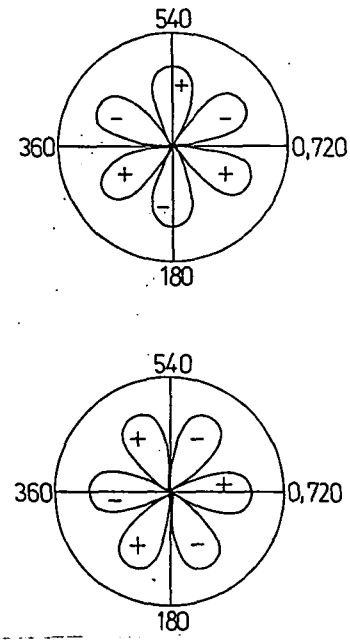

Figure 9. Double–group picture of the $E_{3/2}$ functions

It is therefore interesting to note [2] that the central $Pt_3(CO)_6$ unit in $[Pt_3(CO)_6]_5^{2-}$ is rotated relative to the adjacent units by 27.2° and 28.6°. Of course, this argument requires that the Pt–Pt bonding between adjacent layers is rather insensitive to the angle of rotation between them. The variability of this angle offers some evidence in support of such a speculation, as does the generally lower geometry–sensitivity of

relativistic orbitals: "$p_{1/2}$ is spherically symmetrical".

References

[1] *Gavezzotti A., G. F. Tantardini, H. Miessner*: J. Phys. Chem. *92*, 872 (1988).

[2] *Calabrese, J. C., L. F. Dahl, P. Chini, G. Longoni, S. Martinengo*: J. Am. Chem. Soc. *96*, 2616 (1974).

PRINS REACTIONS OF ALLYL ALCOHOL AND ALLYL ACETATE

R.F. TALIPOV[1], E.D. RAKHMANKULOV[1], M.G. SAFAROV[1] and K. FELFÖLDI[2]

[1] Baskhir State University, Ufa, USSR

[2] Institute of Organic Chemistry, Attila József University,

Dóm tér 8., H–6720 Szeged, Hungary

(*Received May 15, 1990*)

THE CONDENSATIONS OF ALLYL ALCOHOL AND ALLYL ACETATE WITH CH_2O WERE STUDIED. THE MAIN REACTION PRODUCTS DEPARTED FROM THE USUAL MAIN PRODUCTS OF PRINS REACTIONS.

Introduction

The condensations of allyl alcohol and allyl acetate with formaldehyde in the presence of an acid catalyst were studied. The main reaction products were found to be linear formals of allyl alcohol, *trans*–1,4–diacetoxybutene–2 from allyl acetate and, as a result of secondary reactions, 1,2,4–triacetoxy–3–acetoxymethylbutane. The addition products of formaldehyde to the double bonds of allyl alcohol were formed in negligible amounts. Attention was paid to the effects of the reaction conditions (temperature, catalyst concentration, reagent ratio, reaction time) on the yield and product distribution in the reaction of allyl acetate with CH_2O.

Experimental

GLC analysis was performed on an LHM–8MD instrument fitted with a 2m·3mm column of 5% SE–301 on Chromatone N–AW–HMDS and with a flame ionization detector. The column temperature was 373 K or was programmed in the interval

323–423 K, with helium as carrier gas (30 ml/min). ^{1}H–NMR spectra were measured in CCl_4 with a Tesla–BS–487 C spectrometer, and are reported in ppm (δ) relative to internal HMDS. IR spectra were run on a Microlab–620MH spectrometer in neat film. GC/MS spectra were recorded on a Finnigan–4021 instrument (EI 68––70 eV) with a 50 m x 0.32 mm glass capillary column coated with SE–54SIL, temperature–programmed from 50 K to 493 K with helium as carrier gas.

Reaction of allyl alcohol (I) and formalin: A mixture of 238 ml (3.4 mole) I, 290 ml (3.5 mole) 30 % formalin and 8.4 ml cc. H_2SO_4 was heated and stirred at 358–360 K for 2.5 hours. After cooling, the acid was neutralized, the unreacted formaldehyde was bound with gaseous ammonia, and the mixture was extracted with 3x100 ml ether. The organic layer was dried, the solvent was distilled off, and the residue was fractionated on a 15 cm column, to yield 35 g III and 176 g II. The formaldehyde conversion, determined by the sulphite method, was 88–89 %.

Synthesis of IV: A mixture of 46.9 g (1.56 mole) paraformaldehyde, 82 ml water, 13.9 ml cc. H_2SO_4, 144 ml (1.56 mole) butanol–1 and 88.5 g (1.3 mole) I was stirred at 353 K for 9 hours. After the standard working–up, the residue was fractionated, to yield 89 g IV and 37 g dibutylformal.

Reaction of I and formalin in the presence of HOAc: A mixture of 191 ml (1.91 mole) 30 % formalin, 65 ml (0.95 mole) I, 109 ml HOAc and 10.2 ml cc. H_2SO_4 was stirred at 348 K for 4 hours. After cooling, neutralizing and working–up the residue was distilled and separated to yield 62.5 g VIII. This compound was termally unstable above 413 K.

Reaction of I and paraformaldehyde in the presence of $AlCl_3$: To a mixture of 63 ml $CHCl_3$, 10.5 g $AlCl_3$ and 11.8 g (0.39 mole) paraformaldehyde at 273 K 27 ml (0.39 mole) I was added in small portions and the mixture was then stirred at 353 K for 3.5 hours. After the working–up and distilling–off of unreacted I, the residue was

fractionated leading to separation of a fraction with b.p. 343–393 K/3,99 kPa (mainly II) and another one with b.p. 398–423 K/0,799 kPa (a mixture of compounds resulting from the addition of HCl to II).

Reaction of I and paraformaldehyde in the presence of HCl: A mixture of 53.6 g (1.79 mole) paraformaldehyde, 101 ml (1.49 mole) I, 94 ml water and 126 ml cc. HCl was stirred at 343 K for 2 hours. After the working–up and the distilling–off unreacted I (32 g), the residue was fractionated. TLC analysis (on alumina, benzene–EtOH = =10:1, R_F = 0.28) and the ^{1}H–NMR spectrum indicated, that the first fraction (8.6 g) was IX, while the second fraction (16 g, b.p. 429–473 K/1,86 kPa) was a mixture (3:1) of IX and an unknown compound (R_F = 0.63). The total yield of IX was 27 %; the conversion of I was 63 %.

Reaction of I and paraformaldehyde in HOAc: A mixture of 70 g (2.34 mole) paraformaldehyde, 159 ml (2.34 mole) I, 134 ml HOAc and 12.4 ml cc. H_2SO_4 was stirred at 353 K for 6.5 hours. After the working–up and the distilling–off the light fractions (unreacted I, formals II and VIII and allyl acetate), the residue was fractionated. The main fraction (34 g), with b.p. 371–463 K/1,73 kPa was separated by column chromatography (on silicagel, benzene–EtOH = 10:1) into two fractions. The first fraction (R_F = 0.48, n_D^{20} = 1.4516, 5.4 g) was identified as a mixture (5:1) of dioxacyclanes X and XI; the second fraction (R_F = 0.53) was XII.

Reaction of XIII and paraformaldehyde in HOAc: To a mixture of 27 g (0.9 mole) paraformaldehyde, 128 ml HOAc and 16 ml cc. H_2SO_4, 160 ml (1.5 mole) XIII was added dropwise and the mixture was then stirred at 363 K for 3.5 hours. After working–up, the residue was fractionated. In the first fraction (b.p. 346–383 K/3,99 kPa, after redistillation, XVI and 1,2–diacetoxypropane were identified. The second fraction was XVII.

Examination of product distribution (Table III): A sealed ampoule, containing the calculated reagent quantities, was placed into a thermostated bath supplied with a shaker. After the given reaction time, the ampoule was cooled, the mixture was neutralized by Na_2CO_3 and the contents were monitored with GC by the internal standard method.

Discussion

It is known [1,2] that unsaturated alcohols react with formaldehyde to produce compounds with tetrahydrofuran and tetrahydropyran skeletons. Allyl alcohol (I) reacts another way, although there are two directions to produce tetrahydrofurans (Scheme 1).

A more detailed investigation of the reaction showed that the condensation of I and formalin (stabilized by 10–15% MeOH) in the presence of H_2SO_4 produces mainly (stabilized by 10–15 % MeOH) in the presence of H_2SO_4 produces mainly diallylformal II (yield about 40 %) and allylmethylformal III (about 20 %). GC/MS analysis of the reaction mixture showed the presence of

$CH_2{=}CHCH_2(OCH_2)_4OCH_2CH{=}CH_2$ and $CH_2{=}CHCH_2(OCH_2)_4OCH_3$ in traces. Moreover, the GC/MS data demonstrating the presence of V, VI and VII in small quantities in the product mixture support the reality of the reaction pathway shown in Scheme 1. When MeOH was replaced by the more nucleophilic butanol–1, identified products in the reaction mixture included allylbutylformal IV (yield about 50 %) and dibutylformal (about 15 %). Thus the hydroxyl group of I reacts mainly with formaldehyde in aqueous medium, and the structure and ratio of the linear formals formed are determined by the nucleophilicity of the alcohol present.

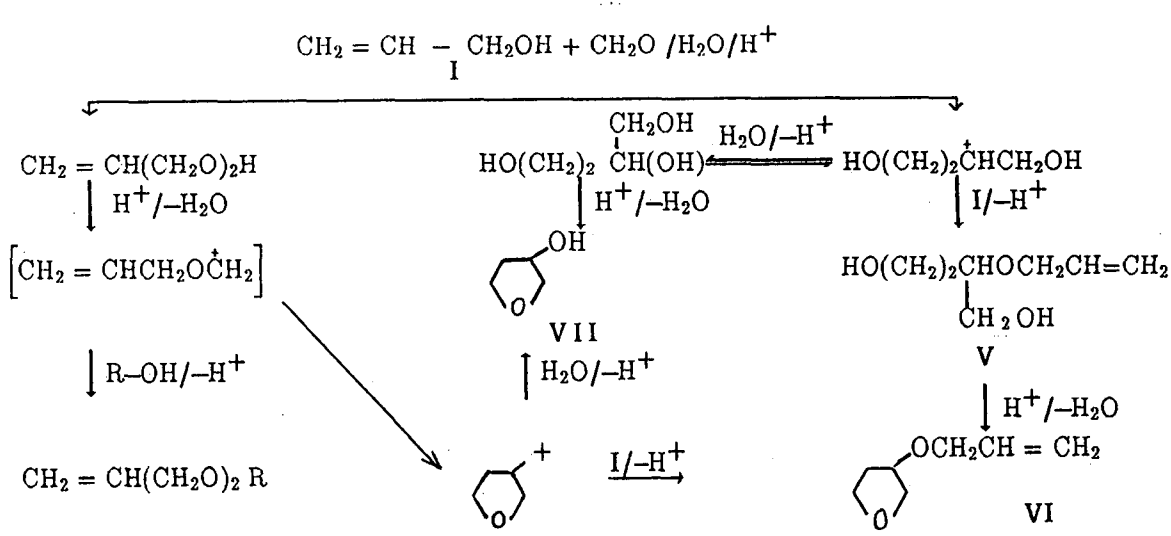

II : R = $CH_2 = CHCH_2$
III : R = CH_3
IV : R = $(CH_2)_3CH_3$

Scheme I

Table I

Physical and analytical data of the compounds

Compounds	Boiling point		Formula	Calcd. %		Found %	
	K/kPa	n_D^{20}		C	H	C	H
II	415–429/101,3	1.4266	$C_7H_{12}O_2$	65.61	9.44	66.01	9.12
III	377–382/101,3	1.4066	$C_5H_{10}O_2$	58.80	9.87	60.09	9.76
IV	323–328/1,19	1.4161	$C_8H_{16}O_2$	66.63	11.18	67.06	10.86
VIII	384–486/101,3	1.4138	$C_7H_{12}O_4$	–	–	–	–
IX	–	–	$C_{11}H_{21}ClO_4$	52.28	8.38	51.66	8.59
X + XI (5 : 1)	–	1.4516	$C_7H_{12}O_4$	52.49	7.55	53.01	7.18
XII	–	1.4642	$C_8H_{14}O_3$	60.74	8.92	61.02	8.49
XVI	328–333/0,13	1.4376	$C_8H_{12}O_4$	60.02	7.56	59.91	8.17
XVII	412–414/0,19	1.4425	$C_{13}H_{20}O_8$	51.32	6.58	51.12	7.32

Table II

Spectral data of the compounds

Compounds	^{1}H–NMR (δ,ppm)	MS (m/2)
II	3.9 m (4H, $C\underline{H}_2CH$); 4.5 m (2 H, $OC\underline{H}_2$); 4.9–5.3 m (4H, $CH=C\underline{H}_2$); 5.8 m (2H, $C\underline{H}=CH_2$)	M–H$^+$ (0.07)(100).
III	as above and 3.2s (3H, $O\underline{CH}_3$)	M$^+$(0.01), M–H$^+$(0.35), 57(100)
IV	0.9t (3H,$C\underline{H}_3$), 1.4 m (4H, $C\underline{H}_2C\underline{H}_2$; 3.4 m (2H, $C\underline{H}_2O$); 3.9 m (2H, $CHC\underline{H}_2O$); 4.5 q (2H, $OC\underline{H}_2O$); 5.1 m (2H, $C\underline{H}_2=CH$); 5.7 m (1H, $CH_2=C\underline{H}$)	–
VIII	1.5 s (3H, $C\underline{H}_3$); 3.5 m (2H, $C\underline{H}_2O$) 4.2 m (4H, $OC\underline{H}_2O$); 4.6 m (2H, $C\underline{H}_2=CH$); 5.3 m (1H, $CH_2=C\underline{H}$)	–
IX	1.3–2.0 m (7H, $C\underline{H}_3$, $C\underline{H}_2$); 3.2 s (1H, OH); 3.3–4.1 m (8H, $C\underline{H}Cl$, $C\underline{H}_2O$, $C\underline{H}OH$, $CHC\underline{H}_2O$); 4.6 m (2H, $OC\underline{H}_2O$); 5.0 m (2H, $C\underline{H}_2CH$); 5.8 m (1H, $CH_2C\underline{H}$)	–
X	1.4–2.0 m (2H,$C\underline{H}_2$); 2.0 s (3H, $C\underline{H}_3$); 3.4–3.9 m (5H,$C\underline{H}_2O$, $C\underline{H}O$); 4.7 q (2H, $OC\underline{H}_2O$)	M–H$^+$(0.4), 100(17.2), 87(55.5), 73(5.3), 72(7.0), 57(16.6), 45(24.4), 43(100), 42(13.5), 45(6.1)
XI	as above	M–H$^+$(1.4), 87(4.7), 73(23.8), 71(10.1), 70(59.7), 54(7.6), 45(16.3), 44(51.1), 43(100), 42(14.4), 41(6.6)
XII	1.4–1.9 m (2H, $C\underline{H}_2$); 3.0–4.0(7H,$C\underline{H}_2O$, $C\underline{H}O$); 4.7 q (2H, $OC\underline{H}_2O$); 5.1 m (2H, $C\underline{H}_2$, CH); 5.7 m (1H, $CH_2C\underline{H}$)	–
XVI	2.0 s (6H, $COOC\underline{H}_3$); 3.8 m (4H, $C\underline{H}_2O$); 5.2 m (2H, $C\underline{H}C\underline{H}$)	70(39.1), 43(100)
XVII	2.0 s (12H, $COOC\underline{H}_3$); 1.9–2.0 m (1H, $C\underline{H}$); 4.0 m (6H, $C\underline{H}_2O$); 5.1 m (1H, $C\underline{H}O$)	159(8.1), 117(13.7), 99(11.7), 70(11.4), 43(100)

Table III

The dependence of the product distribution on the conditions in the reaction of allylacetate (XIII) and formaldehyde[a]

	Reaction				Yield (%)		
No	Temp.(K)	Time (h)	H_2SO_4[b]	[XIII]:[CH_2O]	XIV	XV	XVI
1.	323	0.5	0.5	1:4	16.5	16.9	36.3
2.	323	0.5	10.0	1:4	1.2	–	4.9
3.	323	0.5	10.0	4:1	1.1	–	2.1
4.	323	3.5	0.5	4:1	1.6	14.2	27.9
5.	323	3.5	10.0	1:4	–	3.7	–
6.	323	3.5	10.0	4:1	0.6	3.2	6.8
7.	363	0.5	0.5	1:4	25.1	7.6	–
8.	363	0.5	10.0	1:4	0.3	2.9	8.9
9.	363	3.5	0.5	1:4	2.4	34.0	38.0
10.	363	3.5	10.0	1:4	–	4.6	2.0
11.	363	13.5	10.0	4:1	2.8	–	–
12.	343	2.0	5.3	1:1	–	5.2	8.7
13.	343	2.5	5.8	1:2	1.2	8.4	12.0
14.	343	3.0	6.3	1:3	10.2	22.8	38.1
15.	343	3.5	6.8	1:4	25.8	43.0	26.9
16.	343	3.5	7.3	1:4	14.8	37.1	20.4
17.	343	3.5	7.8	1:4	4.7	10.8	5.2
18.	343	3.5	8.3	1:4	11.0	18.8	13.2

[a] [HOAc] : [CH_2O] = 2 : 1

[b] Mass % to HOAc

The reaction of I and formaldehyde in aqueous HOAc results in the formation of VIII:

$$I + CH_2O + HOAc \xrightarrow[H_2O]{H^+} CH_2 = CHCH_2(OHCH_2)_2\,OAc$$
VIII

The condensation in $CHCl_3$ in the presence of $AlCl_3$ resulted in II, and the GC/MS spectra also revealed a by–product (about 4 %) resulting from the addition of HCl to II:

$$I + (CH_2O)_x \xrightarrow[CHCl_3]{AlCl_3} II + CH_2 = CH(CH_2O)_2CH_2CHClCH_3$$

The reaction in HCl solution resulted the formation of IX:

$$I + CH_2O \xrightarrow{H^+} II \xrightarrow{HCl} CH_3CHClCH_2(OCH_2)_2CH = CH_2$$

$$\overset{H^+}{\downarrow}\ \overset{CH_2O}{\downarrow}$$

$$CH_3CHClCH_2(OCH_2)_2\overset{+}{C}HCH_2CH_2OH$$

$$I \quad \downarrow \ -H^+$$

$$CH_3CHClCH_2(OCH_2)_2\ CHOCH_2CH = CH_2$$

$$\Big|$$

IX $(CH_2)_2OH$

The main products of the condensation in anhydrous HOAc were the linear formals II and VIII, and allyl acetate. X, XI and XII were identified in negligible quantities. These are formed according to the following scheme (R = H or Ac):

It is known [3,4] that the main products of the reaction between allyl acetate (XIII) and formaldehyde in HOAc are 4–acetoxymethyl–1,3–dioxane (X), the

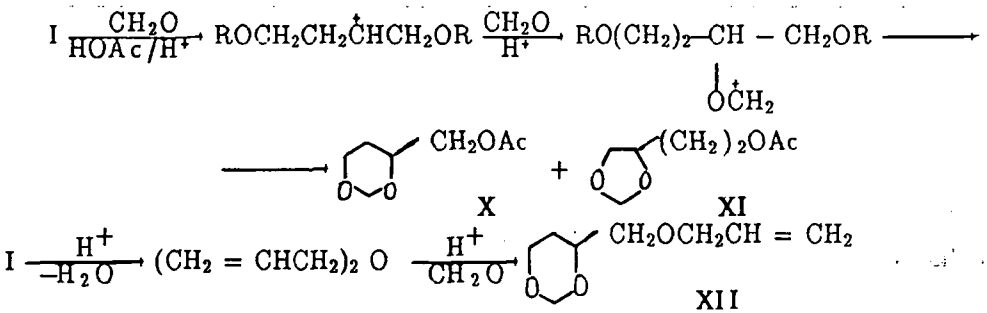

triacetate of 1,2,4–butanetriole (XIV) and 3–acetoxytetrahydrofuran (XV). In the product of our experiments we identified large quantities of *trans*–1,4–diacetoxy–butene–2 (XVI) [1], 1,2,4–triacetoxy–3–acetoxymethylbutane (XVII) and 1,2–diacet–oxybutane as an addition product of HOAc to the double bond of XIII (Scheme 2). It has been found [5] that, in the Prins reaction, the presence of an aqueous organic medium facilitates the formation of 1,3–diols and 1,3–dioxanes, where as anhydrous organic solvents, such as HOAc, facilitate the formation of unsaturated alcohols. In an attempt to increase the yield of XVI, we changed the reaction conditions (Table III), but failed to achieve a selective formation of XVI. This is clearly connected with the fact that the energy barrier of the reaction between allyl acetate and formaldehyde is higher that of a secondary Prins reaction between XVI and CH_2O. It was earlier reported [6] that the presence of more strongly electrondonating substituents facilitates the reaction between a double bound and formaldehyde.

References

[1] *Hanschke, E.:* Chem. Ber. *88*, 1053 (1955).

[2] *Gelin, R., R. Henry, S. Gelin:* C. R. Acad. Sci., Ser. C. *275*, 957 (1972).

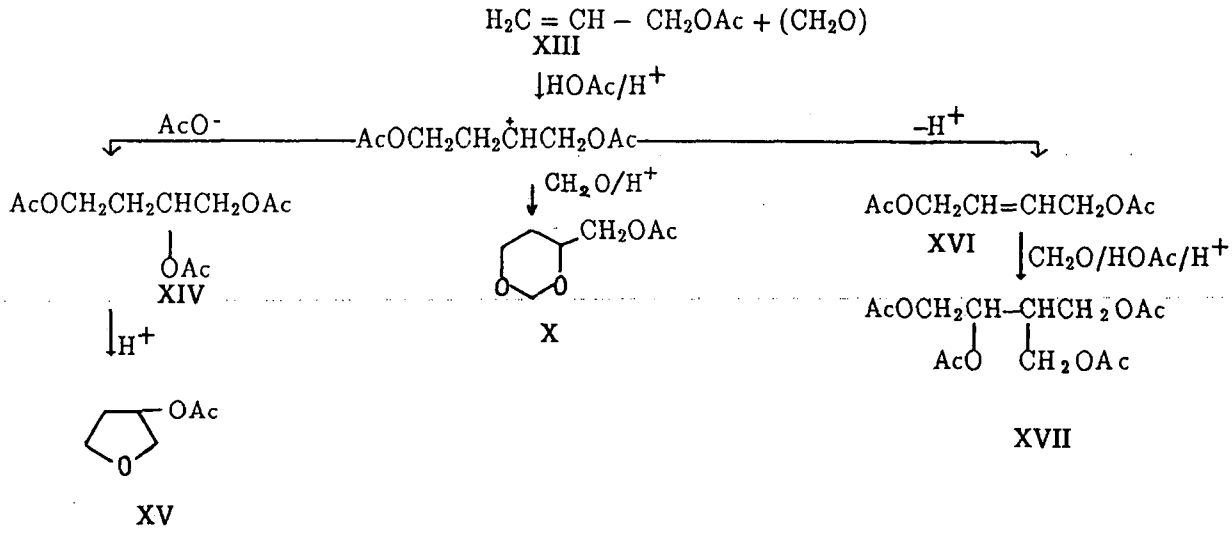
H2C = CH – CH2OAc + (CH2O)
XIII
↓HOAc/H+
AcO-
AcOCH2CH2ĊHCH2OAc
–H+
AcOCH2CH2CHCH2OAc
OAc
XIV
↓H+
OAc
O
XV
↓CH2O/H+
CH2OAc
O
O
X
AcOCH2CH=CHCH2OAc
XVI
↓CH2O/HOAc/H+
AcOCH2CH–CHCH2OAc
AcO
CH2OAc
XVII

Scheme II

[3] *Olsen, S.:* Acta Chem. Scand. *4*, 462 (1950).

[4] *Setinen, K., V. Blazek, M. Kraus, Z. Zitny:* Chem. Prum. *28*, 415 (1978); C. A. *89*, 215140 n (1978).

[5] *Stapp, P. R., J. C. Randall:* J. Org. Chem. *35*, 2948 (1970).

[6] *Tanaka, T., Y. Nishimura:* Mem. Fac. Eng., Kyushu Univ. *28*, 1 (1968); C. A. *70*, 37740 (1969).

CORRELATIONS BETWEEN THE VISIBLE SPECTRA OF $VO(AA)_2$ IN DIFFERENT SOLVENTS AND THE TAFT–KAMLET SOLVENT PARAMETERS

J. CSÁSZÁR and N.M. BIZONY

Institute of Physical Chemistry, Attila József University,

P.O.Box 105, H–6701 Szeged, Hungary

(*Received November 15, 1990*)

THE VISIBLE SPECTRA OF ACETYLACETONATE COMPLEX OF VO^{2+}, $VO(AA)_2$, WERE MEASURED IN THIRTY ORGANIC SOLVENTS. THE CORRELATIONS, BETWEEN THE SPECTRAL AND STRUCTURAL CHARACTERISTICS AND THE TAFT–KAMLET SOLVENT PARAMETERS, π^*, α AND β, ARE DISCUSSED.

Introduction

The ion VO^{2+} with the electronic structure $3d^1$ forms coordination compounds with coordination numbers 5 and 6. The complex $VO(AA)_2$ (AA: acetylacetonate) can be easily prepared [1]; the compound is monomeric in benzene solution[1] [2a] and paramagnetic ($16.044\ 10^{-24}$ A m^2 [3]), with a dipole moment $14.341\ 10^{-30}$ C m [4]. A strong σ–bond forms between the ($2p_z$ + 2s) hybrid of the oxygen and the ($3d_{z2}$ + + 4s) hybrid of the V^{4+}, while the $2p_x$ and $2p_y$ orbitals on the oxygen π–bond with the $3d_{xz}$, $3d_{yz}$ orbitals on the metal ion, so that the high stability of VO^{2+} is obvious. The ($3d_{z2}$ + 4s) hybrid and the orbitals $3d_{x^2-y^2}$ and $4p_x$, $4p_y$, $4p_z$ are capable of five σ–bonds [5] directed in a tetragonal pyramid (the overall molecular symmetry is C_{2v});

[1] KAWATE et al. [2b] have demonstrated the formation of a dimer of $VO(AA)_2$ in toluene–benzene solution at 77 K.

the V^{4+} is located at the centre of gravity of the five oxygen atoms [6].

BALLHAUSEN and GRAY [3] have pointed out that in vanadyl complexes the ground orbital, the b_2 level, is an almost pure vanadium $3d_{xy}$ orbital, and that in their spectra, as in that of $VO(AA)_2$, three crystal field bands are obtained, due to the transitions $e_\pi^* \leftarrow b_2$ (−3Ds + 5Dt): ν_1, $b_1^* \leftarrow b_2$ (10Dq): ν_2 and $a_1^* \leftarrow b_2$ (10Dq − 4Ds − 5Dt): ν_3. The sixth position, *trans* to the vanadyl oxygen, is open and may be coordinated by ligand or solvent molecules, producing a roughly octahedral structure. Thus, changes in the solvent may be expected to perturb the axially oriented MO's, which is manifested in the magnetic, optical and other behaviour [4,7].

We have examined the visible spectra of $VO(AA)_2$ in 30 pure solvents; the maximum data and the caculated parameters are listed in Table I. This permits a discussion of the correlations between the band position and the TAFT–KAMLET [8] solvent parameters π^*, α and β.

Experimental

The complexes were prepared according to a literature procedure [1]. The spectra were measured on a SPECORD M–40 instrument in spectroscopically pure solvents, in 1.0 and 0.1 cm quartz cells.

Conclusions

From the data in Table I, the following conclusions can be drawn.

1.) The frequency of ν_1 reflects the difference between the in–plane and axial ligand(solvent)–to–vanadium bonding. A strong axial perturbation reduces the V–O interaction, thereby lowering the e_π^* level with respect to b_2; ν_1 shifts to bathochromicallly approximately 4000 cm^{-1} on change of the solvent from Cl_2CCCl_2 to water. A

plot of ν_1 *vs.* π^* results in two separate linear correlations (Fig. 1A); for non–alcoholic solvents:

$$\nu_1/cm^{-1} = 18296 - 5422\ \pi^* \qquad (r = 0.982)$$

The alcohols cause a smaller change in the band position:

$$\nu_1/cm^{-1} = 14449 - 2431\ \pi^* \qquad (r = 0.807)$$

ν_1 is also linearly correlated with α (hydrogen donor ability of solvent molecules):

$$\nu_1/cm^{-1} = 15200 - 2611\ \alpha \qquad (r = 0.978)$$

These relations reveal that, the higher the polarizability and hydrogen–bond–forming ability of the solvent, the larger is the bathochromic shift of ν_1.

2.) The value of 10Dq is obtained directly from the transition $b_1^* \leftarrow b_2$. The position of this band should be dependent on both the σ–donor and π–donor strength of the in–plane ligands. The latter quantity does not vary to a large extent, so ν_2 should be directly related to the in–plane field strength. ν_2 varies in only a very narrow interval; it is not sensitive to change in the solvent. A more sensitive parameter is $\nu_{2\text{-}1}$ [9] (changes from 1000 to 5500 cm^{-1}) which shows a spread nearly four times as large that of 10Dq in the series studied. The plots of $\nu_{2\text{-}1}$ *vs.* π^* (Fig. 1B) results in linear correlations for non–alcohols:

$$\nu_{2\text{-}1}/cm^{-1} = -2650 + 7247\ \pi^* \qquad (r = 0.989)$$

and for alcohols:

$$\nu_{2\text{-}1}/cm^{-1} = 2115 + 4062\ \pi^* \qquad (r = 0.937)$$

The plot of $\nu_{2\text{-}1}$ *vs.* α:

$$\nu_{2\text{-}1}/cm^{-1} = 1211 - 3852\ \alpha \qquad (r = 0.946)$$

result in linear correlations with positive slopes, while the correlation between $\nu_{2\text{-}1}$ and β is also linear, but has a negative slope:

$$\nu_{2\text{-}1}/cm^{-1} = 5793 - 1822\ \beta \qquad (r = 0.964)$$

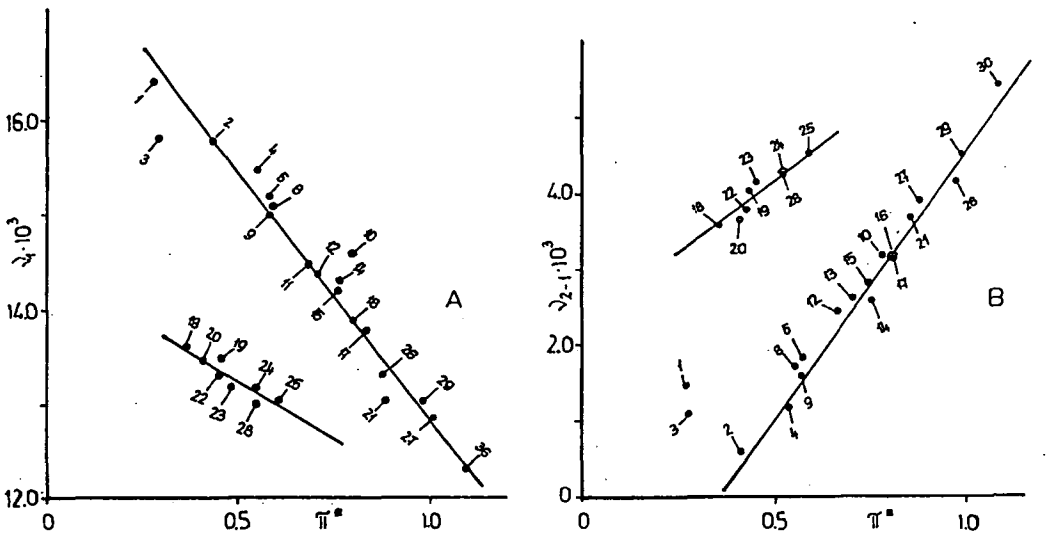

Figure 1: A) Plot of ν_1/cm^{-1} vs. π^*; B) plot of ν_{2-1}/cm^{-1} *vs.* π^*

3.) Ds [$=(\nu_1 + \nu_3 - \nu_2)/7$] and Dt [$=(\nu_1 - 3Ds)/5$] are measures of the tetragonal distortion of the molecule [3]. Both parameters are relatively large, indicating a very considerable distortion. The plots of Ds *vs.* π^* (Fig. 2) for non–alcohols:

$$-Ds/cm^{-1} = -3967 + 993\ \pi^* \qquad (r = 0.942)$$

and for alcohols:

$$-Ds/cm^{-1} = -3430 + 782\ \pi^* \qquad (r = 0.936)$$

show that an increase in the polarizability of the solvent results in a decrease in the distortion; in other words [9] the stronger the sixth ligand (solvent), the weaker is the total axial perturbation due to both the vanadyl oxygen and the sixth ligand. Similar high Ds and Dt are obtained for other vanadyl complexes; for example, for $VO(H_2O)_6^{2+}$, Ds = − 4570 and Dt = 143 cm^{-1} [3].

4.) The parameter ρ [=(1–7Dt)/4Dq], the ratio of the effective axial charge and the effective equatorial charge, can be calculated on the basis of ligand field theory in the knowledge of all three band positions [9]. The increase in ρ on going from $VO(SO_4)$ (–0.440) to $VO(AA)_2$ (+0.041) is consistent with the decrease in the V = 0 double bond distance [5]. Also, the increase observed in ρ when $VO(AA)_2$ is dissolved in a more polar solvent is what on might expect from the consideration that there is an empty axial position which can be occupied by coordinating solvent [10]. Unfortunately, the exact location of ν_3 is problematic because the band appears very close to the intraligand spin–forbidden $\pi^* \longleftarrow \pi$ band; thus the calculated ρ values are uncertain. In spite of this uncertainty, the values in Table I show a similar trend to that of π^*.

5.) The ESR g values $\{g_\perp = 2[1-(c_1^{*2}\ \lambda)/\nu_1]$; $g_\parallel = 2[1-(c_1^{*2}\ \lambda)/\nu_2]$ should be calculated from the optical absorption data (λ = 135 cm^{-1}, while c_1^* is 0.907 and 0.946 for the first and second transitions, respectively [11]). The calculated isotropic <g> values (Table I) agree well with the published data [12]. It is obvious that the average values of g are close to the free electron (g_e = 2.0023) value. The <g> values reported for the vanadyl complexes in the literature are approximately the same for measurements on crystals, powder and solution [3]. Within experimental error, the published <g> values do not vary; the small trend in our data is due to the simplified formulae used for the calculations.

6.) It has been observed [13] that, if there is a ligand–VO^{2+} interaction in the axial direction, the differences ($g_\parallel$ – <g>) and (g_e – <g>) vary approximately inversely to ν_1 and ν_2, respectively. We did not obtain a similar correlation. Our calculated differences are very small (0.0135 – 0.0121 and 0.0300 – 0.0330, respectively), indicating that the solvent–VO^{2+} interaction is weaker than the ligand–VO^{2+} interaction;

Table I
The measured spectral data and calculated parameters on $VO(AA)_2$

No	Solvent	ν_1*	ν_2*	ν_3*	ν_{2-1}*	$-Ds$*	$+Dt$*	ρ	<g>	<g>**	α^2
1	Cl_2CCCl_2	16420	17850	26250	1430	3546	1156	–0.13	1.9730		0.45
2	p–Xylene	15800	16400	26400	600	3686	948	–0.012	1.9710		0.44
3	CCl_4	15790	16860	25970	1070	3557	1024	–0.063	1.9715		0.44
4	Dioxane	15540	16650	25750	1110	3520	996	–0.047	1.9711		0.45
5	Benzene	15220	17000	25500	1780	3389	1011	–0.041	1.9713	1.970	0.45
6	c–Hexanone	15150	17500	25580	2350	3319	1039	0.039	1.9718		0.46
7	CS_2	15080	16660	?	?	?	?	?	1.9709	1.968	0.45
8	$CHCl_3$	15080	16820	25800	1740	3437	954	0.007	1.9710	1.970	0.45
9	THF	15000	16600	25800	1600	3457	926	0.024	1.9707	1.969	0.45
10	CH_3NO_2	14570	17770	25370	3200	3167	1014	0.001	1.9717		0.47
11	Reflectance	14500	16700	24500	2200	3186	988	–0.035	1.9705		0.46
12	Acetone	14450	16900	25000	2450	3221	957	+0.009	1.9707	1.968	0.46
13	Cl–Benzene	14400	17000	25800	2600	3314	892	0.082	1.9708		0.46
14	c–Hexane	14300	16900	25050	2600	3207	936	0.031	1.9706		0.46
15	CH_3CN	14200	17000	25800	2800	3286	868	0.106	1.9706	1.969	0.46
16	o–Cl_2–Benzene	13900	17100	25500	3200	3186	868	0.112	1.9705		0.47
17	CH_2Cl_2	13800	16900	25900	3100	3257	806	0.165	1.9702		0.47
18	Octylalc.	13600	17150	25600	3550	3150	830	0.153	1.9703		0.47
19	c–Hexanol	13520	17550	25660	4030	3090	850	0.152	1.9707		0.48
20	Hexylalc.	13480	17180	25500	3700	3114	828	0.157	1.9702		0.47
21	Pyridine	13340	17040	24800	3700	3014	860	0.117	1.9700	1.970	0.47
22	Amylalc.	13320	17080	25200	3760	3063	826	0.154	1.9700		0.47
23	Butylalc.	13220	17360	25400	4140	3037	822	0.171	1.9702		0.48
24	Propylalc.	13200	17450	25620	4250	3053	808	0.190	1.9703		0.48
25	Methanol	13040	17620	25200	4580	2946	840	0.166	1.9704	1.968	0.48
26	Benzylalc.	13030	17250	24950	4220	2961	829	0.159	1.9700		0.48
27	DMFA	13030	16970	25120	3940	3026	790	0.185	1.9700	1.968	0.47
28	Ethanol	13000	17280	25300	4280	3003	798	0.192	1.9700		0.48
29	DMSO	12850	17350	24990	4500	2927	814	0.179	1.9699		0.48
30	Water	12330	17820	25500	5490	2859	751	0.262	1.9699		0.50

* in cm^{-1}; ** [13] p. 111.

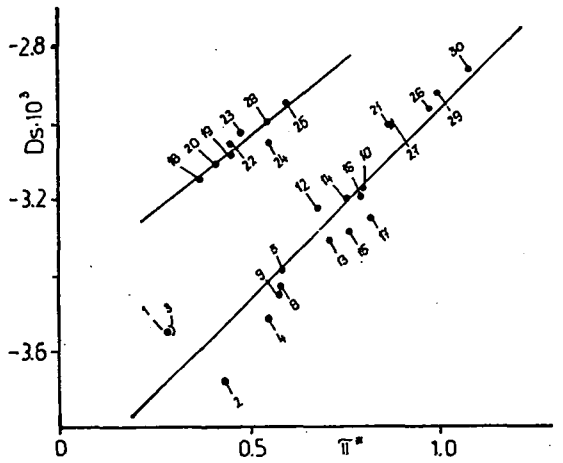

Figure 2. Dependence of Ds/cm^{-1} on π^*

consequently, the field strength does not vary considerably either in–plane axially.

7.) The method of evaluation of the mixing coefficient α^2 $\{=[\nu_2(2-\langle g\rangle)]/8\lambda\}$ [11,14] depends on the fact that the orbital magnetic moment of an unpaired electron is reduced if the magnetic electron is spread in a MO over the entire molecule. $\alpha^2 = 1$ for pure ionic binding and $\alpha^2 = 0.5$ for pure covalent binding. In our case, α^2 varies between 0.46 and 0.50, indicating an almost pure covalent character of the bonds; the somewhat lower values are due to the uncertainty in the optical data.

8.) Several authors have modified the TAFT–KAMLET parameter π^*. For non–––associating solvents, ABE [15] has introduced two polarity parameters, π_1^* , π_2^* , using the optical data on non–polar and weakly polarized molecules such as naphtalene, chlorbenzene and β–carotene. On the other hand, BEKÁREK [16] has found that the modified TAFT–KAMLET parameter, π_n^* $[= \pi^*/(n^2-1)/(2n^2+1)]$ gives a better fit to the experimental optical data than the original parameter. The correlations between these new parameters and our data are very poor; the original

π^* [8], bases on the spectral data on the strongly polar N,N–diethyl–4–nitroaniline, *etc.*, is more useful in our case.

References

[1] Inorg. Syntheses, *5*, 115 (1957).

[2] a.) *Jones, M.M.*: J.Amer.Chem.Soc., *76*, 5995 (1954);
b.) *Kawata, S., H. Yokoi, M. Iwaizumi*: Bull.Chem.Soc.Japan, *63*, 2511 (1990).

[3] *Ballhausen, C.J., H.B. Gray*: Inorg.Chem., *1*, 111 (1962).

[4] *Selbin, J., H.R. Manning, G. Cessac*: J.Inorg.Nucl.Chem., *25*, 1263 (1963); *Boucher, L.J., T.F. Yen*: Inorg.Chem., *8*, 689 (1969); *Chasteen, N.D., R.L. Belford, I.C. Paul*: Inorg.Chem., *8*, 408 (1969).

[5] *Ballhausen, C.J.*: Introduction to Ligand Field Theory., McGraw–Hill. Inc., N.Y., 1962. p. 229.

[6] *Dodge, R.P., D.H. Templeton, A. Zalkin*: J.Chem.Phys., *35*, 55 (1961); *Hon, P.K., R.L. Belford, C.E. Pfluger*: J.Chem.Phys., *43*, 3111 (1965).

[7] *Császár, J.*: Magyar Kémiai Folyóirat, *71*, 110 (1965); Naturwiss., *51*, 158 (1964).

[8] *Kamlet, M.J., R.W. Taft*: J.Amer.Chem.Soc., *98*, 377, 2886 (1976); *Kamlet, M.J., J.L. Abboud, M.H. Abraham, R.W. Taft*: J.Org.Chem., *48*, 2877 (1983).

[9] *Selbin, J., T.R. Ortolano*: J.Inorg.Nucl.Chem., *26*, 37 (1964).

[10] *Kuska, H.A., M.T. Rogers*: Inorg.Chem., *5*, 313 (1966).

[11] *Stewens, K.W.H.*: Proc.Roy.Soc.London, A, *219*, 542 (1953).

[12] *Bernal, J., P.H. Rieger*: Inorg.Chem., *2*, 256 (1963).

[13] *Boucher, L.J., E.C. Tynan, T.F. Yen* in "Electron Spin Resonance of

Metal Complexes"., Ed. T.F. Yen, Hilger Ltd., London, (1969).

[14] *Owen, J.*: Proc.Roy.Soc.London, A, *227*, 183 (1955).

[15] *Abe, T.*: Bull.Chem.Soc.Japan, *63*, 2328 (1990).

[16] *Bekárek, V.*: J.Chem.Soc.Perkin Trans., *2*, 1293 (1983).

FORMATION AND VISIBLE SPECTRA OF SOME MOLECULAR COMPLEXES OF ALIPHATIC AND AROMATIC PRIMARY AMINES WITH IODINE IN CHLORINE–CONTAINING ALIPHATIC SOLVENTS

J. CSÁSZÁR and N.M.BIZONY

Institute of Physical Chemistry, Attila József University,

P.O.Box. 105, H–6701 Szeged, Hungary

(*Received October 15, 1990*)

THE FORMATION AND THE SPECTRAL BEHAVIOUR OF CHARGE–TRANSFER COMPLEXES OF PRIMARY ALIPHATIC (HEXADECYLAMINE, DODECYLAMINE, OCTYLAMINE) AND AROMATIC AMINES (ANILINE, p–TOLUIDINE, p–Cl–ANILINE) WITH IODINE WERE STUDIED IN SIX CHLORINE–CONTAINING SOLVENTS. THE FORMATION CONSTANTS, K_f , OF THE COMPLEXES WERE DETERMINED AND CALCULATIONS WERE MADE ON THE ENERGETICAL RELATIONS OF THE COMPLEX MOLECULES.

Introduction

Several authors (*e.g.* [*1*]) have reported that an increase in the solvating power of a medium for a charge–transfer (CT) complex shifts the CT band to lower energy, but it is often found that an increase in solvent polarity results in a shift in the opposite direction [2]. A specific interaction between the CT complex and the surrounding solvent causing this blue shift should therefore also be considered to be significant in these systems [3]. We earlier [4] discussed the CT complex–forming ability of several aromatic secondary amines with iodine.

As a continuation of this work, we have now studied the formation and the spectral behaviour of molecular complexes of aliphatic [hexadecylamine (HAD), dodecylamine (DDA) and octylamine (OA)] and aromatic [aniline (An), p–toluidine

(pTol) and p–Cl–An (pClAn)] primary amines with iodine in chlorine–containing aliphatic solvents (CCl_4, $CHCl_3$, CH_2Cl_2, $(Cl–CH_2)_2$, $(Cl_2=CH)_2$ and $(Cl_2=C)_2$, and we present the results in this paper.

Experimental

The chemicals were BDH products of p.a. purity, while the solvents were spectroscopically pure; they were used without further purification. The experimental methods have been described elsewhere [4]. For determination of the stoichiometry, stock solutions ($1.2 \cdot 10^{-2}$ mol/dm^3) of the donors (D) and acceptor (A) were prepared. In every case, 1:1 complex formation was found. In determinations of the formation constants, K_f , the concentration of iodine was $1.2 \cdot 10^{-3}$ mol/dm^3, while those of the donors ranged from 5.10^{-4} to 5.10^{-2} mol/dm^3. The K_f values were calculated by the least squares method, using the BENESI–HILDEBRAND [5] equation. Because of the absorption of the solvents, we made measurements only in the spectral range above 250 nm. The optical method used yields values of K_f and ϵ_{CT} which are often concentration–dependent; $1/\epsilon_{CT}$ and $1/K_f \cdot \epsilon_{CT}$ are obtained from the plot, and therefore the evaluated K_f values are very sensitive to ϵ_{CT} . However, the extinction coefficient is also concentration–dependent, a deviation from the BEER's law can be obtained, and thus the BENESI–HILDEBRAND plot does not give strictly true values of K_f and ϵ_{CT} . The calculated values must therefore be treated carefully.

Results and Discussion

Both the n–alkyl and the aromatic amines studied form molecular complexes as n–donors through the lone pair electron(s) on the nitrogen atom, while iodine acts as σ–acceptor; their complexes can be classified as nσ complexes.

The behaviour of the nσ complexes is completely different from that of the other types; for example, their energy of formation is very high, the bonds are strongly localized, the self–absorption of the components varies considerably, *etc.*

When the solutions of the alkylamines studied as donors and iodine as acceptor are mixed, a new band develops in the visible range, between 330 and 430 nm.
Figure 1 shows the absorption spectra of OA, iodine and their mixtures in CCl_4 (A) and $CHCl_3$ (B) solutions.

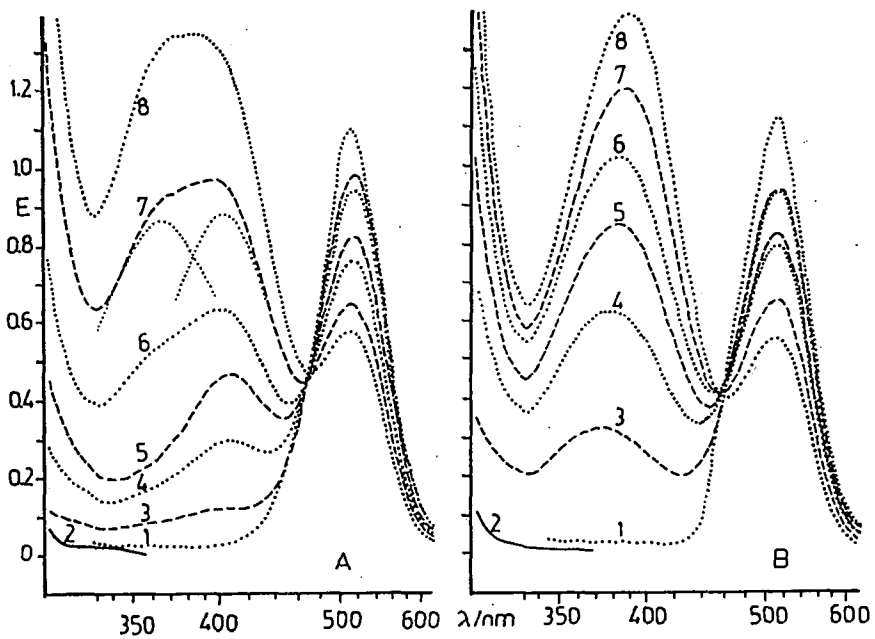

Figure 1: Absorption spectra of iodine (1), OA (2) and their mixtures in CCl_4 (A) and $CHCl_3$ (B) solution. $[I_2]=1.2\cdot10^{-3}$ mol/dm^3. [OA] = (A): (3): $1.89\cdot10^{-4}$, (4): $4.72\cdot10^{-4}$, (5): $7.55\cdot10^{-4}$, (6): $9.44\cdot10^{-4}$, (7): $1.89\cdot10^{-3}$, (8): $2.36\cdot10^{-3}$; (B): (3): $1.97\cdot10^{-4}$, (4): $4.93\cdot10^{-4}$, (5): $7.88\cdot10^{-4}$, (6): $9.85\cdot10^{-4}$, (7): $1.48\cdot10^{-3}$, (8): $1.97\cdot10^{-3}$ mol/dm^3. d=1.0 cm, T=295 K.

Besides the new band, an isosbestic point appears at about 480 nm, indicating equilibrium systems (Figure 2).

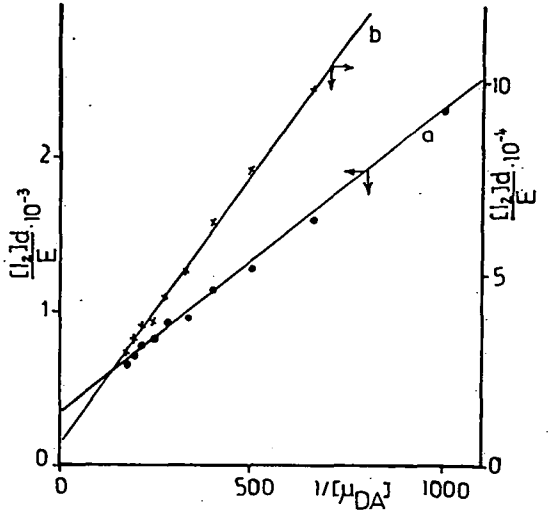

Figure 2. BENESI–HILDEBRAND plot on HDA – iodine systems,
a.) in CCl_4 (r = 0.992) b.) in $CHCl_3$ (r = 0.994)

Since the self–absorption of anilines is not negligible in the region of importance, we find only an inflection at around 340–370 nm. We therefore used the donor at the same concentration as in the mixtures as a blank; in this case the isosbestic point is also observed.

We attribute the new band to the formation of a CT complex. In quantum mechanical terms [16], the wave functions for the ground and excited states are

$$\psi_N = a\psi_o(D\ ,\ A) + b\psi_1(D^+ - A^-) \quad \text{and} \quad \psi_E = a^*\psi_1(D^+ - A^-) - b^*\psi_o(D\ ,\ A)$$

respectively, with $a \approx a^*$, $b \approx b^*$ and $a^2 >> b^2$.

Thus, when light is absorbed, an intermolecular CT occurs, and the transition take place from the structure $\psi_0(A,D)$ ("no–bond" function) to the structure $\psi_1(A^- - D^+)$ ("dative" function), *i.e.* it is an intermolecular CT transition involving a one–electron jump from D to A.

It is just possible, however, that this new band corresponds to the hypsochromically shifted visible band of iodine [6,7], and the true CT band lies in the shorter wavelength region. This blue shift of the iodine band is attributed by MULLIKEN [8] to a greater exchange repulsion between the σ_u excited MO of iodine and the adjacent donor, and an isosbestic point may be observed between the free and complexed iodine bands [9]. On the other hand, the I_3^- ion also exhibits an absorption maximum at around 365 nm [10]. Thus, in the wavelength region mentioned, absorptions of different origins are present and the exact position of the CT band is very difficult to establish. The BENESI–HILDEBRAND [5] method is still applicable here, in spite of the fact that the absorption is a superposition of the CT band and the shifted iodine band, because both arise from the complex; the appropriate plot in every case gives a straight line with reasonable agreement, indicating the formation of 1:1 complexes.

With regard to the effects of the solvents used on the spectral structure of both the iodine and the amine–iodine systems, we can divide the solvent molecules into three groups:

a.) In solutions in the inert CCl_4, the interaction is probably due to van der Waals forces only; the λ_{max} values measured in the vapour phase [11] and in CCl_4 solution differ only slightly (λ_{max}: 520 and 516 nm).

b.) In solutions in $CHCl_3$, CH_2Cl_2, $(Cl–CH_2)_2$ and $(Cl_2=CH)_2$, there are attractive forces due to polarization of the iodine molecule and other species by the electrical field of the solvent molecules [12], and λ_{max} is somewhat lower (498–510 nm).

c.) In the case of solutions in $(Cl_2{=}C)_2$, the spectrum of iodine changes completely, and there is no evaluable change in the presence of aniline donors.
It seems likely that $(Cl_2{=}C)_2$ forms a CT complex with iodine that is more stable than the aniline–iodine complexes. In accordance with literature data [20], we measured the CT band of the tetrachloroethylene–iodine system in n–hexane solution at 279 nm (4.44 eV), ϵ_{CT} = 15950, from which an ionization potential of I_D = 9.27 eV may be calculated.

The tendency is observed that, the higher the relative permittivity of the solvent molecule, the greater is the hypsochromic shift of the visible band of iodine; the data on $(Cl_2{=}CH)_2$ and $(Cl_2{=}C)_2$ deviate strongly from the linear λ_{max} *vs.* ϵ correlation (Figure 3).

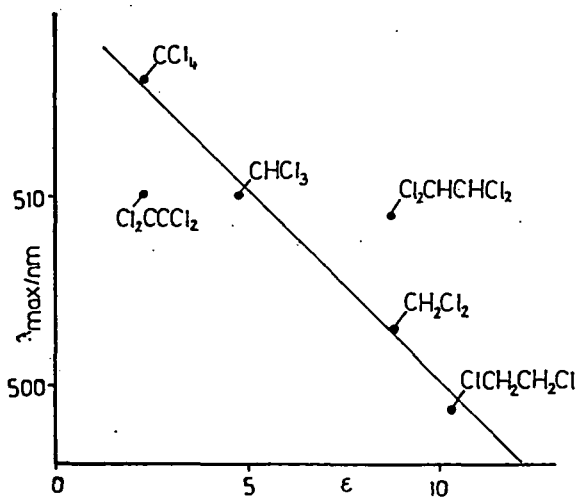

Figure 3. Plot of λ_{max}/nm of the iodine band measured in different solvent *vs.* the relative permittivities of solvent molecules.

In the case of anilines, the equilibrium measurements show that the para–X substituent plays an important role in the complex formation. If X = H, it is easy to follow the spectral change when the blank also contains the aniline in appropriate concentration; a similar set of curves may be measured as presented in Fig. 1. The CT band shifts bathochromically as compared with those for the alkylamine complexes. If an electron–withdrawing substituent is present in the para position, the spectral change is much smaller than in the An–iodine system, suggesting that the complex formation under otherwise the same experimental circumstances and at the same D/A ratios, is limited. It appears that an electron–withdrawing substituent decreases the charge density in the aromatic ring and also on the nitrogen atom to such an extent that the probability of CT is reduced. On the other hand, in the presence of an electron–donating substituent (X = OCH_3), similarly as in the An.I_2 system, a well–defined spectral change is measurable; the determined formation constants are higher than those of An.I_2 (Table I).

The intensity of the CT bands, ϵ_{CT}, does not vary in a systematic way with K_f, which has usually been ascribed to contact CT during molecular collisions, where the internuclear distance is too great for complex formation to contribute to the intensity of the CT band.

The ν_{CT} values do not show a correlation either with the TAFT–KAMLET [13] parameters or with the McRAE [14] and other [15] equations; only the plot of ν_{CT} *vs.* the acceptor number, AN, of the solvents results in a linear correlation. For the HDA.I_2 and An.I_2 systems, the empirical equations are $\nu_{CT} = 128.AN + 23820$ ($r = 0.989$) and $\nu_{CT} = 61.AN + 27250$ ($r = 0.916$), respectively; *i.e.* with higher AN, the CT bands shift hypsochromically.

There is no strict correlation between the formation constants and the solvent

Table I

Measured and calculated characteristics on the iodine complexes studied

Donor		S_1	S_2	S_3	S_4	S_5	S_6
HDA	λ_{CT}/nm	≈401	374	378	380	361	362
	μ_{EN}^{*}	3.01	4.94	3.11	4.04	5.71	
	I_D^{**}	7.69	7.97	7.93	7.91	8.13	8.11
	K_f^{***}	310	200	620	525	75	
	ϵ_{CT}^{****}	1890	5070	2020	3400	6800	
DDA	λ_{CT}/nm	365,401	385	378	380	361	365
	μ_{EN}	5.25	2.90	4.60	4.79	6.32	
	I_D	8.08,7.69	7.86	7.93	7.91	8.19	8.08
	K_f	130	645	450	530	62	
	ϵ_{CT}	5760	1760	4420	4800	8330	
OA	λ_{CT}/nm	360,410	390	377	373	360	365
	μ_{EN}	4.71	3.09	4.29	5.85	599	
	I_D	8.13,7.60	7.80	7.94	8.06	8.13	8.08
	K_f	100	650	880	470	95	
	ϵ_{CT}	4630	2000	3850	7140	7500	
pTol	λ_{CT}/nm	357	356	358	360	355	354
	μ_{EN}	1.33	1.58	1.52	2.02	1.76	
	I_D	8.16	8.18	8.17	8.13	8.19	
	K_f	225	240	245	210	185	
	ϵ_{CT}	370	520	480	850	650	
An	λ_{CT}/nm	360	348	350	352	350	≈340
	μ_{EN}	1.64	2.03	1.97	2.14	1.37	
	I_D	8.13	8.27	8.25	8.23	8.25	
	K_f	200	140	200	180	130	
	ϵ_{CT}	560	860	810	950	390	
pClAn	λ_{CT}/nm	380	350	362	362	358	≈350
	μ_{EN}	1.83	1.68	2.18	2.01	1.26	
	I_D	7.91	8.25	8.16	8.11	8.16	≈8.25
	K_f	40	60	1010	744	310	
	ϵ_{CT}	700	590	990	840	330	

S_1:CCl_4, S_2:$CHCl_3$, S_3:CH_2Cl_2, S_4:$ClCH_2CH_2Cl$, S_5:$Cl_2CHCHCl_2$, S_6:Cl_2CCCl_2;
*[22] p.63, **[22] p. 76, *** dm^3mol^{-1},**** from BENESI–HILDEBRAND plot, $dm^3mol^{-1}cm^{-1}$

parameters, but certain tendencies are recognizable. With an increase in the solvent polarity (π^*) or acceptor number, the K_f value also increases. In the case of chloroform, the values differ, which may be due to both the hydrogen–bond and the iodine–complex–forming abilities of the solvent. It seems that K_f increases with the lengthening of the alkyl chain. The formation constants of the complexes of the anilines are generally lower than those of the n–alkylamine complexes.

It is known that the lower the ionization potential of the donor, I_D, the smaller the transition energies of the CT bands [16,17]. It has been proposed [18] that ν_{CT} is related to I_D and the electron affinity of the acceptor, E_A (for iodine, 1.8 eV [16]):

$$h\,\nu_{CT} = I_D - E_A - \Delta \qquad (a)$$

where Δ is the stabilization energy of the ion pair. Several other correlations can also be found in the literature, for example

$$h\,\nu_{CT} = I_D - D + 2\,\beta^2/(I_D - D) \qquad (b)$$

where β is the exchange integral between electron–donating and electron–acceptor orbitals [19]. The experimental and calculated values agree well if it is assumed that A and D are 1.3 and 6.0 eV, respectively. The binding energy is given by the formula $\beta^2/(I_D - D)$ [19–21]. BRIEGLEB [22] has applied the equation

$$h\,\nu_{CT} = I_D - C_1 + C_2/(I_D - C_1) \qquad (c)$$

where for iodine complexes $C_1(E_A - E_C + W_o) = 5.2$ and $C_2(\beta_o^2 + \beta_1^2) = 1.5$ eV; (b) and (c) are analogous. Several empirical equations can also be found, for example

$$I_D = 2.90 + 1.89 \cdot 10^{-3} \cdot \nu_{CT} \qquad (d)$$

reported by ALOISI and PIGNATARO [23].

The I_D values (Table I) calculated *via* (c) and (d) agree well; I_D(An) is between the values published: I_D(An) = 7.70 [24], 7.85 [25], 7.95 [26], and 8.23 [27] eV. The anilines possess higher I_D values than the n–alkylamines (7.60–8.00 and 8.10–8.40 eV,

respectively). The difference is probable due to the fact that the anilines cannot be classified as either n– or π–donors, as a consequence of the resonance between the amino group and the benzene ring; $n\pi$ mixed orbitals form. It has been concluded [28] that the CT in the complex between N,N–Me_2An and iodine occurs mainly from the lone pair electrons of the nitrogen atom. On the other hand, in An, the ionizing electron may possibly be due to one of the non–bonding electrons [27]. In the primary alkylamines studied, there is no such resonance possibility; a "pure" n–orbital is the donor orbital. The data presented in Table I demonstrate that the I_D values do not change considerably with the solvent. As regards our data and those previously published [29], it seems that, with lengthening of the alkyl chains, I_D decreases; for example, for CH_3NH_2, $CH_3CH_2NH_2$ and n–$CH_3CH_2CH_2CH_2NH_2$, I_D is 8.97, 8.86 and 8.71 eV, respectively [29]. A plot of ΔH against the ionization potential of structurally related donors shows a regular relationship; with increasing I_D, ΔH decreases somewhat.

Using the spectral data discussed above, it is possible to calculate the energy levels of the complexes as described in [22]. The calculated energies (W_N: energy of the ground state, W_O: van der Waals energy in the ground state, R_N: resonance energy in the ground state, E_C: Coulombic energy acting between the ions, W_E: energy of the excited state, R_E: resonance energy in the excited state} are listed in Table II, while the energy level diagrams for HDA.I_2 and An.I_2 are presented in Figure 4. The calculations give only very approximate results, but these are suitable for a qualitative comparison of the changes and of the behaviour. Let us suppose that the maximum value of the dipole moment of the molecular complex, μ_l , after the electron transition D $\longrightarrow$ A, if the distance is $d_{DA} = 3.2 \cdot 10^{-10}$ m [22], is $51.03 \cdot 10^{-30}$ C·m. In the knowledge of μ_l and the transition moment, μ_{EN} [22], and if the overlap integral is small (S

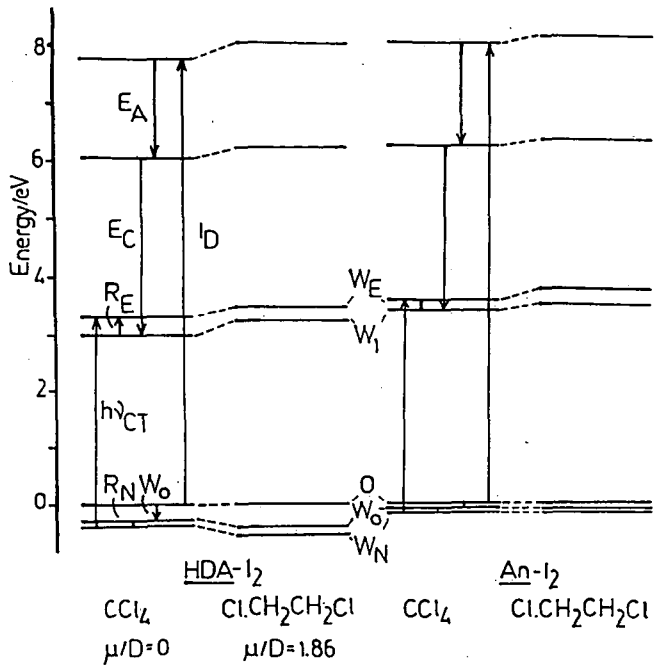

Figure 4: Energy level diagrams of HDA.I_2 (A) and An.I_2 (B) complexes, calculated with spectral data obtained in CCl_4 and $(Cl–CH_2)_2$ solutions; the energy values are summarized in Table II.

= 0.1), it is possible to look for the optimum values of the coefficients a,a*, b,b* and so calculate the parameters listed in Table II.

Thus, it seems that, for the complexes studied, the solvent effect is not particularly considerable. $W_o - W_N$ and $W_1 - W_E$ are the resonance energies, and it generally holds that $W_1 - W_E > W_o - W_N$. For our complexes, these energies lie in the ranges 24–40 and 10–14 kJ/mol, respectively; the energy values for the aniline complexes are somewhat higher. Since $W_N = \Delta H$ [22], *i.e.* the heats of formation for HDA.I_2 and An.I_2 (solvents: CCl_4, μ=0 C·m, and $(Cl–CH_2)_2$, μ=6.20·10^{-30} C·m) are

31.0, 54.6 and 10.9, 16.4 kJ/mol, respectively, the solvent dependence in the cases of the alkylamine complexes are more definite.

BHATTACHARYA and BASU [30] have estimated the stabilization energy of the ion pair $D^+ - A^-$ for a series of iodine complexes of polynuclear aromatic hydrocarbons from ν_{CT}, by using equation (a) and $E_A = 1.80$ eV for iodine. The fact that their Δ value (3.256 eV) is higher than the electrostatic energy between two charges separated by 3–4·10^{-10} m is offered as evidence that polarization and/or covalent forces make some contribution to the binding energy between D and A in the activated state, but the effect of the solvent cannot be excluded. Our Δ values lie in the interval 2.8–3.0 eV; (the effect of the solvent is not determined and the change is not unambiguous.

The calculated binding energies E_B (Table II) are 0.2–0.4 and 0.08–0.10 eV for e two complexes, respectively [$E_B = (\beta_o^2 + \beta_1^2)/(I_D - D)$, $D = 6.0$ eV [19]]. The published E_B values [*e.g.* 19, 20], and presumably also our own data, are generally higher than the actual energy, because the two molecules forming the complex have been pulled together against no–bond state repulsive forces. The calculated E_B for published E_B values [*e.g.* 19, 20], and presumably also our own data, are generally higher than the actual energy, because the two molecules forming the complex have been pulled together against no–bond state repulsive forces. The calculated E_B for benzene.I_2 and dioxane.I_2, for example, are 0.5 and 0.36 eV [19], while the experimental ones are 0.06 [21] and 0.15 eV [20], respectively. Our values agree well with the van der Waals energy W_o in the ground state (Table II). The data show that the resonance energy in the ground state is *arc.* 20–30 and 10–20 per cent, respectively, of the heat of formation ΔH, which is in accordance with other observations [see *e.g.* 22].

The quotient $100\ b^2/(a^2 + b^2)$ is a measure of the participation of the ionic

structure in the ground state. For the discussed two complexes, 2.3, 4.9 and 0.4, 0.8 can be calculated. The low values for the complex An.I_2 are noteworthy similar low values have also been published for the complexes of styrene, diphenylbutadiene, *etc.* with s–trinitrobenzene, for example [22]. With increase in the dipole moment of the solvent, the probability of the presence of the ionic structure also increases. It is interesting that the presence of the ionic structure in the excited state of the two complexes discussed, relative to their ground states, decreases and increases, respectively (see Table II).

Table II

Calculated energetical parameters (eV) on the HDA·I_2 and An·I_2 complexes

	HDA·I_2		An·I_2	
	CCl_4	$ClCH_2CH_2Cl$	CCl_4	$ClCH_2CH_2Cl$
CT_{max}	3.09	3.26	3.44	3.52
I_D	7.69	7.91	8.13	8.25
μ_{EN}	3.01	4.04	1.64	2.14
a	0.970	0.970	0.980	0.980
a*	0.985	0.985	0.990	0.990
b	0.150	0.220	0.060	0.090
b*	0.120	0.180	0.100	0.110
R_N	–0.071	–0.155	–0.013	–0.030
R_E	0.178	0.250	0.088	0.108
E_C	–2.80	–2.85	–2.89	–2.93
W_1	3.09	3.26	3.44	3.52
W_E	3.27	3.51	3.53	3.63
W_o	–0.250	–0.410	–0.100	–0.140
W_N	–0.321	–0.565	–0.113	–0.170
E_B	–0.20	–0.40	–0.08	–0.11
ΔH/kJ/mol	31.0	54.6	10.9	16.4
$100b^2/(a^2+b^2)$	2.3	5.1	0.4	0.8
$100^{*2}/(a^{*2}+b^{*2})$	1.5	3.3	1.0	1.2

In connection with the shape of the CT bands, it is interesting to observe the effects of solvents on it. While the measured CT bands always show asymmetry on the shorter wavelength side in $CHCl_3$, CH_2Cl_2, *etc.* solutions, in CCl_4 solution the bands are extremely broad and their complexity is obvious. Gaussian analysis results in two sub–bands at 365 and 401 nm; the distance between the two maxima is 2500 cm^{-1}. The relative intensities of the bands depend on the ratio D/A; the intensity of the 365 nm band, ϵ_{365}, increases more rapidly than that of the ϵ_{401} band, and the plot of the ratio $\epsilon_{401}/\epsilon_{365}$ *vs.* log[alkylamine] gives a linear correlation (Figure 5).

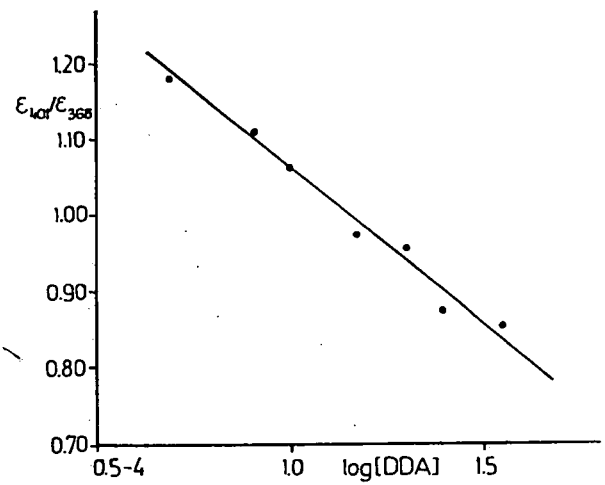

Figure 5: Plot of intensity ratios $\epsilon_{401}/\epsilon_{365}$ *vs.* log[DDA]. Solvent: CCl_4

There may be many reasons for this band splitting. We consider it likely that, as a consequence of splitting of the ground state of the donor cation, the donor component has two ionization energies with close lying values; this supposition, however, requires further theoretical consideration. The complexity of the band is still more obvious

with shortening of the alkyl chain. A similar complexity of the CT bands has been described for several CT complexes [21–33].

References

[1] *Bayliss, N.S., E.G. McRae*: J. Phys. Chem., *58*, 1002 (1954).

[2] *Offen, H.W., M.S.F.A. Abidi*: J. Chem. Phys., *44*, 4642 (1966).

[3] *Davis, K.M.C., M.C.R. Symons*: J. Chem. Soc., 2079 (1965).

[4] *Császár J., N.M. Bizony*: Acta Chim. Hung., Budapest, in press.

[5] *Benesi, H.A., J.H. Hildebrand*: J. Amer. Chem. Soc., *71*, 2703 (1949).

[6] *Tsubomura, H., R.P. Lang*: J. Amer. Chem. Soc., *83*, 2085 (1961).

[7] *Ebara, N.*: Bull. Chem. Soc. Japan, 33, 540 (1960); *El–Aasser, M., F.A. Halim, M.A. Mayoumi*: J. Amer. Chem. Soc., *93*, 590 (1971).

[8] *Mulliken, R.S.*: Rec. trav., *75*, 845 (1966).

[9] *Ham, J.*: J. Amer. Chem. Soc., *76*, 3875 (1954); *Brandon, M., M. Tamres, S. Searle, Jr.*: J. Amer. Chem. Soc., *82*, 2129 (1960).

[10] *Autrey, A.D., R.E. Connick*: J. Amer. Chem. Soc., *73*, 1842 (1951); *Buckles, R.E., J.P. Yuk, A.I. Popov*: J. Amer. Chem. Soc., *74*, 4379 (1952).

[11] *Rabinowitch, E., W.C. Word*: Trans. Farad. Soc., *32*, 540 (1936).

[12] *Walker, O.J.*: Trans. Farad. Soc., *31*, 1432 (1935).

[13] *Kamlet, M.J., R.W. Taft*: J. Amer. Chem. Soc., *98*, 377, 2886 (1976), Acta Chem. Scand., Ser. B., *39*, 611 (1985); *Kamlet, M.J., J.L. Abbound, M.H. Abraham, R.W. Taft*: J. Org. Chem., *48*, 2877 (1983).

[14] *McRae, E.G.*: J. Phys. Chem., *61*, 562 (1957).

[15] *Aihara, J., M. Tsuda, H. Inokuchi*: Bull. Chem. Soc. Japan, *42*, 1824 (1969); *e.g. M. Chastrette, M. Rajzmann, M. Chanon, K.F. Purcell*: J. Amer. Chem. Soc., *107*, 1 (1985).

[16] *Mulliken, R.S.*: J. Amer. Chem. Soc., *74*, 811 (1952), *72*, 600 (1950), J. Phys. Chem., 56, 801 (1952); Rec. trav., *75*, 845 (1956).

[17] *e.g. Leffler, J.E.*: J. Org. Chem., *20*, 1202 (1955); *R.M. Keefer, L.J. Andrews*: J. Amer. Chem. Soc., *77* 2164 (1955).

[18] *McConnel, H., J.S. Ham, J.R. Platt*: J. Chem. Phys., *21*, 66 (1953).

[19] *Hastings, S.A., J.L. Franklin, J.C. Schiller, F.A. Matsen*: J. Amer. Chem. Soc., *75*, 2900 (1953).

[20] *Ketelaar, J.A.A., C. van der Stolpe, A. Goudsmit, W. Dzeubas*: Rec. trav., *70*, 499 (1951), *71*, 1104 (1952).

[21] *Cromwell, T.M., R.L. Scott*: J. Amer. Chem. Soc., *72*, 3825 (1950).

[22] *Briegleb, G.*: Elektronen–Donator–Acceptor–Komplexe., Springer Vlg., Berlin, 1961.

[23] *Aloisi, G.G., S. Pignataro*: J. Chem. Soc. Farad. Trans., *69*, 534 (1973).

[24] *Watanabe, K.*: J. Chem. Phys., *26*, 542 (1957).

[25] *Bier, A.*: Rec. trav., *75*, 866 (1956).

[26] *Foster, K., D.L. Hammick*: J. Chem. Soc., 2685 (1954).

[27] *Baba, H., I. Omura, K. Higasi*: Bull. Chem. Soc. Japan, *29*, 521 (1956).

[28] *Tsubomura, H.*: J. Amer. Chem. Soc., *82*, 40 (1960).

[29] *Yada, H., J. Tanaka, S. Nagakura*: Bull. Chem. Soc. Japan, *33*, 1660 (1960).

[30] *Bhattacharya, R.*, S. *Basu*: Trans. Farad. Soc., *54*, 1286 (1958).

[31] *De Maine, P.A.D.*: J. Chem. Phys., *26*, 1189 (1957).

[32] *Kuboyama, A.*: J. Chem. Soc. Japan, *81*, 558 (1960).

[33] *Mersifield, R.E., W.D. Phillips*: J. Amer. Chem. Soc., *80*, 2778 (1958).

THE SPECTRA OF ESTERS OF OXOHYDROXOBIS–(8–HYDROXY–QUINOLINE)VANADIUM(V)

(Short communication)

J. CSÁSZÁR and L. KISS

Institute of Physical Chemistry, Attila József University,
P.O.Box 105, H–6701 Szeged, Hungary

(*Received November 16, 1990*)

The vanadate ion reacts with 8–hydroxyquinoline in aqueous solution at pH ≈ 6 to give a stable complex compound, I–H [1] (Structure 1). BIELIG and BAYER [2] confirmed the presence of the OH group *via* the IR spectrum; this result, together with the analytical data, leads to the formula $(C_9H_6ON)_2VO.OH$. This complex dissolves in alcohols to give hydrated esters, I'–R (Structure 2) in the first step; in an excess of boiling aliphatic alcohols I'–R next gives intense red solutions [3], from which red crystals of the anhydrous esters, I–R (Structure 3), separate out on cooling.

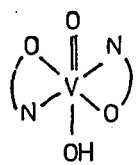

I - H

Structure 1

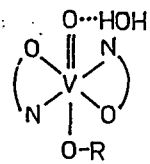

I' - R

Structure 2

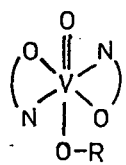

I - R

Structure 3

I–H deposits slowly from concentrated solution of I–R; the solubility of I–R and its tendency to undergo decomposition increase with increasing C atom number in R.

We have prepared the compounds I–H, I'–R and I–R (R = methyl, ethyl, propyl, butyl, amyl, hexyl and octyl) and measured their visible and UV spectra in the corresponding parent n–alcohols and pyridine (py). The spectra were obtained on BECKMAN DU, SPECORD UV–VIS instruments, using spectroscopically pure solvents.

The central V^{5+} ion is a $3d^0$ species, and the complex I–H is diamagnetic [2b]; no d–d bands are expected, and none are observed. The complexes I–H and I–R all give five bands of high intensities (Table I). The bands in the range 240–370 nm are modified bands of 8–hydroxyquinoline due to $\pi^* \leftarrow \pi$ transitions, while the visible band ($\approx$ 490 nm) may be assigned to ligand–to–metal charge–transfer transitions from the phenolate oxygens to the empty d–orbitals of the vanadium (Fig. 1) [4]. Such

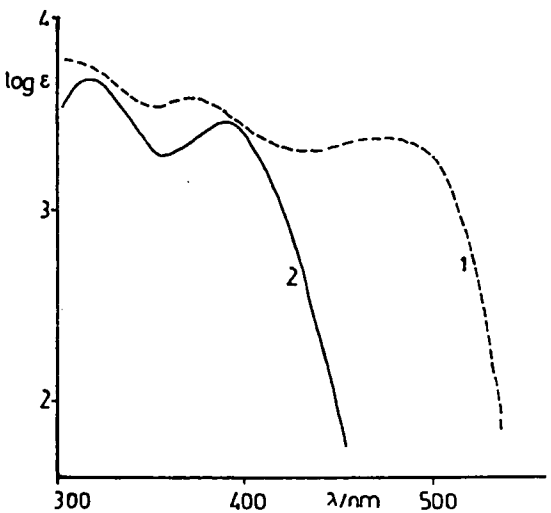

Figure 1:
Absorption spectra of I–C_2H_5 in ethanol(1) and pyridine(2)
c = 3.10^{-4} mol/dm^3,
d = 0.1 cm.

transitions are generally characteristic of phenolate coordination to easily reducible metal ions [5].

It has been reported [6] that the reactions between I–H and aliphatic alcohols result in hydrated esters, I'–R, containing a molecule of water attached by hydrogen–bonding. In excess of boiling alcohol, which may well act as a mild dehydrating agent, the compounds I'–R are transformed to anhydrous esters I–R as final products. In the IR spectra of I–R, no hydroxyl frequencies are observed [6]. For a discussion of the mechanism of ester formation, see *e.g.* [6]. The absorption spectra of the hydrated and the anhydrous compounds are practically the same. Table I shows that the spectra of the red products dissolved in the parent alcohols vary slightly as group R changes from CH_3 to C_8H_{17}; the visible band shifts somewhat hypsochromically and the intensities increase in the sequence $CH_3 \longrightarrow C_8H_{17}$.

Table I

Spectral data on the compounds I–R measured in the parent alcohols ROH and pyridine

R =	λ/nm and (log ε)	
	in alcohols	in pyridine
CH_3	490(2.95)367(3.58)315(3.71)256(4.44)240(4.72)	388(3.50)310(3.73)
C_2H_5	485(3.35)366(3.56)310(3.73)256(4.36)242(4.72)	390(3.49)310(3.72)
C_3H_7	485(3.49)376(3.65)312(3.76)260(4.30)243(4.76)	387(3.49)310(3.71)
C_4H_9	480(3.44)370(3.63)310(3.75)260(4.34)242(4.68)	392(3.51)315(3.74)
C_5H_{11}	480(3.52)372(3.69)310(3.78)260(4.35)242(4.71)	396(3.48)315(3.72)
C_6H_{13}	480(3.58)372(3.65)312(3.80)260(4.32)242(4.68)	392(3.45)313(3.72)
C_8H_{17}	478(3.60)374(3.70)312(3.78)262(4.30)242(4.70)	392(3.48)312(3.72)

When I–CH_3 is dissolved in propanol, for example, and I–C_3H_7 in methanol, we obtain the same spectra as when I–C_3H_7 is dissolved in propanol or I–CH_3 in methanol; consequently, in the presence of a large excess of the other alcohol, a transesterification takes place. When the complexes I–CH_3 – I–C_8H_{17} are dissolved

in mixtures of two different alcohols, an equilibrium system forms; the calculated equilibrium constants are between 2.10^{-2} and 9.10^{-2}, and ΔH varies between 8.5 and 17.5 kJ mol^{-1} [7].

Dissolution of the hydrated esters, I'–R, in py results in yellow solutions. The final spectra are the same for all the complexes, with two characteristic bands at 390 nm ($\log \epsilon = 3.50$) and 310 nm ($\log \epsilon = 3.72$). The red → yellow transformation of the solutions may be followed well spectrophotometrically. From py solutions, yellow crystals can be isolated, the analytical data on which suggest the presence of two py molecules; on heating, two py molecules are released. The IR spectra of the yellow final products contain νV=0 and νOH frequencies at 948 and 3440 cm^{-1}, respectively. The compounds I–H and I'–R yield the same final products.

The spectrophotometric measurements indicate that in py solution, where the py is both a solvent and a reactant, a pseudo–first–order reaction takes place. The rate constants and the calculated thermodynamic parameters are presented in Table II.

Table II

The pseudo–first–order rate constants and the calculated thermodynamic parameters on the reaction of I'–R and pyridine

R =	$k'/10^4\ s^{-1}$			E_a	ΔH^*	$-\Delta S^*$
	298 K	308 K	318 K	$kJ \cdot mol^{-1}$	$kJ \cdot mol^{-1}$	$J \cdot K^{-1} mol^{-1}$
CH_3	5.22	11.31	21.48	55.79	53.23	129.00
C_2H_5	3.91	8.19	17.16	58.30	55.74	123.16
C_3H_7	1.90	4.84	11.24	70.03	67.47	89.68
C_4H_9	1.98	4.89	10.34	65.17	62.61	105.55
C_5H_{11}	1.75	4.61	9.74	67.72	65.16	97.94
C_6H_{13}	1.72	4.53	9.39	66.98	64.42	100.54
C_8H_{17}	1.67	4.53	9.15	67.11	64.55	100.27

The data show that the rate constants decrease in the sequence $C_1 \rightarrow C_5$; for higher alcohols, no further significant change in the reaction rate is observed. The ARRHENIUS activation energy, E_a, and the enthalpy of activation, ΔH^*, increase from I–CH_3 to $_i$–C_5H_{11}. The parameters for I–C_3H_7 differ strongly from the expected ones. The high negative values of the activation entropy, ΔS^*, are noteworthy. The activation parameters vary with the number of carbon atoms, n, according to a zig–zag shape, similarly to the changes in other parameters in the homologous series. On the other hand, a plot of ΔH^* *vs.* ΔS^* results in a linear correlation ($r = 0.997$).

The mechanism of the reaction is problematic. We consider the following mechanism to be possible. On dissolution in py, the HOH molecule and the R group split off to result in I–H. Then, one of the V–O bonds opens and one py molecule, which has a high coordinating ability, is coordinated directly to the central V^{5+} *via* its lone pair electrons. This step is very fast and results in a positive charge on the central ion. The intermediate reacts with a further py molecule more slowly, because the charge on the central ion makes further V–O bond–breaking more difficult. This second step takes place with measurable rate, according to the equation

$$\text{rate} = k[I'\text{–}R][py].$$

Since [py] in py solution is about 12.573 mol dm^{-3}, which is much higher than [I'–R], the reaction takes place as a pseudo–first–order reaction, and we may use the equation

$$\text{rate} = k'[I'\text{–}R].$$

Table II presents the $k' = k/12.573$ values. If we consider that the charged activated complex is formed from two molecules (I'–R and one py molecule), that the final product has a still higher charge, and that the py molecules have a high polarization effect, the highly negative activation entropy values are obvious [8].

References

[1] *Montequi, R., M. Gallego*: Ann. Soc.esp.Fis.Quim., *32*, 134 (1934).

[2] (a) *Bielig, H.J., E. Bayer*: Liebigs Ann., *584*, 96 (1953).

(b) *Bayer, E., H.J. Bielig*: Liebigs Ann., *584*, 116 (1953).

[3] *Bach, J.M., R.A. Trelles*: An.Assoc.quim.argen., *28*, 111 (1940).

[4] *Bonadies, J.A., C.J. Carrano*: J.Amer.Chem.Soc., *108*, 4088 (1986).

[5] *Patch, M.G., C.J. Carrano*: Inorg.Chim.Acta, *56*, 171 (1981).

[6] *Blair, A.J., D.A. Pantony, G.J. Minkoff*: J.Inorg.Nucl.Chem., *5*, 316 (1958).

[7] *Császár, J., J. Balog*: Acta Phys. et Chem. Szeged, *6*, 33 (1959).

[8] *Pearson, R.G.*: J.Chem.Phys., *20*, 1478 (1952).

THEORETICAL STUDY OF THE ADSORPTION OF CO MOLECULES ON STEPPED SINGLE CRYSTAL PT SURFACES

(Preliminary communication)

J. GARDI and M.I. BÁN*

Institute of Physical Chemistry, Attila József University

P.O.Box 105, H–6701 Szeged, Hungary

(*Received November 20, 1990*)

BY EMPLOYING THE SEMIEMPIRICAL QUANTUM CHEMICAL ASED–MO METHOD, ADSORPTION OF CARBON MONOXIDE MOLECULES ON STEPPED PT SURFACES BASED ON (111) TERRACES OF FCC (775), (755) AND (533) STRUCTURES HAS BEEN INVESTIGATED AND, ON BASIS OF THE CALCULATED ELECTRONIC DATA, FAVOURABLE SITES OF ADSORPTION HAVE BEEN PREDICTED.

To understand the elementary steps of heterogeneous catalysis it is important to investigate the chemisorption of small molecules on single crystal surfaces of metals. Theoretical studies promote such investigations and support the explanations of experimental observations. The adsorption of carbon monoxide on a Pt surface is one of the best model both for experimental [1–5] and theoretical [6–10] examinations. Most of the studies are concerned with smooth surfaces, and only a limited number of theoretical works has been dealing with surfaces having terraces, steps, kinks, *etc.* on them. By the present paper, our aim is to calculate the electronic properties of carbon monoxide molecules chemisorbed on stepped Pt(111) surfaces so being able to predict the most favourable adsorption sites and orientations for CO molecules. Another aim

* Author to whom all correspondence should be addressed.

of our work is to determine the minimum size of the substrate–adsorbate system and especially that of the metal cluster which should be used for such model calculations.

Three relatively simple types of stepped surfaces, based on (111) terraces, have been chosen. One of them has step faces of (111) orientation, as with fcc(775), and the other two have step faces of (100) orientation, as with fcc(755) and fcc(533). The bulk cubic Pt lattice parameter of 392.39 pm (nearest–neighbour distance of 277.46 pm) has been used [11] in all the electronic structure calculations by employing the atom superposition and electron delocalization (ASED–MO) method [12] with its modified parameter sets [13]. One–fold top–site positions have been assumed for the CO molecules, preferentially chemisorbed with a constant Pt–C bond length of 198 pm from the surface (carbon end down), with a frozen C–O distance of 115 pm, being based on a structure determination by LEED of CO on Pt(111) [14]. The geometries of the system composed of the substrate and the adsorption overlayer were determined by the computer program PSD [15]. Predictions based on electronic properties could be compared and checked with experimental data available so far only for the orientation of CO molecules on stepped Pt(533) surface, obtained by a NEXAFS study [16]. However, it should be mentioned that the surface structures and so the electronic structures of fcc(533) and fcc(755) are similar therefore it is expected that the corresponding experimental observations would be nearly the same for fcc(755).

By the program PSD, first a metal cluster was separated from the appropriate crystal lattice having the characteristic features: terraces and steps. The size of the cluster was chosen so that it could easily be handled by the ASED–MO method, not consuming too much computing time. In the starting computations a maximum of 45 Pt atoms in three layers (beneath each other) and 6 CO molecules in predetermined arrays were included. Then the numbers of Pt atoms and CO molecules were reduced

systematically to the point when relative values of electronic properties (net charges, overlap populations, sum of one–electron energies, *etc.*), and trends in them, began to change substantially. The determination of the smallest possible cluster size to be used in the calculations, employing the same model, allows us the later use of more sophisticated quantum chemical (*e.g.* "ab initio") methods. When doing calculations on any of the three stepped surfaces it was found [17] that a cluster composed of 15 Pt atoms (three Pt atoms in rows) placed in one layer and 3 CO molecules on top of the Pt atoms in a row supplied the same overall electronic picture (relative values and trends) as the much larger system. Therefore the detailed calculations were carried out with the reduced size metal cluster having the characteristic features of the fcc(775), fcc(755) and fcc(533) structures, respectively. The 3 CO molecules with collinear Pt–C–O axis were placed on one row of Pt atoms parallel to the step edges in different specified positions (on terrace atoms, or at the outside and inside step sites, respectively), and the differences in total electronic energies (the sums of one–electron energies) of the whole substrate–adsorbate system and that of the metal cluster and the 3 COs separately were considered and compared. The dependence of the electronic data on the tilting angle of the CO molecules (the collinear Pt–C–O axis) to the terrace normal has also been investigated, by gradually tilting the CO molecules by the same polar angle at zero azimuth (parallel and zig–zag or fish–bone tilting regarded).

It has been found [17] that layers lying deeper beneath the top layer Pt atoms do not modify significantly the overall electronic picture of the system in any of the three stepped structures, at the approximation level used. In other cases –*e.g.* when calculating fcc(110) crystal lattice [10]– even the presence of third layer atoms in addi–

tion to the top layer ones are quite important for the CO orientation. CO bonding to the surfaces is predominantly a result of 5σ stabilization due to mixing with the metal orbitals having s and d character and back–donation to the CO π^* orbitals from the metal d–orbitals. Our calculations give the orientation of adsorbed CO at both step and terrace sites on stepped Pt(533) surface in accordance with the experimental study of SOMERS et al. [16]. The angular dependence of both the 2π intensity and the $\sigma/2\pi$ intensity ratio indicates that the terrace CO is bonded essentially normal to the terrace and that the step CO is tilted away by only a few degrees towards the macroscopic surface normal. A dramatically large angle of tilt for CO on stepkink sites as observed in the system CO/Pt(321) [18] was not found. The energy of the σ–resonance is identical for both step and terrace CO indicating that there is little change in the C–O overlap population (bond order) even though temperature programed desorption shows that the step species is more strongly bond by ~ 20 kJ mol^{-1} (~ 0.2 eV $molecule^{-1}$) than terrace COs. This means that the carbon–to–metal bond strength is ~ 20 kJ mol^{-1} higher for CO adsorbed at the steps than at terrace sites.

The lowest total energies in any of the three stepped substrate–adsorbate systems investigated are related always with COs in "outside" step (*i.e.* step–edge) positions, at any angles. In "inside" step (step–bottom) positions a tilting angle of 45 degree (off the step) is favoured. Almost exactly the same energies have been found in positions at the ends of the metal cluster. The terrace COs are bonded essentially normal to the terrace. Except "outside" and "inside" step sites the energies are at maximum when the tilting angle is nearly 30°. The lowest energies can always be attributed to the fish–bone (zig–zag) tilting of COs, in any location of them, on the surface. At tilting angles between 60–70 degrees the energy of the system has been found to be almost exactly the same whatever are the positions of COs and it approached the minimum.

When the three CO molecules have been placed at random on the surface the total energy is always larger than at row positions. In accordance with those discussed above, in view of heterogeneous catalysis the adsorption sites on step edges (at any angles) and any sites on terraces of the structures examined (at tilting angles 60–70^{o} to the terrace normal) are favoured and preferred to other sites and angles.

Geometry data, numerical results and details of the calculations are available on request.

Acknowledgement

Thanks are due to Prof. M. A. Van Hove (Berkeley, USA) for suggesting the problem and to Prof. A. B. Anderson (Cleveland, USA) for his advice concerning the parameterization and lending and permitting the use of his program ASED–MO. The support of this work is acknowledged to the Hungarian Academy of Sciences (OTKA Grant No. 393/1988).

References

[1] *Crowell,J.E., E.L. Garfunkel, G.A. Somorjai,*: Surface Sci. *121*, 303 (1982).

[2] *Garfunkel,E.L., J.E. Cromwell, G.A. Somorjai,*: J. Phys. Chem. *86*, 310 (1982).

[3] *Hofmann,P., S.R. Bare, N.V. Richardson, D.A. King*: Solid State Commun. *42*, 645 (1982).

[4] *Bibérian,J.B., M.A. Van Hove*: Surface Sci. *138*, 361 (1984).

[5] *Shincho,E., C. Egawa, S. Naito, K. Tamaru*: Surface Sci. *149*, 1 (1985).

[6] *Ray,N.K., A.B. Anderson*: Surface Sci. *119*, 35 (1982).

[7] *Ray,N.K., A.B. Anderson*: Surface Sci. *125*, 803 (1983).

[8] *Baetzold,R.C.*: J. Chem. Phys. *82*, 5724 (1985).

[9] *Anderson,A.B., M.K. Awad*: Surface Sci. *183*, 289 (1987).

[10] *Bán,M.I., M.A. Van Hove, G.A. Somorjai*: Surface Sci. *185*, 355 (1987).

[11] *Pearson, W.B.*: Handbook of Lattice Spacings and Structures of Metals, Vol.2, p.86, Pergamon Press, Oxford, 1967.

[12] *Anderson,A.B.*: J. Chem. Phys. *62*, 1187 (1975).

[13] *Anderson,A.B., R.W. Grimes, S.Y. Hong,*: J. Phys. Chem. *91*, 4245 (1987).

[14] *Ogletree,D.F., M.A. Van Hove, G.A. Somorjai*: Surface Sci. *173*, 351 (1986).

[15] *Dömötör,Gy., M.I. Bán*: QCPE program QCMP 084; QCPE Bull. *10*, 67 (1990); Computers Chem. *15*, 91 (1991).

[16] *Somers,J.S., Th.Lindner, M. Surman, A.M. Bradshaw*: Surface Sci. *183*, 576 (1987).

[17] *Gardi,J.*: Diploma work, JATE Institute of Physical Chemistry, Szeged, 1990.

[18] *Trenary,M., S.L.Tang, R.J. Simonson, F.R. McFeely*: J. Chem. Phys. *80*, 477 (1984).

THEORETICAL STUDIES ON THE RECOMBINATION REACTION OF *tert*–BUTYL RADICALS

T. KÖRTVÉLYESI and L. SERES

Institute of Physical Chemistry, Attila József University,

P.O.Box 105, H–6701 Szeged, Hungary

(*Received July 2, 1990*)

THE SELF–COMBINATION OF THE *tert*–BUTYL RADICALS (C_{3v}) WAS STUDIED THEORETICALLY AT THE LEVEL OF SEMIEMPIRICAL QUANTUM CHEMICAL METHODS, BY MEANS OF UHF–MINDO/3 AND UHF–AM1, WITH COMPLETE GEOMETRICAL OPTIMIZATION. THE MINIMUM ENERGY REACTION PATH (MERP), AND THE STRUCTURE AND ENERGY OF THE TRANSITION STATE WERE DETERMINED. INCORRECT ACTIVATION AND BOND DISSOCIATION ENERGIES, COMPARED WITH THE EXPERIMENTAL RESULTS, WERE OBTAINED BY MEANS OF UHF APPROXIMATIONS. UHF APPROXIMATION IS NOT ACCEPTABLE TO DESCRIBE THE COMBINATION OF LARGE RADICALS WITH HIGH SYMMETRY.

Introduction

The kinetic and thermochemical characteristics of the *tert*–butyl radical have attracted much attention during the past twenty years. The structure of the radical was studied at the level of *ab initio* quantum chemical calculations by PACANSKY *et al.* [1]. A structure with C_{3v} symmetry was found to be the most stable. The IR spectrum of the radical was also consistent with C_{3v} symmetry [2]. Thus, the structure and the thermochemistry of the radical are well established [3–7].

The recombination reaction has been studied experimentally in different laboratories and the logarithm of the preexponential factor was found to be between 8.4 and 12.38 [8–11]. In the evaluation of the kinetic results in a 400 K temperature interval, McMILLEN and GOLDEN [3] concluded, that the self–combination has zero activation energy. TSANG [12] came to the same conclusion. Laser Induced Fluoro–

escence experimental results were published recently by ANASTASI and ARTHUR [13,14]. A small negative activation energy ($E_A = -0.5$ kJ mol^{-1}) was found.

The self–combination reaction of the methyl radical has been studied in detail at the *ab initio* level [15,16] and by semiempirical SCF–MO methods (UHF–MINDO/3, UHF–MNDO, MNDO–CI, UHF–AM1 and AM1/CI) (*e.g.*[17,18]). The minimum energy reaction path (MERP) calculated by means of UHF–MINDO/3 and UHF–AM1 [19, 20] has no barrier, but the bond dissociation energies (BDEs) were found to be less than the experimental ones. DANNENBERG *et al.* [18] proposed the method of MNDO including configuration interaction (CI 3x3 – open shell excited singlet) and an extended CI (9x9, 27x27, 57x57) method for the combination of radicals containing heteroatoms with lone electron–pairs to model the combination of small alkyl radicals. By the UHF approximation of MNDO and AM1 the combination reactions of large alkyl radicals has not so far been studied. It is of interest to examine whether semiempirical quantum chemical methods with UHF approximation predict acceptable results for the combination of larger radical(s) with high symmetry. The combination of *tert*–butyl radicals was studied in detail and some results are presented here.

Results and Discussion

Our UHF–MNDO and UHF–AM1 calculations on the geometry of the dissociating ethane molecule predict two independent methyl structures at a distance of circ. 230 pm on the MERP. From this distance the energy decreases by less than 0.4 kJ mol^{-1} at every 10 pm. The self–combination of the *tert*–butyl radical can be regarded as that of a substituted methyl radical. The effect of the methyl groups on the self–combination was investigated at the level of semiempirical quantum chemical methods, by means of UHF–MINDO/3 and UHF–AM1 of AMPAC [19]. The MERPs

were investigated in the reverse (bond cleavage) direction, starting from the optimal geometry of 2,2,3,3–tetramethylbutane with the symmetry of D_{3h} (see Fig.1). The calculation of the MERP in the bond forming direction was not successful because of SCF–convergency problems (at around 500 pm) and spin–separation problems (at around 300 pm).

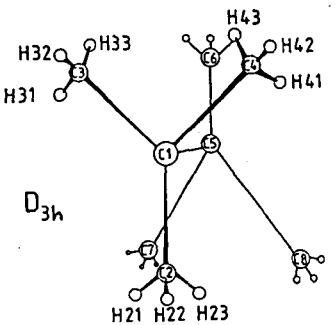

Figure 1: The structure of the reactant in the decomposition reaction of 2,2,3,3–tetramethylbutane (D_{3h})

The calculated MERPs are depicted in Figure 2. The MERP of A–TS–B was calculated by UHF–MINDO/3, and A'–TS'–B' by UHF–AM1. The geometry of the transition state (TS) was established by means of the McIVER–KOMORNICKI method [20] with the keyword of SIGMA [19].

The energies of the reactant (*tert*–butyl radical), the transition state and the product (2,2,3,3–tetramethyl–butane) calculated *via* UHF–MINDO/3 and UHF–AM1, together with the experimentally determined [21] and thermochemically calculated data [22], are included in Table I. The activation energies of the self–combination calculated by UHF–MINDO/3 and UHF–AM1 are 168.2 and 46.5 kJ mol^{-1}, respecti–

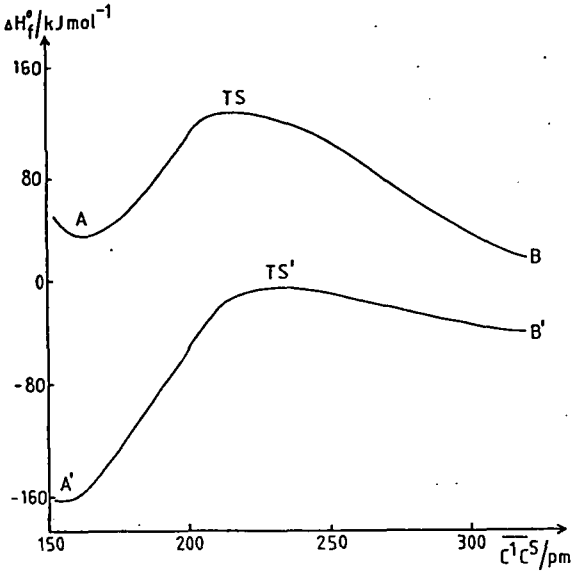

Figure 2. The MERPs of the recombination reaction of *tert*–butyl radicals. A–TS–B was calculated by UHF–MINDO/3 and A'–TS'–B' by UHF–AM1

vely. The former method gives an unrealistically high value which can be due to the number of electron repulsion integrals being reduced greatly by using the core approximation [23]. The calculated energies of the molecules containing crowded (*tert*–butyl) groups are inadequately described by MINDO/3 calculations [23,24]. The activation energies of the C–C bond cleavage reaction are 91.2 kJ mol^{-1} (UHF––MINDO/3) which is evidently an underestimation of the C–C bond strength. UHF––AM1 predicts BDE(*tert*–C_4H_9–*tert*–C_4H_9) = 163.9 kJ mol^{-1} which is an acceptable

result related to the experimental one (158.8 kJ mol^{-1} [21,22]).

The geometries in the TS calculated by means of UHF–MINDO/3 and UHF–AM1 are summarized in Table II. The central bond distances (C^1C^5) in the TS calculated by UHF–MINDO/3 and UHF–AM1 differ by 10.8 pm. The spin contamination in the direction of the TS is increased, the spin separation begins at circ. 200 pm.
AM1/CI 3x3 (open shell excited singlet) method predicts good MERPs (BDEs and activation energies) for the combination of small and medium size alkyl and alkenyl radicals [25]. Further calculations are in progress by means of this method.

Table I

Heats of formation of the reactant (*tert*–butyl radical), the TS and the product (2,2,3,3–tetramethylbutane) calculated by UHF–MINDO/3 and UHF–AM1

Heats of formation/kJ mol^{-1}	UHF–MINDO/3	UHF–AM1	Exp.[20,21]
tert–butyl radical	–22.1	–26.7	48.6
transition state	124.0	–6.9	–
2,2,3,3–tetramethylbutane	32.8	–170.8	–61.6

Conclusion

The calculated distance between the developing radical centres in the TS is approximately of 230 pm which is close to the C–C bond distance at nearly full spin separation in the decomposition of ethane. Both the activation energy of the bond formation and breaking are much greater and less, respectively, than those of the experimental results at UHF–MINDO/3 approximation for the combination of radicals with tertiary carbon radical centre. UHF–AM1 predicts a good BDE, but an unrealistically high activation energy.

Table II

Geometry of the TS of *tert*–butyl radical recombination (see Figure 1)

Geometry	UHF–MINDO/3	UHF–AM1
C^1C^5/pm	220.3	231.7
C^1C^2/pm	150.7	147.9
C^1C^3/pm	150.7	147.9
C^1C^4/pm	150.7	147.9
C^2H^{21}/pm	111.4	112.1
C^2H^{22}/pm	111.1	111.7
C^2H^{23}/pm	111.1	111.7
$\Theta(C^2C^1C^5)$	105.5	109.6
$\Theta(C^3C^1C^5)$	105.5	111.2
$\Theta(C^4C^1C^5)$	105.5	111.2
$\delta(C^2C^1C^5C^6)$	179.7	179.5
$\delta(C^3C^1C^5C^6)$	60.3	60.3
$\delta(C^4C^1C^5C^6)$	59.7	61.2

Acknowledgement

This work was supported by grants from The Hungarian Research Foundation (OTKA Contr.No.394/88).

References

[1] *Pacansky, J., M.Yoshimine:* J.Phys.Chem. *90*, 1980 (1986).

[2] *Pacansky, J., J.S.Chang:* J.Chem.Phys. *74*, 5539 (1981).

[3] *McMillen, D.F., D.M.Golden:* "Hydrocarbon Bond Dissociation Energies" in Annual Reviews of Physical Chemistry, .S.Rabinowitch, Ed.;Annual Rewiews Inc., Palo Alto, CA, p.493, 1982.

[4] *Russell, J.J., J.A.Seetula, R.S.Timonen, D.Gutman, D.F.Nava:* J.Amer.Chem.Soc. *110*, 3084 (1988).

[5] *Tsang, W.:* In "Shock Waves in Chemistry", A.Lifshitz, Ed.;Marcel Dekker, New York, 1981, p.59.

[6] *Walker, J.A., W.Tsang:* Int.J.Chem.Kinet., *11*, 867 (1967).

[7] *Atri, G., R.R.Baldwin, G.A.Evans, R.W.Walker:* J.Chem.Soc., Faraday Trans.I. *74*, 366 (1978).

[8] *Golden, D.M., Z.B.Alfassi, P.C.Beadle:* Int.J.Chem.Kinet. *6*, 359 (1974).

[9] *Parkes, D.A., C.P.Quinn:* J.Chem.Soc., Faraday Trans. I. *72*, 1952 (1976).

[10] *Choo, K., P.C.Beadle, L.W.Piszkiewicz, D.M.Golden:* Int.J.Chem.Kinet. *8*, 45 (1976).

[11] *Kerr, J.A., S.J.Moss:* "Handbook of Bimolecular and Termolecular Gas Reactions", CRC Press, Inc. Boca Raton, Florida, 1981.

[12] *Tsang, W.:* J.Amer.Chem.Soc. *107*, 2872 (1985).

[13] *Anastasi, C., N.L.Arthur:* J.Chem.Soc. Faraday Trans. II. *83*, 277 (1987).

[14] *Arthur, N.L.:* J.Chem.Soc., Faraday Trans.II. *82*, 1057 (1986).

[15] *Carlacci, L.,C.Doubleday,Jr., T.R.Furlani, H.F.King, J.W.McIver,Jr.:* J.Amer.Chem.Soc. *109*, 5323 (1987).

[16] *Darvesh, K.V., R.J.Boyd, P.D.Pacey:* J.Phys.Chem. *93*, 4772 (1989).

[17] *Dannenberg, J.J., J.C.Rayez, M.T.Rayez–Meaume, P.Halvick:* J.Mol.Struct. *123*, 343 (1985).

[18] *Körtvélyesi, T., L. Seres:* React. Kinet. and Catal. Lett., in press.

[19] a.) Dewar Research Group, and *J.J.P.Stewart:* QCPE Bull. *6*,

24 (1986)., b.) QCPE Program 506.

[20] *Komornicki, A., J.W.McIver:* J.Amer.Chem.Soc. *94*, 2625 (1972).

[21] *Russell, J.J., J.A.Seetula, R.S.Timonen, D.Gutman, D.F.Nana:* J.Amer.Chem.Soc. *110*, 3084 (1988).

[22] *Seres, L., L.Zalotai, F.Márta:* Acta Phys.et Chem. Szeged, *23*(4), 433 (1977).

[23] *Bingham, R.C., M.J.S.Dewar, D.H.Lo:* J.Amer.Chem.Soc. *97*, 1294 (1975).

[24] *Dewar, M.J.S., W.Thiel:* J.Amer.Chem.Soc. *99*, 4907 (1977).

[25] *T.Körtvélyesi, L.Seres:* J.Mol.Struct. (THEOCHEM), accepted for publication.

MNDO AND AM1 STUDIES ON THE RESONANCE STABILIZED ALLYL–TYPE RADICALS CONTAINING CC, CN AND NN BONDS

T. KÖRTVÉLYESI and L. SERES

Institute of Physical Chemistry, Attila József University,

P. O. Box 105, H–6701 Szeged, Hungary

(*Received October 1., 1990*)

THE HEATS OF FORMATION AND THE FULLY–OPTIMIZED GEOMETRIES OF 1–METHYLALLYL (1R), 1–METHYL–1–AZAALLYL (2R'), 1–METHYL–2–AZAALLYL (2R') AND 1–METHYL–1,2–DIAZAALLYL (3R) RADICALS WERE CALCULATED AT THE SEMIEMPIRICAL QUANTUM CHEMICAL LEVEL (MINDO/3––UHF, MNDO–HE AND AM1–HE). THE RESONANCE ENERGIES OF THE RADICALS WERE CALCULATED USING THE HEATS OF FORMATION OF THEIR PARENT COMPOUNDS (2–BUTENE (1), N–ETHYLIDENE––METHYLAMINE (2) AND AZOMETHANE (3)). THE RESONANCE ENERGIES OF 2R AND 3R WERE FOUND TO BE LESS THAN THOSE OF 1R, 2R'. ROTATIONAL AND INVERSIONAL MECHANISM OF THE ISOMERIZATION OF THE MOLECULES AND ALLYL–TYPE RADICALS CONTAINING ESSENTIAL DOUBLE BONDS AND PARTIAL CC, CN AND NN DOUBLE BONDS WERE STUDIED. THE CALCULATED BARRIER HEIGHTS PREDICT TOO LOW ACTIVATION ENERGIES FOR THE ROTATION. THE REASON OF THE LOW BARRIERS CALCULATED IS THE UNDERESTIMATION OF THE LONE–PAIR AND THE DOUBLE LONE–PAIR REPULSION IN THE NDDO FORMALISM. ISOMERIZATION AT CC, NN AND CN DOUBLE BONDS AND PARTIAL DOUBLE BONDS BY INVERSION IS UNLIKELY.

Introduction

The thermal decomposition of *cis*– and *trans*–diazenes can be described by complex reaction schemes [1] involving the synchronous (a) or asynchronous (b) decomposition of these compounds. Much effort has been devoted to decide between mechanisms (a) and (b) [2]. Symmetrical dialkyldiazenes cleave by mechanism (a), whereas diazenes with different alkyl (or aryl) substituents do so by mechanism (b) [3,4]. MNDO calculations [5] on the thermal decompositions of *trans*– and *cis*–diethyldiazene predict stepwise decomposition *via* synchronous bond fission and suggest a transition state through *cis* isomers. Experimentally, the *cis*–diazenes are thermally less

stable than the *trans* isomers [1]. The role of the *cis* conformer in the photochemical deazatization of *trans*–1,3–dialkyl–1,2–diazenes has been confirmed experimentally [1,6]. In the thermolyses of *trans*– and *cis*–di(2–propyl)–diazene, FOGEL et al. [7] showed that the decomposition does not occur *via* the labile *cis* conformer, and suggested that the isomerization of the *cis* conformer proceeds with inversion.

For the *cis–trans* isomerization of alkyl–1,2–diazenes, three possible mechanisms have been suggested: rotation [2], inversion and dissociation/combination [8]. The electron configuration $(n_-)^2(\pi)^2(n_+)^2$ for the *trans* ground (π,π^*) state correlates with a doubly excited configuration of the *cis* isomer; rotation is symmetry–forbidden [9]. The rotation around the N=N bond is highly hindered (247–351.8 kJ mol^{-1}) [10], and the rotational barrier is significantly higher than those in the olefins [11]. A detailed INDO–SCF calculation, followed by CI calculations [10a] for the isomerization of azomethane in the ground and some low–lying excited states, showed that rotation of the methyl groups around the N=N double bond was more feasible than inversion. The calculated relative stability of the *trans* and *cis* isomers, $\Delta\Delta_fH^o = \Delta_fH^o(trans) - \Delta_fH^o(cis)$, was found to be 14.2 kJ mol^{-1}, in contrast with the experimental data [12]. As products of radical H–abstractions from 2–butene, N–ethylidenemethylamine and azomethane (*Reaction 1*), resonance–stabilized allyl–type radicals are formed:

$$trans\text{–}CH_3\text{–}X{=}X\text{–}CH_3 + R \rightarrow E\text{–}CH_3\text{–}X{=}X\text{–}CH_2 + RH \qquad (1)$$

$$E\text{–}CH_3\text{–}X{=}X\text{–}CH_2 \rightleftharpoons Z\text{–}CH_3\text{–}X{=}X\text{–}CH_2 \qquad (2,\text{–}2)$$

where X = CH, N.

Results on the reactions of 1–azaallyl and 2,3–diazaallyl radicals are scarce. The last reaction has been studied in the decompositions of dialkyldiazenes [13] and in the radical–initiated gas–phase reactions of dialkyl–diazenes [14]. In further reactions, the

radical can also isomerize (*Reaction 2*), similarly to the allyl radicals, and take part mostly in radical disproportionation and combination reactions forming stable products.

There is an equilibrium between the E and the Z isomer of 1–methylallyl radical at the temperature range 399–439 K [15].

Calculations for the compounds 1, 2 and 3 and the radicals 1R–3R were carried out by means of semiempirical quantum chemical methods (MINDO/3 [16], MINDO/3–UHF [17], MNDO–HE [18], AM1–HE [19,20] and AM1–UHF [21]).

Calculations

The heats of formation and the geometries of the molecules and radicals in the ground state were calculated with full geometrical optimization. In the calculations of the torsional profiles, the twist angle was fixed at different values as the reaction coordinate (Θ = 0°, 15°, 30°, 45°, 60°, 75°, 90°, 105°, 120°, 135°, 150°, 165° and 180°), and an optimization was applied for the remainder geometrical parameters. In the calculation of the inversion profile (AM1–HE), the twist angle of Θ(C–N–N–C) was kept unchanged (Θ = 180° and 0°) and the bending–angle was kept fixed (ϕ = 110°, 120°, 130°, 140°, 150°, 160°, 170°, 180° and 360° – ϕ) values as reaction coordinates.

The resonance energies (RE) were defined similarly to the allyl resonance energies (ARE) [21] (ARE = BDE(CH_3–H) – BDE(($R_\pi CH_2$–H)), using the calculated data for dialkyl–diazenes, methane and methyl radical [19].

The stabilization energies (SE) were calculated by the method of LEROY [22]:

$$SE = \Delta H_a - \Sigma N_i E_i$$

where ΔH_a is the atomization energy and N_i the number of bond i.

The necessary bond terms to determine the atomization heats of radicals were unknown. By using the experimental and calculated heats of formation of dialkyldiazenes with low strain [23] (n–alkyl group substituted diazenes), for the bond energy terms (E) [22] E(C–N=N–C) = 1105.5 ± 0.8 kJ mol^{-1} was obtained [24]. The $(E(C–H)_p^N$ and $E(C–H)_s^N$ were supposed to be equal to $E(C–H)_p^{C–N=N–C}$ and $E(C–H)_s^{C–N=N–C}$, respectively.

Results and Discussion

Resonance and stabilization energies of radicals 1R–3R

The heats of formation of compounds 1–3 calculated by means of MINDO/3, MNDO and AM1, are summarized and compared with the experiments in Table I–II. The best agreement with the experimental values was obtained by AM1. A dramatic improvement was observed at the N–containing compounds with changing the core–core repulsion function (CRF) in MNDO to result AM1 [19]. Table III contains the heats of formation of allyl–type radicals formed in reaction (1). Used the calculated data, the resonance energies were also calculated (Table IV) for the isomers of 1–3. The heats of formation for *cis* (Z) isomers of N–containing molecules suggest higher thermodynamic stability than for the *trans* ones in contradiction with the experimental results available in the literature [23]. (The only exception among the diazenes, the difluorodiimide, is more stable in the *cis* configuration [30].) MINDO/3 predicts an unrealistically small heats of formation for 1–3, because this method reduce the number of electron integrals to be considered using core approximation [25,18]. The lone–pair and double lone–pair interactions are underestimated not only in MINDO/3 [16], but in MNDO [18] and AM1 [25], too. An improvement was found for these compounds in MNDO which is probably due to the inclusion of directional

Table I

Calculated heats of formation of 2–butene and N–ethylidene–methylamine

Method	$\Delta_f H^o$/kJ mol^{-1}			
	1		2	
	cis[a]	*trans*	*cis*[a]	*trans*
MINDO/3	–23.9 [25]	–26.4 [25]	47.6	40.2
MINDO	–16.7 [26]	–21.4 [25]	31.2	27.5
AM1	– 9.2	–14.0	33.6	42.7
exp.[b]	– 8.0	–12.6		

[a] The methyl groups have a staggered–staggered conformation in *cis*–1 and *cis*–2.
[b] See in [27]

Table II

Calculated heats of formation of azomethane

Method	$\Delta_f H^o$/kJ mol^{-1}	
	cis[a]	*trans*
MINDO/3	39.8	86.2 [28a]
MNDO	107.2	96.3
AM1	126.5	146.3
exp.		134.5 ± 3.8 [23a]
		148.8 ± 5.2 [23b]
		149.1 ± 6.2 [23c]

[a] The methyl groups have a staggered–staggered conformation in *cis*–dimethyldiazene; this was demonstrated by *ab initio* calculations to be the most stable geometry with C_{2v} [29a] symmetry.

effects in the two–center electron–electron repulsions and core–electron attractions [18b]. The further improvement in AM1 calculations is due to the modified CRF [19a]. Similar observation was made for the radicals 2R, 2R' and 3R. KAO et al. [31] completed by *ab initio* methods this effect with the strain among the large alkyl groups. The attraction between the alkyl H–atom and the lone–pair of electrons on N–atom can not be negligible either [30]. None of the methods applied in the calculations give good relative stability for the isomers of N–containing molecules.
The resonance energies in the radicals 1R and 3R are practically equal. In radicals 2R and 2R' the resonance energies are very different. In the radical, where the N–atom is in symmetrical position in the delocalized system, the stabilization through delocalization is greater than in the radicals 1R, 2R and 3R [35]. An N–atom in unsymmetrical position has an even lower delocalization effect. The stabilization energies of 1R and 3R calculated by LEROY [22] differ by circ. 10 kJ mol^{-1}. The UHF approximation [32b,33] (UHF–MINDO/3 and UHF–AM1) overestimates the thermodynamic stability of the radicals in each case considering the experimental data available in the literature and the half–electron (HE) approximation [34].

By means of the calculated heats of formation for dialkyl–diazenes the group increments of $\Delta_f H^o[C–(N_A)(H)_2]$ = 90.4 kJ mol^{-1} and $\Delta_f H^o[C–(N_A)(C)(H)]$ = 94.8 kJ mol^{-1} [24] were estimated using the group values for groups in molecules proposed by SCHERER et al. [23g].

The calculated geometries for 3 and 3R are summarized in Table V – VI. The difference between MINDO/3 and AM1 results is significant. As it can be seen in Table V, the geometry calculated by means of AM1 shows the best agreement with the experimental result. A similar observation was made for the allyl radicals [32].

The net atomic charges ($q_X = Z_X - \Sigma_\mu X_{P\mu\mu}$, where Z_X is the core charge of

Table III

Calculated heats of formation of resonance stabilized radicals 1R–3R

Radical		$\Delta_f H^o$/kJ mol^{-1}			
		MINDO/3–UHF	MNDO–HE	AM1–HE	AM1–UHF
1R	E	88.8	103.0	116.8	81.0
	Z	91.8	105.5	119.5	84.0
2R	E	163.9	166.9	196.4	161.2
	Z	173.7	155.5	189.4	173.3
2R'	E	139.7	132.9	147.1	120.3
	Z	145.6	138.2	141.2	115.1
3R	E	115.1 [28a]	214.4	275.4	245.4
	Z	144.0	238.6	264.4	235.9

[a] The heats of formation of the radicals are calculated for the E and Z conformers.

Table IV

Calculated resonance (RE) and stabilization (SE) energies of radicals 1R–3R

Radical		RE/kJ mol^{-1}[a]	SE/kJ mol^{-1}
1R	E	41.7	77.3
	Z	34.2	75.1
2R	E	14.0	
	Z	11.9	
2R'	E	63.3	
	Z	60.1	
3	E	38.6	65.7
	Z	29.8	

[a] The resonance energies are calculated by means of the following expression: RE = $(\Delta_f H^o(CH_4) - \Delta_f H^o(CH_3)) - (\Delta_f H^o(\text{diazenes}) - \Delta_f H^o(\text{1,2–diazaallyls}))$ [21], supposed that 1R–3R to be carbon centered radicals.

atom X, $P_{\mu\mu}$ is a diagonal element of the bond order matrix) on the radicals in position 1 and 3 change slightly. The electron densities on the C– and N–atoms are very similar, while substantial deviation was found at the reactive centres (C– or/and N–atom). The π–spin density correlates with the reactivity of the radicals in combination reactions [17,36] and with the coupling constants of ESR measurements [37b]. A reactivity difference was proposed for the C– and N–atoms in radical 3R by means of UHF–AM1 and AM1/C1 3x3 calculations [24].

In radical combinations, the SOMOs (Singly Occupied MOs) interact with each other and correlate with the reactivity of the radicals [36]. The calculated SOMO energies show, that the nucleophilicity of alkyl radicals increases with the alkyl–substitution [28b,32]. In radicals 1R–3R, the nucleophilicity increases when one of the alkyl C–atoms is substituted for N in the order 2R'>2R>1R>3R.

Rotational and inversional barriers of 1–3 and 1R–3R

The (AM1–HE) calculated rotational profiles of 1 and radical 1R (around the C=C and C–C bonds), those of 2 and radical 2R and 2R' (around the C=N and C–N bonds) and those of 3 and radical 3R (around the N=N and N–N bonds) are depicted in Figs. 1–3. The characters of the rotation profiles of molecules are similar. The maxima of the rotational barriers are at $\Theta = 90^{\circ}$ in 1 and at $\Theta = 105^{\circ}$ in 3. The profile of 2 has a plateau in the range of 75–125°. This departure is due to lone–pair repulsions in molecules [18b].

The calculated height of the barrier of rotation around the N=N bond (182.3 kJ mol^{-1}) is considerably higher than those around the C=C bond (136.3 kJ mol^{-1}) in butene–2 (AM1–HE) and around the C=N bond (105.0 kJ mol^{-1}). A recent experimental value for 2–butene is 271.7 ± 8.8 kJ mol^{-1} [11a]. The calculated (AM1–HE)

Table V

The calculated and experimental geometries of *trans*– and *cis*–azomethane

	MINDO/3	MNDO	AM1	exp.[b]
r(N=N)/pm	119.2	122.2	122.5	124.7 [29a]
	(116.2)	(120.8)	(120.6)	(125.4) [29b]
r(C–N)/pm	140.0	147.5	145.5	148.2 [29a]
	(143.4)	(147.8)	(145.5)	(148.0) [29b]
< CNN/degree	127.6	116.6	119.5	112.0 [29a]
	(138.9)	(127.3)	(126.9)	(119.3) [29b]

[a] The geometrical parameters of the *cis* isomer are in parenthesis.

[b] The symmetries of the most stable *trans* and *cis* isomers are C_{2h} and C_{2v} [29], respectively.

Table VI

The calculated geometries of 1–methyl–1,2–diazaallyl radical[a]
$C^1H_3 - N^1 \doteq N^2 \doteq C^2H_2$

		MINDO/3–UHF	MNDO–HE	AM1–HE	AM1–UHF
$r(N^1–N^2)$/pm	E	118.0	126.5	126.8	
	Z		(124.2)	(124.5)	(124.8)
$r(C^1–N^1)$/pm	E	127.0	135.5	134.0	
	Z		(136.3)	(134.9)	(135.6)
$r(C^2–N^2)$/pm	E	138.9	145.9	144.6	
	Z		(146.7)	(143.7)	(144.8)
$<C^1N^1N^2$/ degree	E	151.3	115.6	120.0	
	Z		(126.0)	(128.2)	(127.8)
$<C^2N^2N^1$/ degree	E	133.1	117.3	118.0	
	Z		(128.8)	(126.4)	(125.6)

[a] The geometries of the E conformers are in parenthesis.

rotational barrier is significantly lower for the rotation around the N=N bonds than the barrier heights determined by other theoretical methods (*ab initio* with different

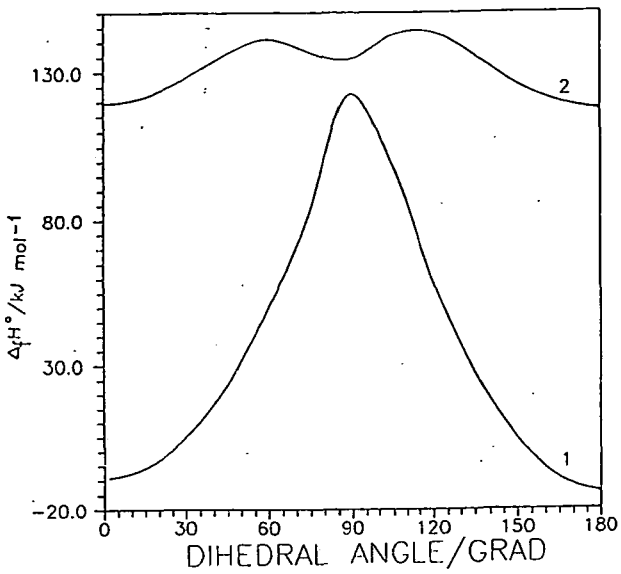

Figure 1: Rotational barriers of the 2–butene and the 1–methylallyl radical, calculated by means of AM1–HE: 1: rotation around the C=C bond, 2: rotation around the C–C bond.

basis sets, MNDO CI, *etc.*: 247.0–351.8 kJ mol^{-1}) [10], too.

The character of the rotational profiles of the radicals is similar: all have a valley – a local minima at $\Theta = 90^{o}$, which is the less stable allenic form of the radical. The heights of the barriers of radical 1R and 3R are 26.3 and 10.7 kJ mol^{-1}, respectively. The barrier height around the N–N σ–bond in hydrazines, determined by means of ESR–techniques, is 24 kJ mol^{-1} [38] (which is higher than the barrier for rotation around the C–C σ–bond by circ. 4 kJ mol^{-1}). The allyl radical delocalization energies (ADE) [37b] were calculated from the barrier heights of allyl–type radicals (determi–

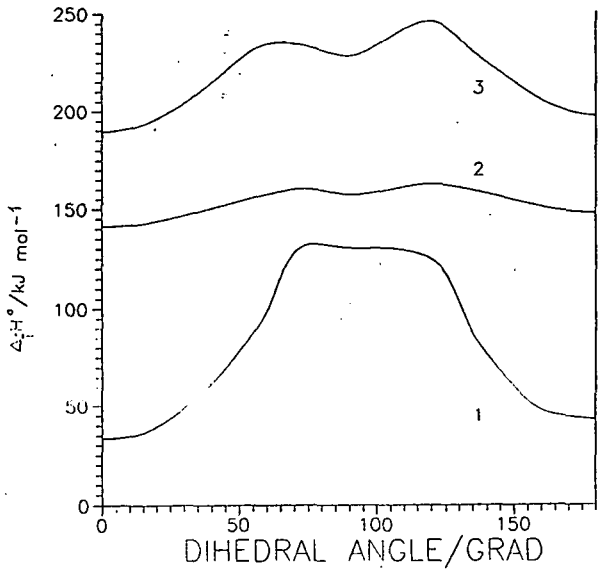

Figure 2: Rotational barriers of N–ethylidenemethylamine around N=N double bond (1), 1–methyl–1–azaallyl (2R) around C–N (2) and 1–methyl–2––azaallyl (2R') radicals around C–N bonds (3), calculated by means of AM1–HE.

ned by ESR–technique) and from that of the σ–bond. The calculated ADE for the allyl radical was found to be circ. 48 kJ mol^{-1} [37b]. Since the calculated values of the barrier heights are significantly lower than expected on the basis of the experimental data (for allyl–type radicals (see *e.g.*[37])), only a qualitative approximation can be made for the delocalization energy of 3R. (MNDO and AM1 underestimate the rotational barrier heights [20].) The rotational barrier in 3R is less than that in 1R. Thus,for ADE a smaller value is predicted than for the allyl–type radicals, considering the greater rotational barrier for the N–N σ–bond [38] than that for the C–C σ–bond.

The barrier heights of the radicals 2R and 2R' are also different – 2R' has a greater barrier (35 kJ mol^{-1}). We have found that 2R' is a more stable radical than 1R, 2R and 3R (see Table IV). On the basis of the calculations a qualitative conclusion was drawn to explain the possible mechanism of the isomerization and the experimental results [14b]. The barrier height of inversion in azomethane (Fig. 4) was found to be lower than the rotation barrier, 134.7 and 182.3 kJ mol^{-1} (related to the *cis* isomer), respectively. The situation in radical 3 is reversed (Fig.4). The barrier height for inversion and rotation are 112.8 and 12.7 kJ mol^{-1}. Isomerization is preferable by a rotational mechanism. The rotational and inversional barriers at compound 2 are almost the same (Fig.5). At radical 2R and 2R' the rotation is more favourable than the inversion.

Under the experimental conditions (around 400 K) [14b], for which the reactions of alkyl– substituted 1,2–diazaallyl radicals were studied, an equilibrium is expected between Z and E radicals. The lack of *cis*–products can be attributed to the lower reactivity of Z than E radicals and the unstability of the products of Z radicals.

Conclusions

The AM1 method predicts greater stability for the *cis* and *syn* isomers of the compounds 2–3 and the radicals 2R, 2R' and 3R. The nucleophilicity increases in the order 2R' > 2R > 1R > 3R while the thermodynamic stability (RE and SE) decreases in the order 2R' > 1R > 3R > 2R. On the basis of the height of the barrier of rotation around the N–N and C–C bonds, the delocalization energy is lower in radical 3 than in 1R. On the basis of relative barrier heights of the rotation and inversion, an equilibrium was proposed between the E and Z conformers of the radicals at 400 K. The absolute values of the barrier heights are not acceptable because the semiempi–

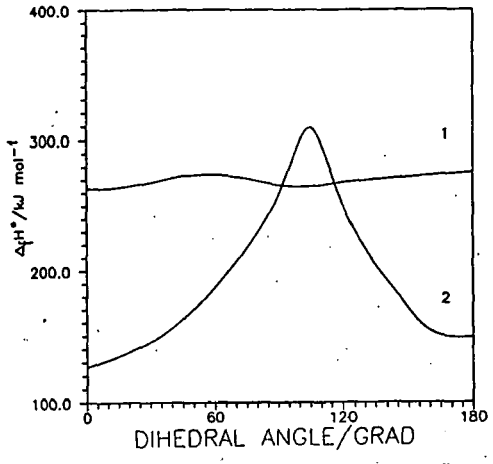

Figure 3: Rotational barriers of dimethyldiazene and the 1–methyl–1,2–diazaallyl radical, calculated by means of AM1–HE: 1: rotation around the N=N bond, 2: rotation around the N–N bond.

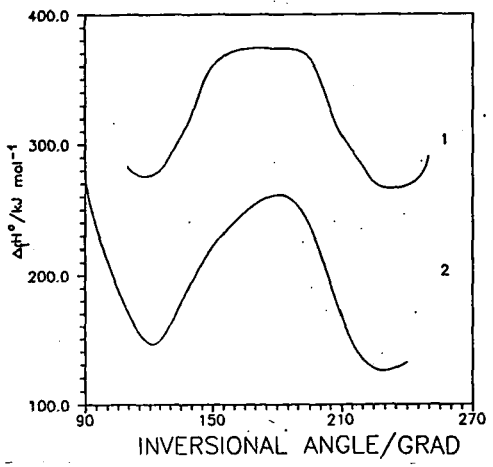

Figure 4: MEPs of inversion of the 1–methyl–1,2–diazaallyl radical (1) and azomethane (2), calculated by means of AM1–HE.

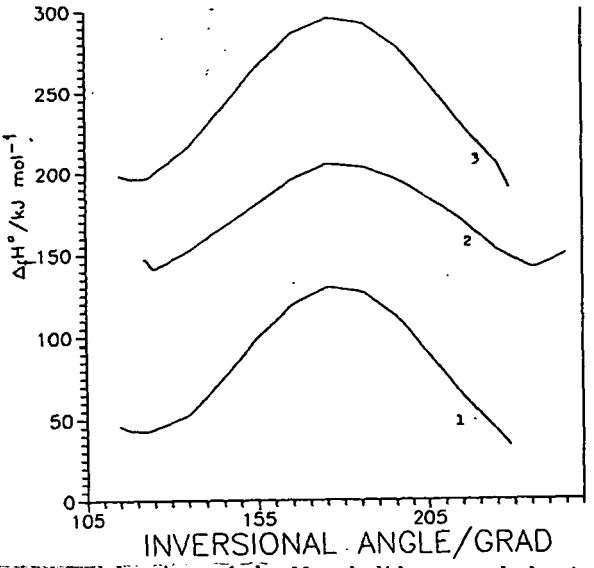

Figure 5: Inversional barriers of the N–ethylidene–methylamine and 1–methyl–
–1–azaallyl and 1–methyl–3–azaallyl radical, calculated by
means of AM1–HE. 2: 1; 2R: 2; 2R': 3.

rical quantum chemical methods applied for the calculations handle the interactions of lone–pair and double lone–pairs of electrons with error.

Acknowledgement

This work was supported by grants from the Hungarian Research Foundation (OTKA Contr.No.394/88) and the Hungarian Ministry of Education (Contr. No. 749/ /86). The authors are grateful to S. Lovas and Gy. Tasi for a modified version of AM1.

References

[1] *Engel, P.S.:* Chem.Rev. 80, *99* (1980).

[2] a.) *Strausz, O.P., J.W.Lown, and H.E.Gunning:* Compr.Chem.Kinet. (ed. Bamford, C.H. and C.F.H.Tipper), Elsevier, p.5, 1972. b.) *Koenig, T.:* in "Free Radicals"; ed. Kochi, J.K., p.1, 1973, c.) *Koga, G., N.Koga, J.–P.Anselme:* in "The Chemistry of the Hydrazo, Azo, and Azoxy Groups"; ed. Patai, S, Wiley, New York, 1975. d.) *Hinz, J., A.Oberlinner, and C.Rüchardt:* Tetrahedron Lett., 1975, 1973. e.) *Schmittel, M., and C.Rüchardt:* J.Amer.Chem.Soc. *109*, 2750 (1987).

[3] a.) *Porter, N.A., and L.J.Marnett:* J.Amer.Chem.Soc. *95*, 4361 (1973). b.) *Porter, N.A., G.R.Dubay, and J.G.Green:* ibid. *100*, 920 (1978). c.) *Kopecky, K.R., P.M.Pope, and J.Sastre:* Can.J.Chem. *54*, 2639 (1976).

[4] *Barton, D., M.Hodgett, P.Skirving, M.Whelton, K.Winter, C.Vardy:* Can.J.Chem. *61*, 1712 (1983).

[5] *Dannenberg, J.J., and D.Rocklin:* J.Org.Chem. *47*, 4529 (1982).

[6] *Porter, N.A., M.O.Funk:* J.C.S.Chem.Comm., *263*, 1973.

[7] *Fogel, L.D., A.M.Rennert, and C.Steel:* J.C.S.Chem.Comm. *536* (1975).

[8] a.) *Neuman, R.C., Jr., and G.A.Binegar:* J.Amer.Chem.Soc., *105*, 134 (1983). b.) *Green, J.G., G.R.Dubay, and N.A.Porter:* J. Amer. Chem. Soc. *99*, 1264 (1977).

[9] *Baird, N.C., and J.R.Swenson:* Can.J.Chem., *51*, 3097 (1973).

[10] a.) *Olbrich, G.:* Chem.Phys. 27, 117 (1978). b.) *Baird, N.C., P.de Mayo, J.R.Swenson, M.C.Usselmann:* J.Chem.Soc.Chem.Comm. 1973, 314. c.) *Talaty, E.R., J.C.Fargo:* Chem.Comm. *2*, 65 (1967). d.) *Kearns, D.R.:* J.Phys.Chem. *69*, 1062 (1965). e.) *Camp, R.N.,*

I.R.Epstein, C.Steel: J.Amer.Chem.Soc. *99*, 2453 (1977).

f.) *Howell, J.M., L.J.Kirschenbaum:* ibid., *98*, 877 (1977).

g.) *Talaty, E.R., A.K.Schwartz, G.Simons:* ibid. *97*, 972 (1975).

h.) *Winter, N.M., R.M.Pitzer:* J.Chem.Phys. *62*, 1269 (1975).

[11] a) *Doering, W.v.E., W.R.Roth, F.Bauer, R.Breuckmann, T.Ebbrecht, M.Herbold, R.Schmidt, H.–W.Lennartz, D.Lenoir, R.Boese:* Chem.Ber. *122*, 1263 (1989). b.) *Wiberg, K.B., E.Martin:* J. Amer. Chem. Soc. *107*, 5035 (1985).

[12] *Engel, P.S.,D.J.Bishop:* J.Amer.Chem.Soc. *97*, 6754 (1975).

[13] a.) *Paquin, E., W.Forst:* Int.J.Chem.Kinet. *5*, 691 (1973).

b.) *Sandhu, H.S.:* J.Phys.Chem., *72*, 1857 (1968).

c.) *Martin, G., A.Maccoll:* J.Chem.Soc.Perkin Trans. *2*, 1887 (1977).

[14] a.) *Péter, A., G.Ács, P.Huhn:* Int.J.Chem.Kinet. *16*, 753 (1984).

b.) *Görgényi, M., L.Seres:* in preparation.

[15] a.) *Roberts, C., J.C.Walton:* J.C.S.Perkin II 1981, *553*.

b.) *Roberts, C., J.C.Walton:* ibid. 1985, *1073*.

[16] *Bingham, R.S., M.J.S.Dewar, D.H.Lo:* J.Amer.Chem.Soc. *97*, 1285 and 1294 (1975).

[17] a.) *Bischof, P.:* J.Amer.Chem.Soc. *98*, 6844 (1976).

b.) *Bischof, P.:* QCPE *11*, 309 (1975).

[18] a.) *Dewar, M.J.S., W.Thiel:* J.Amer.Chem.Soc., *99*, 4899 (1977).

[19] *Dewar, M.J.S., E.G.Zoebisch, E.F.Healy, J.J.P.Stewart:* J. Amer. Chem. Soc. *107*, 3902 (1985).

[20] a.) *Dewar Research Group and J.J.P.Stewart:* QCPE Bull. *6*, 924 (1986). b.)AMPAC Program Package, QCPE Program 506.

[21] a.) *Szwarc, M., A.H.Sehon:* Proc.R.Soc.London, Ser.A, *202*, 263 (1950).
b.) *Szwarc, M., A.H.Sehon:* J.Chem.Phys. *18*, 237 (1950).
c.) *Szwarc, M., B.N.Gosh, A.H.Sehon:* J.Chem.Phys. *18*, 1142 (1950).
d.) *Benson, S.W.:* Thermochemical Kinetics, 2nd Ed., Wiley, New York, N.Y., 1976.

[22] a.) *Leroy, G.:* Int.J.Quant.Chem. *23*, 271 (1983). b.) *Leroy G.*: Adv.in Quant.Chem. *17*, p. 1. 23.

[23] a.) *Rossini, F.D.:* J.Chem.Thermodyn. *8*, 651 (1976). b.) *Rossini, F.D., R.L.Montgomery:* J.Chem.Thermodynamics, *10*, 465 (1978).
c.) *Montgomery, R.L., F.D.Rossini:* J.Phys.Chem., *82*, 575 (1978).
d.) *Inagaki, S., N.Goto:* J.Amer.Chem.Soc. *109*, 3234 (1987).
e.) *Engel, P.S., R.A.Melaugh, M.Mansson, J.W.Timberlake, A.W.Garner, F.D.Rossini:* J.Chem.Thermodynamics, *8*, 607 (1976).
f.) *Engel, P.S., D.B.Gerth:* J.Amer.Chem.Soc., *105*, 6849 (1983).
g.) *Scherer, K.V., Jr., L.Batt, P.H.Stewart:* 9th International Symposium on Gas Kinetics, Bordeaux, 1986.

[24] Körtvélyesi, T., L.Seres: J.Mol.Struct.(THEOCHEM), accepted for publication.

[25] *Bingham, R.C., M.J.S.Dewar, D.H.Lo:* J.Amer.Chem.Soc. *97*, 1294 (1975).

[26] *Dewar, M.J.S., W.Thiel:* J.Amer.Chem.Soc. *99*, 4907 (1977).

[27] *Cox, J.D., G.Pilcher:* "Thermochemistry of Organic and Organometallic Compounds", Academic Press, New York, N.Y. 1970.

[28] a.) *Körtvélyesi, T., L.Seres:* React.Kinet.Catal.Lett. *40*, 65 (1989).
b.) *Körtvélyesi, T., L.Seres:* ibid. *37*, 403 (1988).

[29] a.) *Pamidimukkala, P.M., D.Rogers, G.B.Skinner:* J. Phys. Chem. Ref. Data, *11*, 83 (1982). b.) *Stevens, J.F., Jr., R.F.Curl, Jr., P.S.Engel:* J.Phys.Chem. *83*, 1432 (1979).

[30] *Armstrong, G.T., S.Marantz:* J.Chem.Phys. *38*, 169 (1962).

[31] a.) *Kao, J.J., T.–N.Huang:* J.Amer.Chem.Soc. *101*, 5546 (1979). b.) *Kao, J.J., D.Leister:* J.Amer.Chem.Soc. *110*, 7286 (1988).

[32] a.) *Vajda, E., J.Tremmel, B.Rozsondai, I.Hargittai, A.K.Maltsev, N.D.Kagramanov, O.M.Nefedov:* J.Amer.Chem.Soc. *108*, 4352 (1986). b.) *Körtvélyesi, T., S.Lovas, L.Seres:* to be published in J.Comp.Chem.

[33] *Pople, J.A., R.K.Nesbet:* J.Chem.Phys. *22*, 571 (1954).

[34] *Dewar, M.J.S., J.A.Hashmall, C.G.Venier:* J.Amer.Chem.Soc. *90*, 1953 (1968).

[35] *Cocks, A.T., K.W.Egger:* Int.J.Chem.Kinet. *4*, 169 (1972).

[36] a.) *Epiotis, N.D.:* "Theory of Organic Reactions", Springer Verlag, Berlin–Heidelberg–New York, 1978, p. 195. b) Fukui, K.: "Theory of Orientation and Stereoselection", Springer Verlag, Berlin, 1975, p.10. c.) *Minato, T., S. Yamabe, H.Fujimoto, K.Fukui:* Bull.Chem.Soc.Jpn., *51*, 1 (1978). d.) *Fukui, K., H.Fujimoto:* Bull.Chem.Soc.Jpn. *41*, 1989 (1968).

[37] a.) *Feller, D., E.R.Davidson, W.T.Borden:* J.Amer.Chem.Soc. *106*, 2513 (1984). b.) *H.–G. Korth, H.Trill, R.Sustmann:* J.Amer.Chem.Soc. *103*, 4483 (1981). c.) *R.Sustmann, D.Brandes:* Chem.Ber. *109*, 354 (1976). d.) *Ondruschka B., U.Ziegler, G.Zimmermann:* Z.phys.Chem., Leipzig, *267*, 1127 (1986).

[38] *Lunazzi, L., D.Macciantelli,* Tetrahedron *41*, 1991 (1985).

STUDIES OF HIGH–T_c SUPERCONDUCTORS IN Y–Ba–Cu–O CERAMIC SYSTEM

Béla KOZMA, József CSERÉNYI and Ildikó KOVÁCS

Institute of Solid State and Radiochemistry, Attila József University

Aradi Vértanúk tere 1., H–6720 Szeged, Hungary

(*Received November 10, 1990*)

BULK SUPERCONDUCTORS $YBa_2Cu_3O_{7-x}$ WITH ZERO RESISTANCE AT 90 K AND NARROW T_c TRANSITIONS (3–4 K) WERE SYNTHESIZED. THE EFFECTS OF THE PROCESS PARAMETERS, THE OPTIMUM OF THE SINTER CYCLE AND THE TEMPERATURE DEPENDENCE OF THE RESISTANCE OF $YBa_2Cu_3O_{7-x}$ SAMPLES WERE INVESTIGATED.

Introduction

The discovery of superconducting compounds in the system La–Ba–Cu–O by BEDNORZ and MÜLLER [1] stimulated activity on high–temperature superconductivity, most of the work concentrating on the compound $YBa_2Cu_3O_{7-x}$ since it has a high transition temperature, T_c = 90 K [2]. The discovery of superconducting compounds with even higher transition temperatures (up to 125 K) in the systems Bi–Sr–Ca–Cu–O [3] and Tl–Ba–Ca–Cu–O [4] shows that recent developments in the field of superconducting oxides are very promising.

Most ceramic $YBa_2Cu_3O_{7-x}$ samples are prepared by powder–ceramic techniques, generally involving three main steps: powder preparation and calcining, sintering, and adjustment of the oxygen content [5]. The reactions can be written as

$$Y_2O_3 + 6\ CuO + 4\ BaCO_3 \longrightarrow 2\ YBa_2Cu_3O_{6.5} + 4\ CO_2 \qquad (1173\ K)$$

and

$$4\ YBa_2Cu_3O_{6.5} + 1/4\ O_2 \longrightarrow 4\ YBa_2Cu_3O_7. \qquad (1193–1203\ K)$$

The microstructure is directly affected by the annealing parameters used to obtain the desired oxygen content. Hence, the conditions are of decisive importance as concerns the ultimate mechanical and superconducting properties of the material. The various stages of $YBa_2Cu_3O_{7-x}$ production are dealt with below, and their effects on the superconducting properties are discussed.

Experimental

Powder preparation

The starting compounds were Y_2O_3 (Fluka, 99.9 %), $BaCO_3$ (Reanal, p.a.) and CuO (Merck, p.a.). The morphology of the powders was established with the BET method. The Y_2O_3 and $BaCO_3$ powders consisted of particles with a mean size of 2–4 μm, and the CuO powder of particles 5–10 μm in size (agglomerates). The starting Y_2O_3 , $BaCO_3$ and CuO were mixed in a molar ratio of 1:4:6. The simplest kind of powder preparation, manual dry mixing in a mortar, yielded very inhomogeneous samples. By contrast, very homogeneous powder mixtures (mean particle size approximately 0.7 μm) were obtained by trituration for 2 hours in isopropanol with agate grinding balls (10 mm in diameter). Mixing in an agate mill avoids contamination by the grinding media. The powder mixtures were annealed in air, oxygen and nitrogen atmosphere at 1173 K for 12–24 hours and then cooled to room temperature at 3 K/min. The product was a compact black mass. It was remilled to less than 20 μm grain size. The course of reaction and the formation of $YBa_2Cu_3O_{7-x}$ were studied by X–ray diffraction analysis (Philips–3100) with monochromatized Cu–K_α radiation.

Compacting and sintering

Cylindrical compacts 4 mm thick and 10–12 mm in diameter were prepared for use in the sintering experiments by powder–pressing at 60 MPa. The samples were sintered at 1193 K for 8–10 hours in electric oven (Fig.1), followed by cooling to room in air and oxygen. The sintering properties were investigated by thermal analysis [7,8]. The samples were heat–treated up to 1373 K in a derivatograph (Erdey–Paulik, G–425).

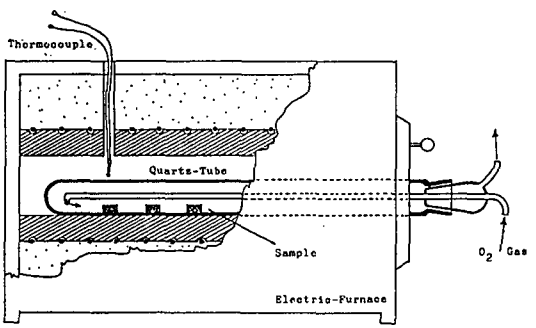

Figure 1: Sintering experiments on specimens in a programmable electrical furnace

The effects of the sintering temperature on the structure and the thermal expansion were studied at 1173 K with an electronic dilatometer (Netzsch), at a heating rate of 5 K/min in air [9]. The microstructure was investigated by means of optical and scanning electron microscopy (JEOL–JSM) with an electron beam–microanalyser to examine several points of the samples.

Superconductivity was first tested *via* the MEISSNER–effect. The transition temperature (T_c) was determined by the resistive four–point method in the temperature range 80–250 K at 0,133 Pa. Thin copper wires were attached to the specimens with conductive silver paint, as power leads and voltage taps. The specimen temperature was measured with a chromel–alumel thermocouple. Resistivity was measured at 10 mA. The four–point voltage was registered with a digital multimeter. For data analysis, a personal computer (ZX–Spectrum) and home–made software were used. This system can measure resistance of samples in vacuum or in any gas atmosphere in the temperature range 77–900 K (Fig.2).

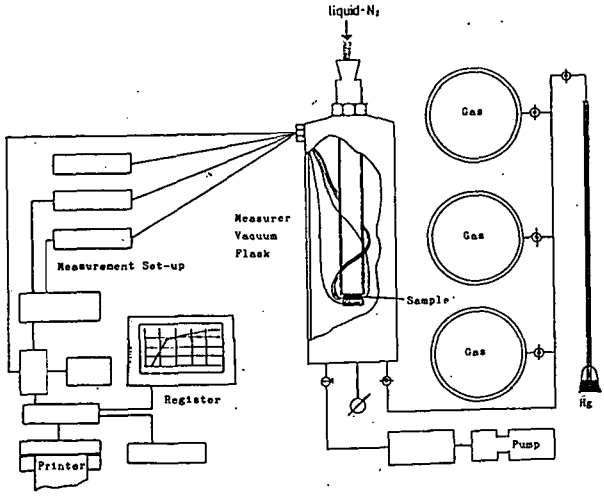

Figure 2. A computer–controlled system for measurement of superconducting samples in vacuum or a gas atmosphere in the temperature range 77–990 K.

Results and discussion

X–ray phase analysis of the powder calcined at 1173 K, indicated the formation of $YBa_2Cu_3O_{7-x}$. After calcination for 2 hours, CuO and Y_2O_3 reflection were no longer observed. The relative intensities of the $BaCO_3$ reflections gradually diminished with increasing time of reaction. The $YBa_2Cu_3O_{7-x}$ phase reflections were observed after 3 hours and the phase formation was almost complete within 4 hours. After compacting, on sintering at 1193 K for 10 hours the reflections of $YBa_2Cu_3O_{7-x}$ very slowly increased in intensity (Fig.3).

The results of derivatographic measurements are shown in Fig.4. Y_2O_3 and CuO did not undergo any change up to 1373 K (Fig.4/1,2). The well–known polymorphic changes of $BaCO_3$ were observed at 1093–1103 K and around 1243 K (Fig.4/3). A significant weight loss and a small endothermic peak were observed in the 1:5 mixture of Y_2O_3 and CuO (Fig.4/4). This weight change may be caused by the reduction of CuO.

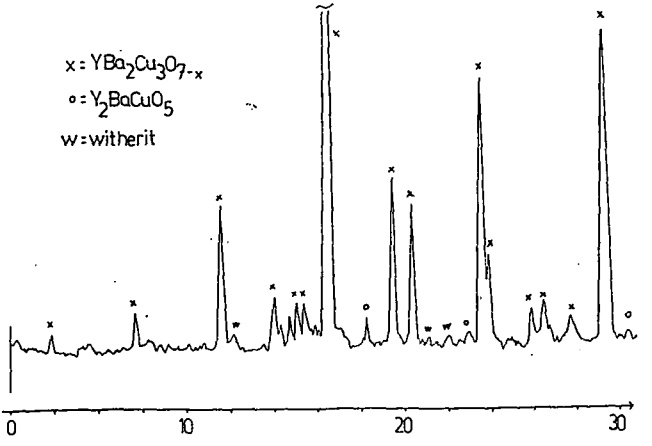

Figure 3: X–ray analysis of superconducting $YBa_2Cu_3O_{7-x}$.

The 1:4 mixture of Y_2O_3 and $BaCO_3$ revealed only the polymorphism of $BaCO_3$ (Fig.

4/5). The 4:6 mixture of CuO and $BaCO_3$ exhibited a chemical reaction at 1263 K (Fig.4/6). The 1:4:6 mixture of Y_2O_3, CuO, and $BaCO_3$ displayed several new endothermic effects (Fig.4/7). The peak at 1133 K is attributed to the perovskite structure transition and the peaks at around 1273 K decomposition.

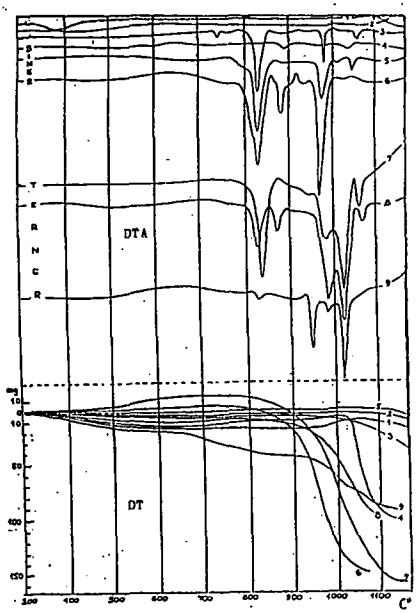

Figure 4: Simultaneous TG and DTA measurements on the starting oxides and their mixtures.

The mixture of the base materials after a 12–24 hours annealing at 1173 K and those compacting and sintering at 1193 K during 4–6 hours exhibit similar decompositions in

the derivatograph oven (Fig.4/8,9).

The different changes in weight during the first two steps in the interval 673–943 K are important. The superconducting properties of the material can change in this temperature range due to oxygen desorption and adsorption and a phase transition from the orthorhombic to the tetragonal state.

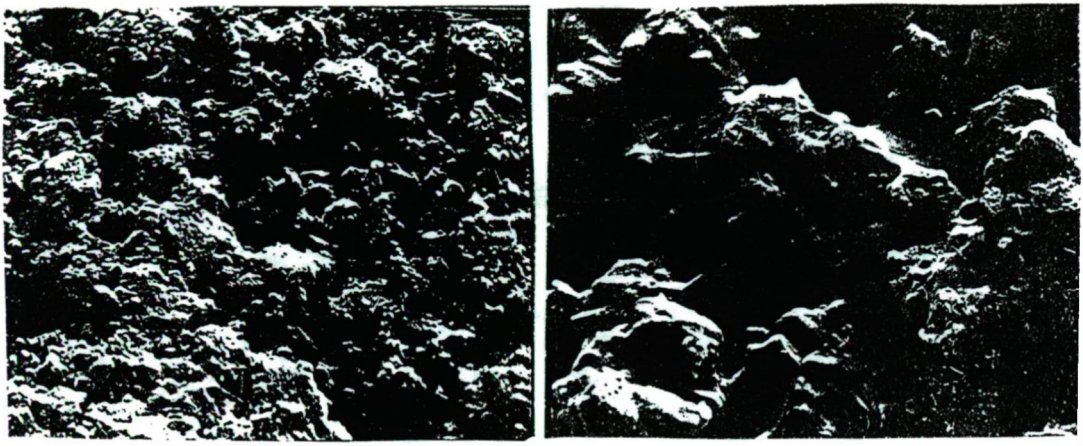

Figure 5: SEM micrographs of a superconducting specimen sintered at 1193 K (M=1050 X and M=13000 X)

The SEM investigations confirmed the results of X–ray diffractometric and thermo–gravimetric analyses. After calcining for 3 hours sinter–necks appear and pronounced grain sets grow (Fig.5).

The sintering conditions exerted marked influence on the microstructure and superconductivity. Specimens sintered at 1173 K displayed a sharp drop in resistance, beginning at about 100 K and reaching zero at 90–85 K. Specimens heat–treated at 1183–1203 K had transition points at 90–92 K (Fig.6/6,7). Samples sintered at 1213 K or higher did not become superconducting. The change in superconductivity at elevated

temperatures can be seen in connection with the formation of liquid phase that separates the superconductive particles.

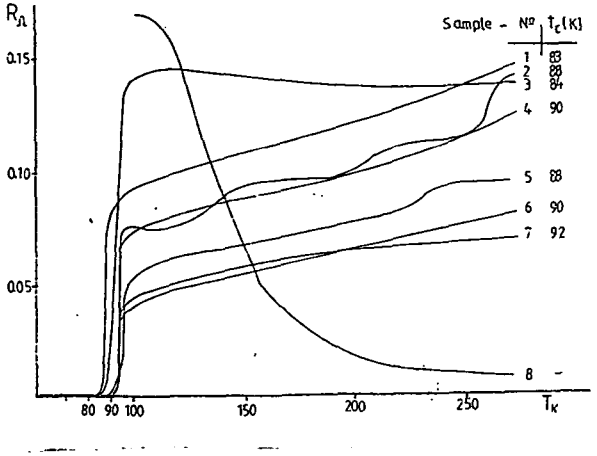

Figure 6: Resistivity as a function of $YBa_2Cu_3O_{7-x}$ specimens sintered at 1173–1213 K.

Dilatometric measurements on the sintered material indicated the existence of a liquid phase. Beginning at 1093 K such specimens showed a rapid increase in shrinkage that could not be attributed to solid–phase sintering. There was an enormous difference in dilation behaviour within a small temperature range (Fig.7). Since the composition of $YBa_2Cu_3O_{7-x}$ is situated very close to the melting zone, even a slight local stoichiometric deviation in Y_2O_3 deficit suffices to cause the formation of a liquid phase.

Heat treatment makes the high–temperature grain boundary phase crystallize extensively into $YBa_2Cu_3O_{7-x}$ thereby restoring the integrity between the superconducting particles and hence converting the specimens into superconductors.

Porosity examination (by water absorption) of the specimens revealed a porosity of 18–25 % caused in part by the formation of carbon dioxide during sintering. The porosity could be reduced by optimizing the calcining conditions.

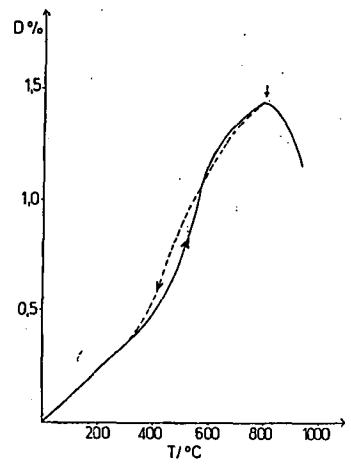

Figure 7: Thermal expansion of superconducting $YBa_2Cu_3O_{7-x}$

SEM and dilatometric measurement demonstrated the phase states which are important for the preparation of superconducting ceramics. The thermal expansivity was also sensitive to temperature change (Fig.7).

Single–phase specimens were obtained only within a narrow temperature range

(1173–1203 K). The broad resistance transitions of specimens sintered below 1183 K indicated the presence of nonsuperconducting volume fractions in such samples (Fig.6/2).

Summary

Reproducible single–phase superconducting ceramic material was obtained by optimizing the various preparation steps. Each individual preparation step exerted a substantial influence on the structural formation and hence on the conducting properties. A homogeneous powder mixture is an important prerequisite for rapid and complete reaction. Investigation of the reaction during calcining revealed the relative rapid formation of a superconducting phase. A single–phase was obtained only within a narrow temperature range. The liquid phase appearing at approximately 1203 K contributed substantially to specimen densification. Slow cooling of the samples after sintering led to the uptake of oxygen and the formation of a superconducting structure.

References

[1] *Bednorz, J.G., K.A. Müller:* Z.Phys. B *64*, 189 (1986).

[2] *Chu, C.W., P.H. Hor, R.L. Meng, L. Gao, Z.Z. Huang, J.Q. Wang:* Phys.Rev.Lett. *58*, 405 (1987).

[3] *Maeda, H., Y. Tanaka, M. Fukutomi, T. Asano:* Jap.J.Appl.Phys.Lett. *27*, 208 (1988).

[4] *Seng, Z.Z., A.M. Herman:* Nature, *332*, 138 (1988).

[5] *Cava, R.J., B. Batlogg, D.W. Murphy:* Phys.Rev.Lett. *58*, 1676 (1987).

[6] *Hor, P.H., L. Gao, R.L. Meng:* Phys.Rev.Lett. *58*, 911 (1987).

[7] *Liang, J.K., X.T. Xu, S.S. Xie, G.H. Rao, Z.G. Duan:*

Z. Phys. B. Cond. Matter, *69*, 137 (1987).

[8] *Ozowa, T., A. Hegishi, Y. Takahasi, R. Sukamoto, H. Ihara:* Thermochimica Acta, *124*, 147 (1988).

[9] *Sytula, A., G. Mawrodiew, S. Koneska, M. Fukarova:* Acta Phys. Polonica, A *73*, 785 (1988).

LIST OF PAPERS PUBLISHED BY THE AUTHORS OF THE DEPARTMENT OF PHYSICS AND THE DEPARTMENT OF CHEMISTRY, IN SCIENTIFIC JOURNALS, DURING 1990.

DEPARTMENT OF PHYSICS

Institute of Experimental Physics

1. *Bali, K., L. Nánai:* Laser induced oxidation of Tantalum. Spectrochim. Acta, A*46*, 499 (1990).
2. *Mizser, A., K. Szatmáry, I. Tepliczky:* Some results of Hungarian variable star observers. First European Meeting of the AAVSO, Brussels, 1990. (in press).
3. *Nánai L.:* Laser light induced dissipative structure on solid surfaces. SPIE, *1352*, 297 (1990).
4. *Nánai, L., I. Hevesi, N.F. Bunkin, B.A. Zon, S.V. Lavrishev, B.S. Luk'yanchuk, G.A. Shafeev:* Influence of electric field on heterogeneous reactions stimulated by laser light. Part I. Theory. Appl. Phys., A*50*, 27 (1990).
5. *Nánai, L., I. Hevesi, N.F. Bunkin, B.A. Zon, S.V. Lavrishev, B.S. Luk'yanchuk, G.A. Shafeev:* Influence of electric field on heterogeneous reactions stimulated by laser light. Part II. Experimental. Appl. Phys., A*50*, 101 (1990).
6. *Szatmáry, K.:* UX Draconis 1976–1989. Meteor, No. *7–8*, 32 (1990).
7. *Szatmáry, K.:* Pulsoting variable stars in binary systems. First European Meeting of the AAVSO, Brussels, 1990. (in press).
8. *Szatmáry, K.:* The planet's moons in the solar system (in Hungarian). Fizikai Szemle, *40*, 350 (1990).

Institute of Optics and Quantum Electronics

1. *Bor, Zs.:* Femtosecond optics. IQEC'90 Conference. Proceedings p. 256 (1990).
2. *Bor, Zs., K. Osvay, B. Rácz, G. Szabó:* Group refractive index measurement by Michelson interferometer. Opt.Commun. *78*, 109 (1990).
3. *Bor, Zs., G. Szabó, Z. Gogolák. Z. Benkö:* Distortion of femtosecond light pulses in optical systems and their applications. Conference, New Orleans (1990).
4. *Dane, C.B., T. Shapr, T. Hofmann, W.L. Wilson Jr., F.K. Tittel, P.J. Wisoff, G. Szabó:* Amplification of high intensity ultrashort blue–-green laser pulses using a XeF(C–A) excimer amplifier. LEOS'90 Boston, November 4–9 (1990).
5. *Hilbert, M., Zs. Bor, M. Benedict:* Relation between the Heisenberg uncertainty principle and the resolution of spectrographs (in Hungarian). Fizikai Szemle *40*, 368 (1990).
6. *Seres, J., J. Hebling, Zs. Bor:* Stability of distributed feedback dye laser excited by excimer laser. Acta Phys. et Chem. Szeged, *96*, 5 (1990).
7. *Sharp, T.E., Th. Hofmann, C.B. Dane, W.L. Wilson Jr., F.K. Tittel, P.J.K. Wisoff, G. Szabó:* Ultrashort laserpulse amplification in XeF(C–A) amplifier. Opt. Letters *15*, 1461 (1990).
8. *Szabó, G., Zs. Bor:* Broad band frequency drubler for femtosecond pulses. Appl. Phys. B50 51 (1990). *Szatmáry, S., F.P. Schäfer:*

Femtosecond pulse generation at 193 nm. The Int. Congr. on Opt. Sci. and Engng. The Hague, 1990.

9. *Szörényi, T., K. Piglmayer, D. Bauerle:* Growth kinetics of laser chemical vapor deposited tungsten. Spectrochim. Acta, *46*A, 505 (1990).

10. *Szörényi, T.:* Laser chemical vapor deposition (LCVD) of silicon oxide thin films. Proc. Symp. Electr. Technol. *'90*, 439 (1990).

11. *Szörényi, T., P. Gonzalez, M.D. Fernandez, J. Pou, B. Leon, M. Pérez–Amor:* Large area silica films deposited on silicon substrates by a CO_2 laser, Laser Assisted Processing II., Proc. SPIE *1279*, 144 (1990).

12. *Szörényi, T., P. Gonzalez, M.D. Fernandez, J. Pou, B. Leon, M. Pérez–Amor:* Silicon oxide films deposited by excimer laser CVD. Thin Solid Films *193/194*, 619 (1990).

13. *Szörényi, T., P. Gonzalez, M.D. Fernandez, J. Pou, B. Leon, M. Pérez–Amor:* Gas mixture dependency of the LCVD of SiO_2 films using an ArF laser. Appl. Surf. Sci. *46*, 206 (1990).

14. *Tittel, F.K., P. Canarelly, C.B. Dane, Th. Hofmann, R. Sauerbrey, T.E. Sharp, G. Szabó, W.L. Wilson, P.J. Wisoff, S. Yanaguchi:* Advanced concept of electron beam pumped excimer lasers. Conf. on Gas and Chem. Lasers, Madrid, Spain. September 10–14, 1990. SPIE Vol. *1397*, 21 (1990).

15. *Tóth, Zs., Z. Kántor, P. Mogyorósi, T. Szörényi:* Surface patterning by pulsed laser induced transfer of metals and compounds. Laser Assisted Processing II., Proc. SPIE *1279*, 150 (1990).

Institute of Theoretical Physics

1. *Bartha, F., F. Bogár, E Kapuy:* Localization of virtual orbitals. Int. J. Quantum Chem. *38*, 215 (1990).
2. *Benedict, M.G., A.I. Zaitsev, V.A. Malyshev, E.D. Trifonov:* Mirrorless bistability in passing of light ultrashort pulse through a thin layer with resonant 2–level centers. (in Russian). Optika i Spektroskopiya, *68*, 812 (1990).
3. *Hilbert, M., Zs. Bor, M. Benedict:* Relation between the Heisenberg Uncertainty Principle and the resolution of spectrographs. (in Hungarian). Fizikai Szemle, *40*, 368 (1990).
4. *Kapuy, E., F. Bartha, F. Bogár, Z. Csépes, C. Kozmutza:* Applications of the MBPT in the localized representation. Int. J. Quantum Chem., *37*, 139 (1990).
5. *Kozmutza, C., E. Kapuy:* Localized orbitals for the description of molecular interaction. Int. J. Quantum Chem., *38*, 665 (1990).
6. *Kozmutza, C., Zs. Ozoróczy, E. Kapuy:* The structure of the CH_2O–NH_3 System. Part I. Study of configurations. J. Mol. Structure (Theochem), *204*, 101 (1990).
7. *Kozmutza, C., Zs. Ozoróczy, E. Kapuy:* The structure of the CH_2O–NH_3 System. Part II. Effect of the basis–set superposition. J. Mol. Structure (Theochem) *207*, 259 (1990).
8. *Varga Zs., I.K. Gyémánt:* 1s core level shifts of Al and Ar atoms in Aluminium clusters. Int. J. Quantum Chem. *38*, 351 (1990).

Institute of Applied Chemistry

1. *Dabbagh, H.A., B. Chawla, J.Halász, B.H. Davis:* Quantitative separation and evaluation of Fischer–Tropsch reaction products having low ^{14}C–isotopic activity. Fuel Sci. Techn. Intern., *8*, 719 (1990).
2. *Hannus, I., I. Kiricsi, Gy. Schöbel, P. Fejes, I. Bertóti, T. Székely:* Reactions of zeolites with volatile halides, III. Investigations of the interaction between mordenites and phosgene. (in Hungarian). Magy. Kém. Folyóirat, *96*, 78 (1990).
3. *Hannus, I., I. Kiricsi, P. Fejes, H. Pfeifer, D. Freude, W. Oehme:* Reactions of zeolites with volatile halides, IV. Thermal stability of hydroxy groups in dealuminated mordenites. (in Hungarian) Magy. Kém. Folyóirat *96*, 84 (1990).
4. *Hannus, I., I. Kiricsi, Gy. Tasi, P. Fejes:* Infrared spectroscopic study of adsorption of phosgene and carbon tetrachloride on zeolites; Fermi resonance. Appl. Catal. L7, 66 (1990).
5. *Kiricsi, I., S.Kh. Akopjan, A.V. Mikhailov, H. Förster:* UV–VIS spectroscopic study of interaction and transformation of allyl alcohol on zeolites HZSM–5. React. Kinet. Catal. Lett., *42*, 145 (1990).
6. *Kiricsi, I., Gy. Tasi, P. Fejes, H. Förster:* Formation of carbocations in zeolites, VII. Chemisorption of 1–hexene, cylohexene, cyclohexane, cyclohexadiene and benzene. (in Hungarian). Magy. Kém. Folyóirat, *96*, 161 (1990).
7. *Kiricsi, I., Gy. Tasi, I. Hannus, P. Fejes, H Förster:* Transformation of allene over zeolites. J. Mol. Catal., *62*, 215 (1990).

8. *Kiricsi, I., Gy. Tasi, H. Förster, P. Fejes:* UV–VIS spectroscopic and theoretical studies on carbocation formation on solid surfaces. J. Mol. Struct., *218*, 369 (1990).

9. *Kiricsi, I., Gy. Tasi,* Á. *Molnár, H. Förster:* Surface intermediates in the transformation of allylalcohol over zeolites. J. Mol. Struct., *239*, 185 (1990).

Institute of Colloid Chemistry

1. *Dékány, I., T. Marosi, Z. Király, L.G. Nagy:* Surface modification and surface thermodynamic potential functions at the S/L interface. Colloids and Surfaces, *49*, 81 (1990).

2. *Dékány, I., T. Marosi, Z. Király, L.G. Nagy:* Characterization of the surface hydrophobicity by solid–liquid interfacial thermodynamic potential functions. (in Hungarian). Magy. Kém. Folyóirat, *96*, 170 (1990).

3. *Dékány, I., A. Weiss:* The liquid–crystal structure of adsorbed layers and the stability of dispersed systems in organic liquids. (in Hungarian). Magy. Kém. Folyóirat, *96*, 206 (1990).

4. *Dékány, I., L.Gy. Nagy:* Thermodynamics of the immersional wetting and adsorption of displacement on solid surfaces. (in Hungarian). Magy. Kém. Folyóirat, *96*, 409 (1990).

5. *Dékány, I., E. Tombácz, A. Szűcs, P. Valastyán:* The effect of corrosion inhibitors on the stability of gasoline–ethylene glycol–water emulsions.

Proc. Third Symp. on Mining Chem. 15–18 Oct. 1990, Siófok, Hungary 239 p.

6. *Dékány, I., J. Müller, S. Puskás, I. Regdon, J. Balázs, M. Gilde:* The influence of asphaltenes and hydrophobic solid particles on the stability of crude oil emulsions. Proc. Third Symp. on Mining Chem. 15–18 Oct. 1990, Siófok, Hungary p. 231.

7. *Dékány, I.:* In memory of Professor F. Szántó. Colloids and Surfaces, *49*, VII (1990).

8. *Erős, I., J. Balázs, I. Péter, M. Tacsi:* Investigation of drug–containing multiple phase emulsions. Pharmazie, *45*, 419 (1990).

9. *Erős, I., J. Balázs, I. Csóka, Sz. Musztafa:* Investigation of the stability of drug–containing (multiple–phase) emulsions. Acta Phys. et Chem. Szeged, *96*, 16 (1990).

10. *Király, Z., I. Dékány:* Enthalpy and entropy effects in adsorption and displacement. Colloids and Surfaces, *49*, 95 (1990).

11. *Marosi, T., I. Dékány:* Adsorption of alcohol–water mixtures on hydrophilic and hydrophobic surfaces, I. Results for methanol–water systems (in Hungarian). Magy. Kém. Folyóirat, *96*, 289 (1990).

12. *Marosi, T., I. Dékány:* Adsorption of alcohol–water mixtures on hydrophilic and hydrophobic surfaces, II. Results for n–propanol–water systems (in Hungarian). Magy. Kém. Folyóirat, *96*, 357 (1990).

13. *Tombácz, E., I. Ábrahám, F. Szántó:* The possibility of hetero–coagulation between montmorillonite and humic substances. Applied Clay Science, *5*, 101 (1990).

14. *Tombácz, E., M. Gilde, I. Ábrahám, F. Szántó:* Effect of sodium chloride on interactions of fulvic acid and fulvate with montmorillonite. Applied Clay Science, *5*, 101 (1990).

15. *Tombácz, E., I. Ábrahám, M. Gilde, F. Szántó:* The pH–dependent colloidal stability of aqueous montmorillonite suspensions. Colloids and Surfaces, *49*, 71 (1990).

16. Tombácz, E., E. Meleg: A theoretical explanation of the aggregation of humic substances as function of pH and electrolyte concentration. Org. Geochem. *15*, 375 (1990).

17. *Váradi, T., I. Dékány:* The fractionation of alkyd resins with various methods. XX^{e} Congrés Fatipec. Nice, 17–21 Sept. 1990. p. 209.

18. *Várkonyi, B., L. Sántha:* Konsistenzgrenzen der konzentrierten wässrigen Pigmentsuspensionen. XX^{e} Congrés Fatipec. Nice, 17–21 Sept. 1990. p. 28.

Institute of Inorganic and Analytical Chemistry

1. *Burger, K.:* Biocoordination Chemistry. Coordination equilibria in biologically active systems. Chapter VI: K. Burger and L. Nagy: Metal complexes of carbohydrates and sugar–type ligands. pp. 236––284 (1990).

2. *Burger, K., Zs. Nemes–Vetéssy, A. Vértes, E. Kuzman, M. Suba, J.T. Kiss, H. Ebel, M. Ebel:* Mössbauer study of mixed–ligand complexes of europium(III). Struct. Chem., Vol. I., 251 (1990).

3. *Csányi, L.J.:* On the peroxidation reactions of monomolybdates. Transition Met. Chem., *15*, 371 (1990).

4. *Csányi, L.J., K. Jáky:* Peroxo–oxometallate formation under phase transfer conditions. J. Mol. Catal, *61*, 75 (1990).

5. *Darzynkiewicz, E., J. Stepinski, S.M. Tahara, R. Stolarski, I. Ekiel, D. Haber, K. Neuvonen, P. Leikoinen, I. Labádi, H. Lönnberg:* Synthesis, conformation and hydrolytic stability of p^1,p^3–dinucleoside triphosphate related to mRNA 5'–cap, and comparative kinetic studies on their nucleoside and nucleoside monophosphate analogs. Nucleosides & Nucleotides, *9*, 599 (1990).

6. *Gaizer, F., H.B. Silber:* A PC computer program minimix for the calculation of the stability constants of $M_qL_pL'_p$, type mixed or the mixture of M_qL_p and M_q,L'_p, complexes from spectrophotometric measurements. Acta Phys. et Chem. Szeged, *36*, 28 (1990).

7. *Gajda, T., L. Nagy, K. Burger:* Proton and zinc(II) complexes of 2–(polyhydroxylalkyl)thiazolidine–4–carboxylic acid derivatives. J. Chem. Soc. Dalton Trans., 3155 (1990).

8. *Kettle, S.F.A.:* Chemistry in a spin. Acta Phys. et Chem. Szeged, *36*, 36 (1990).

9. *Nagy, L., T. Yamaguchi, L. Korecz, K. Burger:* Comparison of the local structures of common (Cu, Fe, Mn, Zn) toxic (Ni, Ag) and therapeutic (Sn) metal complexes formed with carbohydrates and nucleosides. Trace Elements in Medicine, *7*, 99 (1990).

10. *Sipos, P., T. Kis:* Spectroscopic and potentiometric study of protonation and copper(II) complex formation of 3–amino–l–tyrosine.

J. Chem. Soc. Dalton Trans., 2909 (1990).

11. *Sirokmán, G., F. Lukács, Á. Molnár, M. Bartók:* Transformation of compounds containing C–N bonds on heterogeneous catalysis–7. The stereochemistry of the dehydrogenation of 2–alkyl–3–dimethylamino––1–phenylpropan–1–oils. Tetrahedron, *46*, 5347 (1990).

Institute of Organic Chemistry

1. *Bartók, M., Gy. Wittmann, G. Bozóki–Bartók, Gy. Göndös:* Homogeneous and heterogeneous catalytic asymmetric reactions. IV. Hydrogenation of the Ni complexes of cinnamic acid salts over MRNi catalyst. J. Organomet. Chem. *384*, 385 (1990).
2. *Burger, K., Zs. Nemes–Vetéssy, A. Vértes, E. Kuzmann, M. Suba, J.T. Kiss, H. Ebel, M. Ebel:* Mössbauer study of mixed–ligand complexes of europium(III). Struct. Chem. *1*, 251 (1990).
3. *Göndös, Gy., J.C. Orr:* Synthesis and oxidation of pregna–3,5–dien––20–one. Liebigs Ann. Chem. 213 (1990).
4. *Göndös, Gy., L. Gera, M. Bartók, J.C. Orr:* Homogeneous and hetero–geneous catalytic asymmetric reactions, II. Assymetric hydrogenation on stereoid ketones (in Hungarian). Magy. Kém. Folyóirat *96*, 65 (1990).
5. *Katona, T., Z. Hegedüs, Cs. Kopasz, Á. Molnár, M. Bartók:* Amorphous alloy catalysis, II. Effects of dehydrogenation of 2–propanol on the structure and catalytic activity of an amorphous copperzirconi–

um alloy sample. Catalysis Lett. *5*, 361 (1990).

6. *Kiricsi, I., Gy. Tasi, Á. Molnár, H. Förster:* Surface intermediates in the transformation of allyl alcohol over zeolites. J. Mol. Structure *239*, 185 (1990).

7. *Láng, K.:* Some observations of the determination of organic bases with cobalt(II) thiocyanate for the identification of synthetic pharmacological products. Microchem. J. *410*, 191 (1990).

8. *Meskó, E., Gy. Schneider, Gy. Dombi, D. Zeigan:* Steroids, XLII. Configurational analysis of 3–methoxy–16–methylestra–1,3,5(10)–trien––17–ol derivatives. Leibigs Ann. Chem. 419 (1990).

9. *Molnár, Á., J.T. Kiss, I. Bucsi, T. Katona, M. Bartók:* Reactions of organosilicon compounds on metals. Part IV. Effects of alkylhydro–silanes on activity of copper and noble metals in transformations of 1–pentene. J. Mol. Catal. *61*, 307 (1990).

10. *Notheisz, F., I. Pálinkó, M. Bartók:* Hydrogen pressure–dependence in the ring–opening reactions of substituted cyclopropanes over Rh/SiO_2 catalyst. Catal. Lett. *5*, 229 (1990).

11. *Pálinkó, I., F. Notheisz, M. Bartók, D. Ostgard, G.V. Smith:* Self–recognition in the liquid–phase hydrogenation of an optically active compound over Pd/SiO_2 catalysts. J. Mol. Catal. *57*, 353 (1990).

12. *Pálinkó, I., Á. Molnár, J.T. Kiss, M. Bartók:* Activity, selectivity, and stereochemical features in the copper–catalyzed hydrogenative ring––opening of alkyl–substituted cyclopropanes – Nature of active sites. J. Catal. *121*, 396 (1990).

13. *Pálinkó, I., F. Notheisz, M. Bartók:* Low– and high–temperature hyd–

rogenative ring–opening of alkyl–substituted cyclopropanes and methyl–oxirane over Pd/SiO_2 catalyst: detection of β–hydride by a chemical method. J. Mol. Catal. *63*, 43 (1990).

14. *Sárkány, J., M. Bartók:* IR study of the effects of Lewis bases on CO coadsorbed on Pt/SiO_2. Vacuum *40*, 109 (1990).

15. *Sirokmán, G., Á. Mastalir, Á. Molnár, M. Bartók, Z. Schay, L. Guczi:* Structure and catalytic activity of copper, nickel and platinum graphimets prepared from graphite intercalation compounds. Carbon *28*, 35 (1990).

16. *Sirokmán, G., F. Lukács, Á. Molnár, M. Bartók:* Transformation of compounds containing C–N bonds on heterogeneous catalysts – 7. The stereochemistry of the dehydrogenation of 2–alkyl–3–dimethylamino–1––phenylpropan–1–ols. Tetrahedron *46*, 5347 (1990).

17. *Wittmann, Gy., G. Bozóki–Bartók, M. Bartók, G.V. Smith:* Homogeneous and heterogeneous catalytic asymmetric reactions, Part III. New investigations concerning the preparation of reproducible MRNi catalyst. J. Mol. Catal. *60*, 1 (1990).

18. *Wittmann, Gy., Gy. Göndös, M. Bartók:* Homogeneous and heterogeneous asymmetric reactions, Part 5. Diastereoselective and enantioselective hydrogenation of cyclic β–keto esters on modified Raney–nickel catalysts. Helv. Chim. Acta *73*, 635 (1990).

Institute of Physical Chemistry

1. *Bán, M.I., Gy. Dömötör, A. Vize–Orosz, G. Pályi:* Electronic

structures, bonding properties and photoelectron spectra of (μ_2–1––alkyl–2–phosphacetylene) hexacarbonyldicobalt (Co–Co). J. Mol. Struct. (THEOCHEM), *209*, 339 (1990).

2. *Beck, M., I. Nagypál:* Chemistry of Complex Equilibria. Akadémiai Kiadó, Budapest, 1990. 402 pp.

3. *Bockris, J.O'M., M. Szklarzyk, Á. Szűcs:* The electrochemical background to the study of electropharmacology. Eds.: Eckert, G.M. – Gutmann F. – Keyzer H.: Electropharmacology. Chapter 2. 25–91. CRC Press, Boca Raton, USA, 1990.

4. *Boga, E., G. Peintler, I. Nagypál:* Propagating reaction front in the cobalt(II)–catalyzed autooxidation of benzaldehyde. J. Am. Chem. Soc., *112*, 151 (1990).

5. *Boga, E., S Kádár, G. Peintler, I. Nagypál:* Effect of magnetic fields on a propagating reaction front. Nature, *347*, 749 (1990).

6. *Boga, E., I. Nagypál:* The effect of magnetic field on the propagating chemical wave in the cobalt(II)–catalyzed autooxidation of benzaldehyde. React. Kinet. Catal. Letters, *42*, 413 (1990).

7. *Császár, J.:* Some correlations between the spectroscopic characteristics of salicylidene para–X–anilines (Preliminary communication) Acta Chim. Hung., *127*, 165 (1990).

8. *Császár, J.:* Spectral studies of molecular complexes of aromatic Schiff bases with picric acid. Acta Chim. Hung., *127*, 277 (1990).

9. *Császár, J.*: Visible spectra of picric acid derivatives of Ni[4'–X–N(2––hydroxy–benzylidene)aniline]$_2$ type chelates. (Short communication). Acta Chim. Hung., *127*, 313 (1990).

10. *Császár, J.:* Spectral studies of picrates of pyridine and pyridine derivatives. (Short communication). Acta Chim. Hung., *127*, 414 (1990).

11. *Császár, J.:* Spectral studies of the ternary compound N,N'–bis (salicylidene)ethylenediamines–picric acid–pyridine. (Short communication). Acta Chim. Hung., *127*, 697 (1990).

12. *Császár, J., N.M. Bizony:* Formation and visible spectra of some molecular complexes of aliphatic and aromatic primary amines with iodine in chloride–containing aliphatic solvents. Acta Phys. et Chem. Szeged, *36*, 66 (1990).

13. *Császár, J., N.M. Bizony:* Correlations between the visible spectra of $VO(AA)_2$ in different solvents and the Taft–Kamlet solvent parameters. Acta Phys. et Chem. Szeged, *36*, 56 (1990).

14. *Császár, J., L. Kiss:* The spectra of esters of oxohydroxobis–(8–hydroxy–quinoline)vanadium(V). (Short communication). Acta Phys. et Chem. Szeged, *36*, 83 (1990).

15. *Dömötör, Gy., M.I. Bán:* QCMP 084 Program: PSD; QCPE, Bloomington, Indiana, USA, 1990.

16. *Dömötör, Gy., M.I. Bán:* A program for surface design. QCPE Bulletin, *10* (*3*), 67 (1990).

17. *Görgényi, M., L. Seres:* Radical–initiated tautomerization of azoethane to acetaldehyde–ethylhydrazone; reactivity of the $CH_3CH{=}NNC_2H_5$ radical. Tetrahedron Letters, *31*, 7447 (1990).

18. *Gardi, J., M.I. Bán:* Theoretical study of the adsorption of CO molecules on stepped single crystal Pt surfaces. (Short communication).

Acta Phys. et Chem. Szeged, *36*, 89 (1990).

19. *Illing, G., T. Porwol, I. Hemmerich, Gy. Dömötör, H. Kuhlenbeck, H.J. Freund, C.M. Liegener, W. von Niessen:* Electron spectroscopy of absorbates *via* autoionization of core–to bound excited states: experiment and theory. J.Electron Spectr. and Related Phenomena, *51*,149 (1990).

20. *Kankare, J., J. Lukkari, T. Pajunen, J. Ahonen, Cs. Visy:* Evolutionary spectral factor analysis of doping undoping processes of thin conductive polymer films. J. Electroanal. Chem., *294*, 59 (1990).

21. *Körtvélyesi, T., L. Seres:* Theoretical studies on the recombination reaction of tert–butyl radical. Acta Phys. et Chem. Szeged, *36*, 95 (1990).

22. *Körtvélyesi, T., L. Seres:* MNDO and AM1 studies on the resonance stabilized allyl–type radicals containing CC, CN and NN bonds. Acta Phys. et Chem. Szeged, *36*, 103 (1990).

23. *Körtvélyesi, T., M. Görgényi, L. Seres:* On the stability of substituted 1,2–diazaallyl radicals. Z.phys.Chemie, Leipzig, *271*, 000 (1990).

24. *Micskei, K., I. Nagypál:* Kinetic studies in aqueous solutions of iron(II)–glycinate–ethylenediamine, and –malonate complexes. J. Chem. Soc. Dalton Trans., 743 (1990).

25. *Micskei, K., I. Nagypál:* Comparison of the formation rate constants of some chromium(II) and copper(II) complexes. J. Chem. Soc. Dalton Trans., 1301 (1990).

26. *Micskei, K., I. Nagypál:* Kinetic studies in aqueous solutions of cobalt(II)–ethylenediamine–malonate, and –glycinate complexes. J. Chem. Soc. Dalton Trans., 2581 (1990).

27. Peintler, G., I. Nagypál, R.R. Epstein: Kinetics and mechanism of the reaction between chlorite ion and hypochlorous acid. J. Phys. Chem., *94*, 2954 (1990).

28. Rauscher, Á., Gy. Kutsán, Z. Lukács: Effects of hydrogen sulphide and temperature on passivation behaviour of titanium. Corrosion Science, *31*, 255 (1990).

29. Porwol, T., I. Hemmerich, G. Illing, Gy. Dömötör, H.J. Freund, W. von Niessen, M. Neuber, M. Neumann: Autoionisation molekularer Adsorbate: Co(Ni(110), NO/Ni(110), N_2/Ni(110)–Experiment und Theorie. BESSY Jahresbericht, 289 (1990).

30. Szirovicza, L., I. Nagypál, E. Boga: Design of acidic front reactions (in Hungarian). Magy. Kém. Folyóirat, *96*, 72 (1990).

31. Visy, Cs., M. Novák: Role of water in the electrochemical chlorination of cyclo–olefins in nitromethane solution. J. Electroanal. Chem., *296*, 571 (1990).

32. Visy, Cs., J. Lukkari, T. Pajunen, J. Kankare: Spectroelectrochemical study of the anion effect on the transient redox behaviour of poly(N––methylpyrrole) in anhydrous acetonitrile. Synth. Metals, *39*, 61 (1990).

Institute of Solid State and Radiochemistry

1. Berkó, A., F.P. Coenen, F.P. Bonzel: Structure sensitivity of methanation on Nickel. Vacuum *41*, 147 (1990).

2. *Berkó, A., W. Erley, D. Sander:* Layer growth mechanism and dipole–dipole interactions of CH_3Cl on Pd(110): an infrared and thermal desorption study. J. Chem. Phys. *93*, 1 (1990).

3. *Buchanan, D., F. Solymosi, J.M. White:* CO–induced structural changes of Rh on TiO_2 support. J. Catal., *125*, 456 (1990).

4. *Erdőhelyi, A., A. Anneser, Th. Bauer, K. Stephan, D. Borgmann, G. Wedler:* Interaction of carbon dioxide and oxygen on iron films at 273 K. Surface Science *227*, 57 (1990).

5. *Kozma, B., J. Cserényi, I. Kovács:* Studies of high–T_c superconductors in Y–Ba–Cu–O ceramic systems. Acta Phys. et Chem. Szeged, *36*, 121 (1990).

6. *Solymosi, F., J. Kiss, K. Révész:* Effects of illumination on the surface behavior of CH_3Cl on a clean and a K–dosed Pd(100) surfaces. J. Phys. Chem. *94*, 2224 (1990).

7. *Solymosi, F., H. Knözinger:* Infrared spectroscopic study of the adsorption and reactions of CO_2 on K–modified Rh/SiO_2. J. Catal. *122*, 166 (1990).

8. *Solymosi, F., A. Erdőhelyi:* Partial oxidation of ethane over supported vanadium pentoxide catalysts. J. Catal. *123*, 31 (1990).

9. *Solymosi, F., J. Kiss, L. Bugyi:* Interaction of NO with clean and K–dosed Rh(111) surfaces II. EELS and PES studies. Surf. Sci. *233*, 1 (1990).

10. *Solymosi, F., H. Knözinger:* An infrared study on the interaction of CO with alumina supported Rhodium. JCS Faraday I., *86*, 389 (1990).

11. *Solymosi, F., É. Novák, A. Molnár:* Infrared spectroscopic studies on

CO–induced structural changes of Ir on alumina support. J. Phys. Chem. *94*, 7250 (1990).

12. *Solymosi, F., É. Novák:* Effects of potassium on the formation of isocyanate species in the NO+CO reaction on Rhodium catalyst. J. Catal. *125*, 112 (1990).

INDEX

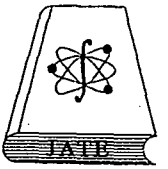

Publisher: The Dean Dr. L. Hatvani
(JATE TTK Dean's Office)
Published by the Editorial Office of Acta Phys. et Chem.
at JATE Institute of Physical Chemistry, Szeged
Wordprocessing and copying by *T. Annus, S. Kádár*
Size: B/5
No. of copies: 400

Fk.: Dr. Hatvani László
Készült az Acta Phys. et Chem. szerkesztőségében
(JATE, Fizikai Kémiai Tanszék, Szeged)
Szövegszerkesztési és sokszorosítási munka: *T. Annus, Kádár Sándor*
Engedélyszám: 16–3007/54–9/1991.
Méret: B/5, Példányszám: 400